# FIRE-RESISTANT GEOPOLYMER CONCRETE

# AND ITS APPLICATION IN

# CONCRETE FILLED STEEL TUBES

YI-FANG CAO

WESTERN SYDNEY
UNIVERSITY

**2017**

# FIRE-RESISTANT GEOPOLYMER CONCRETE

# AND ITS APPLICATION IN

# CONCRETE FILLED STEEL TUBES

YI-FANG CAO

A THESIS SUBMITTED

FOR THE DEGREE OF MASTER OF PHILOSOPHY

CENTRE FOR INFRASTRUCTURE ENGINEERING

SCHOOL OF COMPUTING, ENGINEERING AND MATHEMATICS

WESTERN SYDNEY UNIVERSITY

**August 2017**

# Declaration

I hereby declare this thesis is my original work and it has been written by me in its entirety. I have duly acknowledged all the sources of information which have been used in this thesis.

This thesis contains no material which has been accepted for the award of any other degree or diploma in any university.

(Signature)

Yi-Fang Cao

21-August -2017

# Dedication

*This thesis is dedicated to my parents who have always been*

*a source of encouragement and stamina to undertake my research and to*

*face the eventualities of life with zeal, enthusiasm and fear of god.*

# ABSTRACT

Concrete-filled steel tubular (CFST) columns, composed of core concrete and outer tubes, have been extensively used as main structural elements in high-rise buildings to carry loads. Due to the composite action between the steel and core concrete, this type of composite construction has been reported to have many constructional and structural benefits, such as easy construction from the omission of formwork, restraint to local buckling of the steel tube provided by the core concrete, high strength, stiffness and ductility. Recently, there is increased interest in adopting CFST columns in composite frame systems.

In recent years, fire disasters have frequently been reported worldwide, and seriously threatened personal and public safety. Exposure of concrete and steel to fire will lead to serious structural deterioration and possible failure of columns, thus resulting in local or global collapse of a building. However, in most cases, unprotected CFST columns are not able to maintain structural integrity for sufficient time under fire conditions. External insulating coating or internal reinforcing steel are required to improve the fire resistance of CFST columns, but these two methods tremendously increase the cost of CFST columns and the difficulty of construction.

Although ordinary Portland cement (OPC) concrete is classified as a fire-resistant construction material, during fire exposure severe spalling may occur, as well as significant deterioration of strength and stiffness. Therefore, there is a need to find alternative materials to replace OPC to further improve the fire resistance of concrete. Geopolymer is aluminosilicate synthesised from a material of geological origin or industry by-products (e.g. fly ash) with alkaline solutions. In Australia, fly ash is abundantly available from numerous thermal power plants. The use of fly ash to

manufacture construction materials can promote the better utilisation of this industry by-product, avoiding disposal into landfill. Previous studies have demonstrated that geopolymer can be successfully used as a binder to make geopolymer concrete. The absence of OPC in geopolymer concrete (GPC) can significantly reduce $CO_2$ emissions for the construction industry. Recent research has proved that GPC has substantially better fire performance than OPC concrete. Therefore, GPC has the potential to be used in CFST columns to improve their fire performance. So far, very little research has been conducted to investigate the behaviour of geopolymer concrete-filled steel tubular (GCFST) columns, and this research aims to address this knowledge gap.

In this thesis, salient parameter analysis of GPC mix was conducted based on the Taguchi method, and three optimised GPC mix designs were proposed. Material properties such as slump, density, Young's modulus, compressive strength, flexural strength and splitting tensile strength were experimentally studied. The measured values of Young's modulus, flexural strength and splitting tensile strength of GPC are compared favourably to the predictions of existing standards. The measured hot strength and displacement of GPC under combined loading and elevated temperature were reported. Full-range stress-strain curves of GPC and reference OPC after exposed to elevated temperatures were evaluated. The results further confirm that GPC has the potential to improve the fire performance of CFST columns.

A total of 15 tests were carried out on GCFST columns and conventional CFST columns to compare their behaviours. The main experimental parameters included: (1) Concrete type (geopolymer concrete and OPC concrete); (2) Curing procedure of GPC (ambient curing and elevated temperature curing); (3) Strength of geopolymer concrete

(37.4, 58.6 and 68.4 MPa); (4) Test method (tested at ambient temperature, in fire, or after fire exposure). The axial load, axial strain and lateral strain were measured for ambient temperature tests and residual property tests. The axial displacement versus the temperature curves were recorded for the specimens tested under combined load and temperature increase. The results were compared to predictions of numerical models developed with ABAQUS, and the agreement between them is reasonable.

This research confirms that the behaviour of GPC at an ambient temperature is comparable to that of OPC concrete at an ambient temperature. However, GPC has better fire performance and a higher post-fire residual strength than OPC concrete. This study has proved the potential of using GPC as fire-resistant concrete in CFST columns. Thus, the use of external insulating coating or internal reinforcing steel could be potentially eliminated for CFST columns.

# Acknowledgements

I would like to acknowledge and offer thanks to many people who helped me during the journey to my degree. This journey of discovery would not have been possible without their support, advice and contributions.

First and foremost, I would like to express my deepest gratitude to my supervisors, Prof. Zhong Tao Dr. Zhu Pan and Dr. Richard Wuhrer, not only for providing me guidance, but also for encouraging me to pursue an academic career. I never felt helpless in the whole process as a candidature of MPhil degree. Their knowledge, wisdom and feedback during various stage of this study are highly appreciated. I would also like to thank them for editing my thesis chapters and manuscripts despite their busy schedule.

My sincere appreciation is dedicated to all lab staff at the Structural Research and Testing Laboratory, especially Robert Marshall, Murray Bolden, Zachariah White and Ali Gharizadeh for their help in tackling all experimental challenges.

I extend my gratitude to all staff in Advanced Materials Characterisation Facility (AMCF) for vital equipment support. Special thank was addressed to Timothy Murphy, Laurel George and Shamila Salek for their technical assistance and training.

My thanks were acknowledged to Dr. Md Kamrul Hassan and Utsab Katwal for giving me important support in CFST modelling. The help of Dr. Xin Yu was appreciated for his valuable suggestions. I am grateful to David Batten, Bec Breust, Ashley Bertholdand and other administrative staffs. They offered a professional support to my study. I am deeply thankful to Ann-Marie Blanchard for editing my

thesis who also gave me some insightful advice on word choice. Thanks also go to Ms. Xue Liu for proofreading and constant help.

Last but certainly not the least, I would like to express my gratitude to my friends and colleagues who made my past 2 years much more enjoyable and memorable: A/Prof. Yongjin Li, Prof. Qingxin Ren, Dr. Mengning Lyu, Dr. Yang An, A/Prof. Zhibin Wang, Dr. Ee Loon Tan, A/Prof. Xingqiang Wang, A/Prof. Guihan Peng, Dr. Rui Li, Dr. Parveen Khanehzaei, Dr. Graeme McKenzie, Ms. Soheila Peyrovi Cheshnasar, Mr. Richard Abubakar Shuaibu and Mr. Neelam Bajracjarya.

# List of Publications

**Refereed Journal Paper:**

Y.M. Wang, Y.B. Shao and **Y.F. Cao** (2017), Static behavior of steel tubular structures considering local joint flexibility, *Steel and Composite Structures*, 24(4) 425-439.

**Submitted Journal Paper:**

Pan Z., Tao Z., **Cao Y. F**., Wuhrer R., Murphy T. Compressive strength and microstructure of alkali-activated fly ash/slag binders at high temperature. *Cement and Concrete Composites*, Minor revision.

**Refereed Conference Papers:**

**Y.F Cao**, Z. Tao, Z. Pan T. Murphy & R. Wuhrer (2016), Influence of calcium aluminate cement on strength development of geopolymers cured at room temperature, pp. 927-932, *Mechanics of Structures and Materials: Advancements and Challenges*, 24th Australasian Conference on the Mechanics of Structures and Materials (Perth), 2016, Taylor & Francis Group (London).

Z. Pan, Z. Tao, **Y.F. Cao** & N. Bajracharya, T. Murphy & R. Wuhrer (2016), Comparative performance of alkali-activated slag and fly ash at elevated temperatures, pp. 415-420, *Mechanics of Structures and Materials: Advancements and Challenges*, 24th Australasian Conference on the Mechanics of Structures and Materials (Perth), 2016, Taylor & Francis Group (London).

**Submitted Conference Papers:**

**Y.F Cao**, Z. Tao, Z. Pan T. Murphy & R. Wuhrer (2017), Fire resistance of fly ash-based geopolymer concrete blended with calcium aluminate cement, submitted to 1st *International Conference on Structural Engineering Research (iCSER)*, Sydney, 2017.

Z. Pan, Z. Tao, **Y.F. Cao** & N. Bajracharya, T. Murphy & R. Wuhrer (2016), Effect of temperature on thermal properties of alkali-activated fly ash/slag binders, submitted to *1st International Conference on Structural Engineering Research (iCSER)*, Sydney, 2017.

Z. Tao, **Y.F. Cao**, Z. Pan & Hassan, M, (2017), Behaviour of Geopolymer Concrete-Filled Steel Tubular Columns at Ambient and Elevated Temperatures, submitted to *The 9$^{th}$ Chinese Conference on Fire Resistance of Structures*, Lanzhou.

# Table of Contents

**Abstract……..……..……i**

**Acknowledgements……...…….iv**

**List of Publications……..……..vi**

**Table of Contents……...…..viii**

**List of Figures……...……...…..xv**

**List of Tables……..……...xx**

**Abbreviations, Acronyms and Symbols……...…...……..xxii**

**Chapter 1 Introduction…….……...…..1**

1.1 General……...……..1

1.2 Background…….…...……..……....3

1.2.1 Fire hazard in structures…….…….3

1.2.2 Fly ash-based geopolymer…… …….…..…....5

1.2.3 Concrete filled steel tubular columns…….…….....…..5

1.3 Research motivation……...……..6

1.4 Research objectives, limitation and scope of work……..8

1.4.1 Research objectives...…… …….…..……...8

1.4.2 Research limitation.…… ……..….....9

1.4.3 Research scope…..…….…….…….…..…...9

1.5 Layout of the thesis…….……..……..……..9

**Chapter 2 Literature Review……...…...…..…….12**

2.1 General……...…...…12

2.2 Geopolymer concrete (GPC)…….…….……12

2.2.1 Current development…….…….…….…….....12

2.2.2 Effect of alkali solution.…….....……..13

2.2.3 Effect of curing procedures……..…….……...……..……..16

2.2.4 Effect of additives.……..…..… ….……..…….…….17

2.3 Properties of GPC at an ambient temperature…….……..…..….19

2.3.1 Workability…….……..…...…..…..19

2.3.2 Compressive stress-strain models…...…….……..…...20

2.4 Properties of GPC at elevated temperatures……..……..…….…….…..24

2.4.1 Hot strength ……..…….…….…….....24

2.4.2 Residual strength…….…….....26

2.5 CFST columns……...…….…….…..…….29

2.5.1 Development of CFST columns……..…….…….....29

2.5.2 CFST columns at elevated ambient temperature……..……..……30

2.5.3 CFST columns at elevated temperatures……..…..…….33

2.6 Summary……...……..…...…....35

**Chapter 3 Experimental Program…….…..……37**

3.1 Introduction……...……...…..37

3.2 Materials…...……...…...……...……37

3.2.1 Fly ash and calcium aluminate cement (CAC)…..……..…….....37

3.2.2 Alkaline activators……..…….…....……..39

3.2.3 Aggregates…….....…..……...…….……...40

3.2.4 Superplasticiser…….……40

3.3 Concrete experimental method…….……..41

3.3.1 Sample preparation……....……...……41

3.3.2 Testing regime…….…….……..42

3.4 CFST experimental method……..…..…….50

3.4.1 Sample preparation…….……...…….....….…….50

3.4.2 Testing regime…….…….…….51

3.5 Summary……..……..…...…….....54

**Chapter 4 Development of Optimised Mix Design for Geopolymer Concrete…55**

4.1 Introduction……..……..55

4.2 Background of Taguchi method….…….…….…..55

4.3 Controlling ratios in GPC….……...……..……57

4.3.1 Alkali solution concentration…….……..…..57

4.3.2 Calcium aluminate cement replacement ratio...…...…….…….…58

4.3.3 Activator to binder ratio…….…...……..……..……..……...58

4.4 Salient parameter analysis and optimised mixing design...…….…….…..59

4.4.1Salient parameter analysis on workability……..……..……..61

4.4.2 Salient parameter analysis on compressive strength….……...…….62

4.4.3 Optimised mixing design…….....…..…….…...66

4.5 Summary…….……..……..……...……..…67

**Chapter 5 Behaviour of GPC at Ambient Temperature…….…….…….69**

5.1 Introduction……...……...……...…..……..69

5.2 Test results and discussion of GPC…….…..…….69

5.2.1 Workability of fresh concrete……..……..……...…….....70

5.2.2 Density of hardened concrete……..…..…..…….72

5.2.3 Young's modulus……..…..……..…….…..…….....72

5.2.4 Compressive strength……..…..…..73

5.2.5 Splitting tensile strength……..……..…….…….…….74

5.2.6 Flexural strength……..…….……....…….…….....74

5.3 Microstructure characterisation of geopolymer pastes……..……..75

5.3.1 Conversion of CAC…….……...……....……...……..76

5.3.2 Thermal gravimetric analysis (TGA)..……..……...…….....…….....79

5.3.3 Scanning electron microscopy (SEM) analysis..…….…..……80

5.4 Comparison of experimental results with existing models.…..…..……..84

5.4.1 Comparison of Young's modulus……...…….…….…….....84

5.4.2 Comparison of splitting tensile strength …….....….86

5.4.3 Comparison of flexural strength…….....…...…….…….…….....88

5.5 Summary……..……...……..…..……89

**Chapter 6 Performance of GPC at Elevated Temperatures…….....…….91**

6.1 Introduction……...…….…….91

6.2 Performance of geopolymer mortar at elevated temperatures…….……92

6.2.1 Specimen preparation...92

6.2.2 Test method. ...93

6.2.3 Test results ...95

6.2.4 Parameter analysis on hot strength...97

6.3 Performance of GPC at elevated temperatures...101

6.3.1 Hot strength...101

6.3.2 Deformation of GPC at high temperature under constant load ...102

6.4 Residual properties of GPC after exposure to elevated temperatures.....105

6.4.1 Experimental setup...105

6.4.2 Density ...106

6.4.3 Stress-strain relationship curve...107

6.5 Summary...109

**Chapter 7 Performance of GCFST Columns at Ambient Temperature and Elevated Temperature...111**

7.1 Introduction...111

7.2 Experimental investigation...112

7.2.1 Specimen preparation...112

7.2.2 Test setup……..……..……114

7.3 Experimental results and discussion…..…….……116

7.3.1 Performance of CFST columns at ambient temperature…….……116

7.3.2 Comparison between test results and FE predictions……..……125

7.3.3 Performance of CFST columns after elevated temperature exposure.133

7.3.4 Performance of CFST columns under combined temperature and loading……...……..……..…..138

7.4 Summary……..……..139

**Chapter 8 Conclusions and Future Research Needs...….....……141**

8.1 Conclusions…….……..……141

8.2 Recommendations for future research…….…….…….……...…143

**References...…...…….…….…….…….…….……145**

# List of Figures

Figure 1.1World's tallest buildings by year (Gable, 2016) ……..1

Figure 1.2Fire engulfs a 63-story Hotel in Dubai (AHMED JADALLAH, Reuters)...4

Figure 2.1 Stress-strain curves for OPC and GPC (Noushini et al., 2016) …...…..…22

Figure 2.2 Typical buildings using CFST columns……..……29

Figure 2.3Load versus longitudinal strain relation of geopolymer concrete filled columns from a modified model (Shi et al., 2015) ……..……..……31

Figure 3.1 SEM images of raw materials…….……38

Figure 3.2 Sieve analysis of combined coarse aggregate and fine aggregate. ...……39

Figure 3.3 Mini-slump mould…….……41

Figure 3.4 Young's modulus test setup…….…….……..42

Figure 3.5 Flexural strength test setup…….……43

Figure 3.6 Stress-strain relationship experiment setup…….…….……..44

Figure 3.7 Fire test setup of concrete cylinder…….……...……45

Figure 3.8 Heating regime……...…..……...46

Figure 3.9 Bruker D8 Advance Powder Diffractometer X-ray diffraction ……..…..47

Figure 3.10 JEOL 6510 LV Scanning electron microscope…….……..48

Figure3.11 Bruker Vertex 70 coupled Netzsch 449C Jupiter DSC-TGA instrument...48

Figure 3.12 Fire test setup of steel coupon…….…….....50

Figure 3.13 Setup and location of strain gauges and LVDTs……..……..…51

Figure 3.14 Fire test setup of CFST……...…….52

Figure 4.1 Average effect of factors on the workability of fresh geopolymer paste……...……....61

Figure 4.2 Average effect of factors on the compressive strength of geopolymer mortar…….……64

Figure 5.1 Slump test of fresh GPC…….……..…….70

Figure 5.2 Conversion curing temperature and humidity…….……..76

Figure 5.3 TGA results of geopolymer pastes…….....…….78

Figure 5.4 Geopolymer paste sample for SEM…….....79

Figure 5.5 SEM images of pastes at a) 3 days and b) 7 days……..…….80

Figure 5.6 SEM images and EDS results of pastes at 28 days……...……..……82

Figure 5.7 Relationship of modulus of elasticity with compressive strength……..…83

Figure 5.8 Relationship of splitting tensile strength with compressive strength…..…85

Figure 5.9 Relationship of flexural strength with compressive strength……....….87

Figure 6.1 Setup of GPM fire test……..……..92

Figure 6.2 Typical fracture patterns of specimens during elevated temperature Exposure…….……93

Figure 6.3 Influence of activator concentration……..……..97

Figure 6.4 Influence of CAC replacement ratio……..……..…..…….97

Figure 6.5 Influence of activator to binder ratio……...…….……98

Figure 6.6 Hot strength of concrete……...……..…….…100

Figure 6.7 Deformation of concrete under constant load and high temperature…..…101

Figure 6.8 Deformation of concrete under constant load and high temperature…….102

Figure 6.9 Experimental setup of GPC residual properties…….....…...103

Figure 6.10 GPC specimens before and after heat process……..……..105

Figure 6.11 Stress-strain relationship curve of concretes……..…….106

Figure 7.1 Heating regime……..…113

Figure 7.2 Tested specimens at ambient temperature……114

Figure 7.3 Comparison between N-ε curves of GCFST columns with different strength levels…….……...…….115

Figure 7.4 Comparison between N-ε curves of GCFST columns with different heating regimes……..…….……..…..116

Figure 7.5 Comparison between N-ε curves of GCFST and conventional CFST columns……...…….116

Figure 7.6 Comparison of different strength indexes…...…….……117

Figure 7.7 Comparison of compressive stiffness……...……...…….……119

Figure 7.8 Comparison of different ductility indexes……...…….……121

Figure 7.9 Axial load versus strains at mid-height of test specimens…….…....…122

Figure 7.10 Development of lateral-to-axial strain ratio for CFST columns…..……123

Figure 7.11 3D FE model of CFST column……...…...124

Figure 7.12 Model of concrete in CFST column…….....126

Figure 7.13 Model of steel in CFST column…….…...……..……128

Figure 7.14 Comparison of N-ε curves for GCFST columns with FE model…….…129

Figure 7.15 Comparison of compressive stiffness for GCFST columns with FE model ……...……....130

Figure 7.16 Tested specimens after exposed to elevated temperature……..…..…131

Figure7.17 Comparison of N-ε curves for CFST with different concretes after exposure to elevated temperature……..……...……...…….132

Figure 7.18 Comparison of different strength indexes……..…..…..……134

Figure 7.19 Comparison of compressive stiffness of CFST columns at ambient and post-fire test……..…..…..……..135

Figure 7.20 Failed specimens under constant load and elevated temperature…..….136

Figure 7.21 Axial deformation-time curves of CFST columns at heating stage…….137

# List of Tables

Table2.1 Stress-strain models for unconfined concrete under uniaxial compression……19

Table 3.1 Chemical analysis by X-ray fluorescence of fly ash and CAC……..……37

Table 3.2 Weight of NaOH pellets of solution per kilogram in different molarities…38

Table 4.1 Orthogonal experimental factors……...…...…..56

Table 4.2 Mixture proportions of geopolymer mortar (kg/m$^3$) ……..…....58

Table 4.3 Results of nine geopolymer mortar mixtures……..…….…...59

Table 4.4 Range analysis on workability……...……..…60

Table 4.5 Range analysis on early-age strength…….……..……...62

Table 4.6 Range analysis on strength at 28 days……..…..62

Table 4.7 Range analysis on long-term strength…….…….....63

Table 5.1 GPC mixing proportions……..…..…..69

Table 5.2 Workability test of fresh GPC……...……..70

Table 5.3 Density of hardened GPC……...…...….71

Table 5.4 Young's modulus test results……...…...72

Table 5.5 Compressive strength……...……...72

Table 5.6 Splitting tensile strength……...…….....73

Table 5.7 Flexural strength……...……...……...73

Table 5.8 Geopolymer paste mixing proportions…….…..……74

Table 5.9 Conversion test……...…...…….77

Table 6.1 Orthogonal experimental factors……...…..91

Table 6.2 Compressive strengths of GPMs at different temperatures……...…..95

Table 6.3 Concrete mixing proportions (kg/m$^3$). ……...…99

Table 6.4 Concrete mixing proportions (kg/m$^3$) ……..……..……104

Table 6.5 Density of different concrete……..…….105

Table 7.1 Proportions of concrete mixes (kg/m$^3$) ……..……..…...111

Table 7.2 Summary of CFST stub column specimens……..……..……112

Table 7.3 Compressive stiffness (kN) ……..……..……..……119

Table 7.4 Compressive stiffness (kN) ……..……..……131

# Abbreviations, Acronyms and Symbols

**AMCF:** Advanced Materials Characterization Facility

**ASTM:** American Society for Testing and Materials

**CAC:** calcium aluminate cement

**CFST:** Concrete-filled steel tubular

**C-S-H:** Calcium silicate hydrate

**DSC:** Differential scanning calorimeter

***DI*:** Ductility index

$E_c$**:** Young's modulus of concrete

$E_s$**:** Young's modulus of steel

**EA**: Compressive stiffness

**EDS:** Energy-dispersive X-ray spectroscopy

$f_B$**:** Confining stress for circular CFST

$f_c'$**:** Mean value of compressive strength

$f_u$**:** Ultimate strength of steel

$f_r$: Residual stress of confined concrete

**FE:** Finite element

**GPC:** Geopolymer concrete

$G_F$**:** Fracture energy

**GGBFS:** Ground granulated blast furnace slag

**GCFST:** Geopolymer concrete-filled steel tubular

**GPC:** Geopolymer concrete

**GPM:** Geopolymer mortar

**HGPC:** heat cured GPC

***K*c:** Compressive meridian

**LVDT:** Linear variable differential transducers

***M*s:** Modulus of silicate ratio

***N:*** Measured axial load

$N_{ue}$**:** Measured ultimate strengths

$N_{u,r}$**:** Residual ultimate strengths after elevated temperature

**N-A-S-H**: Sodium alumina silicate hydrate

**OPC:** Ordinary Portland cement

***RSI*:** Residual strength index

***REA*:** Residual compressive stiffness

**SFRC:** Steel fibre reinforced concrete

**SEM:** Scanning electron microscopy

***SI*:** Strength index

**TGA:** Thermal gravimetric analysis

**XRF:** X-ray fluorescence spectroscopy

**XRD:** X-ray Diffraction Analysis

**ν:** The normalized axial load ratio

***Ψ*:** Dilation angle

***e*:** Flow potential eccentricity

$\varepsilon_{c0}$: Strain at peak stress under uniaxial compression

$\varepsilon_y$: Yield strain of steel

# Chapter 1 Introduction

## 1.1 General

In recent years, fire disasters have frequently been reported worldwide, and have seriously threatened personal and public property safety. High temperatures lead to serious damage to concrete structures, resulting in significant mechanical decay of concrete and even fatal effects at the structural level, due to the spalling phenomenon of concrete (Connolly, 1995). Geopolymer is a relatively new construction material and has fire-resistant properties that are much better than those of Portland cement concrete (Fernández-Jiménez et al., 2008a). Composite structures have been widely used in civil engineering, such as high-rise buildings shown in Figure 1.1.

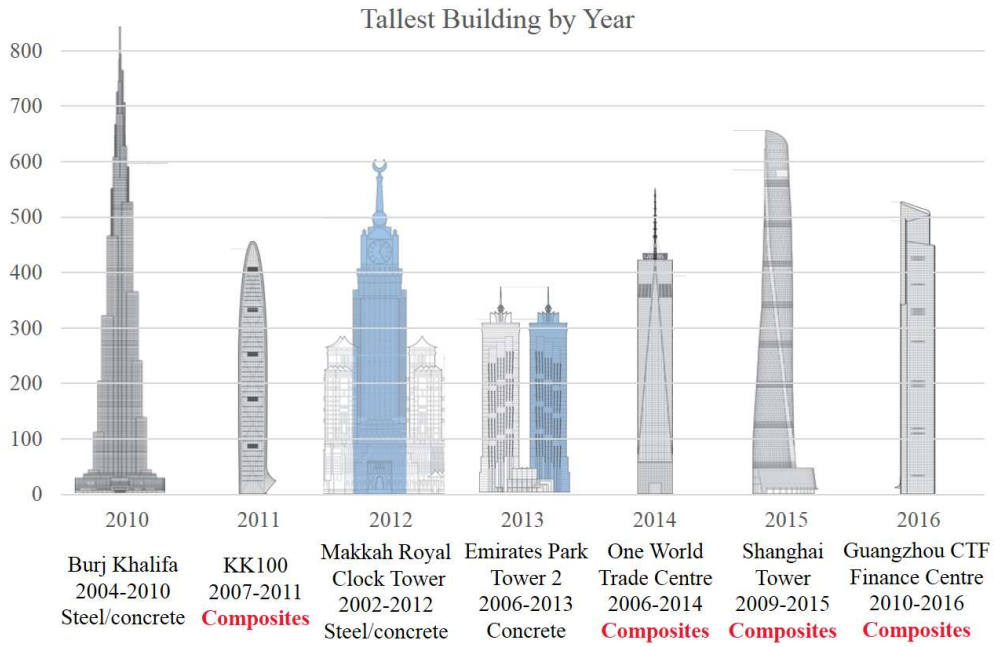


Figure 1.1 World's tallest buildings by year (Gable, 2016)

The tallest buildings completed in 2011, 2014, 2015 and 2016 used a composite structure, which utilises a combination of both steel and concrete acting compositely in the main structural elements. Concrete-filled steel tubular (CFST) columns have

been extensively used for years (Han et al., 2014). Although the fire performance of CFST columns is better than that of hollow tubular columns (Yin et al., 2006), some extra procedures need to be implemented to protect CFST from a fire. In order to improve the fire performance of CFST members, this research aims to use geopolymer concrete for manufacturing of fire-resistant concrete-filled steel tubes.

Concrete is one of the most commonly used materials on the earth, and it is conventionally produced by using ordinary Portland cement (OPC) as a binder which is a calcium silicate hydrate (C-S-H) gel. In contrast, the chemical composition of geopolymers is similar to zeolites, but shows an amorphous microstructure. The mechanism of geopolymerisation may consist of dissolution, transportation, and polycondensation, and takes place through an exothermic process (Provis and van Deventer, 2014). The main chemical process in geopolymers is polymerisation, unlike concretes made with Portland cement and blended cement, where the main product of hydration is C-S-H gel, which is the major provider of concrete strength. Strength of OPC concrete decreases when subjected to fire conditions, and this is mainly caused by the $Ca(OH)_2$ ingredient which decomposes under elevated temperatures (Arioz, 2007). However, $Ca(OH)_2$ is not a main ingredient of geopolymer. Pan and Sanjayan (2012) reported that geopolymer samples retained a higher strength at elevated temperatures, in contrast to OPC concrete

CFST combines the advantages of concrete and steel, and has further benefits, namely its high load bearing capacity, stiffness and ductility, convenience for fabrication and construction, large energy dissipation, and it is also considerably cost-effective. When CFST columns are exposed to fire, concrete can absorb the heat from the steel tube, whereas the steel tube can prevent the concrete from spalling. However,

suitable measures are often still required in practice to ensure its fire resistance, which leads to increased costs and difficulties in construction. By using geopolymer concrete, it is possible to significantly increase the fire resistance of CFST columns. This chapter will provide the knowledge background, aims of this project and layout of the report.

## 1.2 Background

### 1.2.1 Fire hazards in structures

Fire hazards are a major concern in structural engineering. Most of structures need to consider the measurements of most structures to reduce the destruction caused by fire. The weak spots and strengths of structural members should be checked in the design to ensure the highest possible level of safety. If it is necessary, fire insulation materials need to be used to protect structural members by slowing down heat transfer. In addition, fire sprinkler systems, fire extinguishers, fire alarms and smoking detectors can be used for suppression of fire.

As shown in Figure 1.2, an immense fire erupted on a 63-story luxury hotel in Dubai, caused by fireworks on New Year's Day of 2016. Luckily, the fire did not spread inside the building, and the building maintained its good integrity after the fire was extinguished. Fire in high-rise buildings presents a significant threat to residents' properties and safety. On one hand, the fire spread very rapidly across the Dubai high-rise because of the wind; a witness described that the entire side of the building was engulfed in flames within seven minutes. In addition, the sheer height limited the use of normal water hoses, and fire fighters had to enter the building to find the outbreak and extinguish the fire; these minutes allowed the fire to spread further before the fire crews could find the location of the outbreak.

Figure 1.2 Fire engulfs a 63-story Hotel in Dubai (AHMED JADALLAH, Reuters)

Generally, the fire behaviour of structural members depends on the applied loads and the duration of the fire, so fire resistance varies in different structural forms. In the event of a fire, the strength of the materials in structural members is gradually reduced as temperatures increase, while the speed of heat transfer depends on the thermal conductivity and heat absorption capacity of the materials. However, fire protection materials can help to slow the speed of heat transfer. During the fire exposure of a CFST member, the temperature of the steel tube rises faster than that of the concrete, due to its direct exposure to fire and higher thermal conductivity, and then the loads are distributed to the concrete. If the concrete cannot support an increased load, the composite column will collapse. These findings demonstrate that concrete plays an important role in CFST columns under fire conditions.

### 1.2.2 Fly ash-based geopolymer

OPC concrete is very sensitive to fire hazards for chemical and physical reasons. To improve the fire performance of concrete, fly ash-based geopolymer can be used as the binder to produce concrete, instead of Portland or any other hydraulic cement paste. To form the geopolymer concrete (GPC), fly ash-based geopolymer paste concretes the fine aggregates, coarse aggregates and other un-reacted materials together, with or without the addition of admixtures. The manufacturing of GPC can be carried out applying standard concrete technology methods.

Similar to OPC concrete, the aggregates in geopolymer concrete occupy the largest volume, normally about 75-80% mass. The silicon and aluminium in low calcium (ASTM Class F) fly ash are not only activated by a combination of sodium hydroxide and sodium silicate solutions to form the geopolymer paste that binds all the aggregates. In addition, calcium aluminate cement (CAC) is well known for high temperature resistance; it is also found to have rapid hardening properties which are favourable for many practical applications as an additive in geopolymer. Throughout this research project, CAC is used as a small ingredient of the binder in geopolymer to achieve desirable mechanical properties, as well as fire resistance.

### 1.2.3 Concrete filled steel tubular columns

CFST does combine the advantages of concrete and steel. The strength of filled concrete can be enhanced by the confinement effect provided by the steel tube, while the local buckling of the steel tube can be delayed or even prevented by the concrete core. Moreover, the steel tube can serve as a permanent formwork for concrete casting and thus the construction period can be shortened and the cost can be reduced.

The cross-sections for the CFST are various and circular; square and rectangular sections are commonly adopted in engineering design. Basically, only plain concrete was used to fill the steel tube. Sometimes in order to improve the strength and ductility of concrete, glass or steel fibres will be added to the concrete. In addition, steel bars or I-section steel can be encased in the concrete core to improve the resistance as well as reduce the section sizes. In general, CFST columns are better than conventional steel and columns in terms of fire resistance, due to the fact that the concrete can absorb the heat from the steel tube while the steel tube can prevent the concrete from spalling.

## 1.3 Research motivation

Due to the fast development of population and growth of economies in many cities, high-rise buildings have long been a necessity. According to a report completed by Gable (2016), the composite structure system has become popular in multi-storey and high-rise buildings over the last few decades. CFST columns have been widely applied in high-rise buildings with great success. Fire hazards are a major threat to life and property in buildings, and can lead to building collapse. Unfortunately, large resident density in high-rise buildings increases the probability of the occurrence and severity of fire hazards. Engineers regularly adopt suitable measures to maintain structural integrity under fire conditions. Conventional CFST columns usually cannot satisfy fire resistance requirements. In practice, a large amount of internal steel reinforcement is put in the steel tube to retain the strength of CFST columns during a fire outbreak. However, the use of reinforcement substantially increases the construction cost and time, while reducing the constructability. This thesis aims to develop fire-resistant CFST without internal steel reinforcement.

To improve the fire endurance of CFST columns, this research proposes to replace OPC with GPC. The manufacture of OPC is responsible for 5% global carbon dioxide emission while consuming a lot energy. As an alternative, GPC uses geological origin (e.g. metakaolin) or industrial by-products (e.g. fly ash) as raw material. In Australia each year, 12 million tonnes of coal combustion ash is produced, of which only 40% is effectively utilised in construction application. The application of GPC is not only able to reduce the $CO_2$ emission but also save the land fill from industry by-products.

The majority of unused ash is low calcium fly ash. Conventional GPC synthesised by low calcium fly ash was cured at elevated temperatures to obtain adequate strength. Many attempts were made to eliminate the elevated temperature curing procedure, which impedes the onsite application of GPC in buildings. Most recently, researchers have investigated some additives, including OPC (Nath and Sarker, 2015) and ground granulated blast furnace slag (GGBFS) (Nath and Sarker, 2014), to make geopolymer cured at an ambient temperature. Very little information is available about the use of CAC as an additive and its influence on properties of geopolymer, although it has been widely used in making refractory concrete. Moreover, the fire performance of geopolymer has been conducted on GPC (Rivera et al., 2016), and it exhibited better fire performance. However, less research can be found on the study of using CAC, which is a fire-resistant cement, to improve the fire performance of geopolymer.

It was reported that GPC exhibited different mechanical properties from OPC (Hardjito, 2005). Compared to the extensive knowledge of geopolymer materials, much less research has been done on the behaviour of GPC structural members.

Extensive research was conducted on CFST, but little research has been done on geopolymer concrete-filled steel tubular (GCFST) columns. Espinos et al. (2015) reported an improvement in the fire performance of GPC filled double-skin steel tube. No fire tests have been reported on the fire performance of GCFST. Without the knowledge of GCFST, it will not be possible to generalise the application of using geopolymer in construction. In this thesis, the fire resistance of GPC and behaviour of GCFST under ambient and elevated temperatures will be fully explored, modelled and predicted.

## 1.4 Research objectives, limitation and scope of work

### 1.4.1 Research objectives

As previously discussed, there is no widely accepted holistic approach for the mix design of geopolymer, and limited research work has been done on GCFST. The aims of this research is as follows:

- To identify and study the salient parameters that affect the properties of fly ash-based geopolymer.
- To develop a fire-resistant concrete using geopolymer and study its properties.
- To study the fire performance and mechanical properties of GCFST.
- To develop a finite element (FE) model for GCFST and verify it with test results.

### 1.4.2 Research limitation

Due to the limit of time and knowledge of the author, this research is focused on the static behaviour of geopolymer concrete. The FE prediction of GCFST was mainly limited to performance at an ambient temperature.

### 1.4.3 Research scope

The salient parameter analysis of geopolymer was conducted, and the performance of optimised GPC mix designs under elevated temperatures was studied. The properties of GPC studied included workability, hot strength and residual compressive strength, Young's modulus, tensile strength and indirect tensile strength.

Therefore, the GPC was fully comprehended and used to manufacture fire-resistant GCFST. The GCFST was tested at ambient temperature, then a proposed FE model was verified by the test results. The residual strength of GCFST was also tested after elevated temperature exposure. Finally, the deformation of GCFST at combined load and elevated temperature was analysed.

## 1.5 Layout of thesis

This thesis investigates the performance of fire-resistant geopolymer concrete and its application in CFST columns. Eight chapters are included:

**Chapter 1:** Introduces the general background of building fire hazards, geopolymer and CFST columns. The research motivation is introduced, along with the objectives, limitations and scope.

**Chapter 2:** Reviews the existing knowledge of alkali-activated materials with an emphasis on low calcium fly ash based geopolymers. The current research is covered

of GPC at ambient and elevated temperatures. Subsequently, a review of research of CFST is presented to appreciate the potential of using GPC to improve the performance of CFST.

**Chapter 3:** Describes the experimental program throughout this research.

**Chapter 4:** Details the methodological approach towards optimised mix design of ambient cured GPC. The salient factors that influence the workability and compressive strength of geopolymer paste and mortar are identified, respectively. The mix design optimised process is illustrated with the help of the Taguchi method.

**Chapter 5**: Presents the mechanical properties of GPC at ambient temperature, including density, Young's modulus, compressive strength, splitting tensile strength and flexural strength. The microstructure characterisation of geopolymer was conducted. The measured mechanical properties were compared with standard prediction.

**Chapter 6:** Presents the performance of GPC at elevated temperatures. Firstly, studies are presented of the residual strength of GPC after being exposed to elevated temperatures, followed by studies of the deformation of GPC under combined load and elevated temperatures. The performance of GPC at elevated temperatures is compared to that of OPC.

**Chapter 7:** Investigates the experimental study on the mechanical properties of GCFST at ambient temperatures. The comparisons of test results with standard prediction, simplified model prediction and FE prediction are presented.

The test results of GCFST at elevated temperatures are also reported. Firstly, the residual strength of GCFST is tested after exposure to elevated temperatures. Secondly, the deformation of GCFST was studied under constant load and elevated temperatures.

**Chapter 8:** Draws conclusions and proposes recommendations for future research.

# Chapter 2 Literature Review

## 2.1 General

Chapter 1 introduced an overview of the question and motivation for the research. The main scope of this thesis is to evaluate the potential of using GPC as a fire resistant material and its application in CFST columns. This chapter summarises the development of geopolymers and CFST columns. A literature review is presented on the applications of geopolymers and CAC in concretes, along with the past research on the properties of concretes, focusing on, but not limited to, mechanical properties and fire performance. Furthermore, the mechanical properties of CFST columns at ambient and elevated temperatures are presented.

## 2.2 Geopolymer concrete (GPC)

### 2.2.1 Current development

After lime and OPC, geopolymer has been commonly considered as the third generation cement (Li et al., 2010). The potential of geopolymer binders to extensively use in industrial construction is supported by the fact that there are abundant industrial wastes generated in various industries that are found to be suitable to use as geopolymer raw materials. Geopolymers are commonly referred to “alkali-activated materials” which are produced from a series of reactions between alkaline activator and an aluminosilicate rich source. A repeating unit of silicate monomer (Si-O-Al-O) is created in this reaction, and following this the monomers are converted into silicate polymers. The amorphous sodium alumina silicate hydrate (N-A-S-H) gel is produced from a reaction of alkali and alumina-silicate (Davidovits, 1991). The main criteria for developing suitable geopolymer is that the source material should be highly

amorphous and have a low water demand, sufficient reactive glassy content and be able to release aluminium easily. Despite this variety of nomenclature in the reaction, the term geopolymerisation describes all materials synthesised utilising the same chemistry (Duxson et al., 2007). Although a variety of aluminosilicate materials, such as kaolinite, fly ash, GGBFS, have been used as solid raw materials in the geopolymerisation technology, this research mainly focuses on fly ash-based geopolymer due to the abundance of fly ash in Australia.

### 2.2.2 Effect of alkali solution

Alkali activator plays an important role in the initiation of the geopolymerisation reaction. The concentration of alkali activator has an effect on the compressive strength of geopolymer because a strong alkaline solution is useful to help the dissolution of aluminosilicate in raw materials.

The alkaline activators—such as sodium hydroxide (NaOH), potassium hydroxide (KOH), sodium silicate ($Na_2SiO_3$) and potassium silicate ($K_2SiO_3$)—can be used to activate aluminosilicate materials. Compared to NaOH, KOH shows a higher level of alkalinity. However, in practice, it has been found that sodium hydroxide possesses a better capacity to liberate silicate and aluminate monomers than potassium hydroxide (Duxson et al., 2007). Shaikh and Hosan (2016) studied the performance of steel reinforced geopolymers using Na and K based activators. Steel fibre reinforced geopolymer concrete (Na) was slightly stronger than steel fibre reinforced concrete (SFRC) in terms of residual indirect tensile strength and residual compressive strength. However, K activated geopolymer lost strength quickly under high temperatures. In

this research, sodium hydroxide was used in alkali solution to obtain better fire performance.

Nematollahi and Sanjayan (2014) studied the effect of two different activators and superplasticisers on the workability of fly ash based geopolymer pastes, i.e 8 M sodium hydroxide and multi-compound activator composed of 8 M NaOH solution and sodium silicate solution with a $SiO_2/Na_2O$ ratio of 2.0. The experimental results indicated that using 8 M NaOH solution as the activator, naphthalene based superplasticiser was an effective type; whereas modified Polycarboxylate based superplasticiser was the most efficient type when the multi-compound activator was used. Fernández-Jiménez and Palomo (2005) studied the mechanical strength of alkali-activated fly ash, with several activators in which the $Na_2O$ content changed from 5% to 15%. They concluded that the $SiO_2/Na_2O$ molar ratio affects mechanical strength. They noticed that using a $Na_2O$ content of 5.5% by fly ash mass leads to a very low pH, affecting the reaction development in a negative way and also that the $Na_2O$ content increase leads a mechanical strength increase. The use of 14% of $Na_2O$ by fly ash mass leads to optimum mechanical performance. Duxson et al. (2007) studied the alkali-activation of metakaolin geopolymers with a mixture of sodium or potassium hydroxide with sodium waterglass or potassium waterglass. Those authors reported that using a combination of sodium hydroxide and sodium waterglass leads to higher mechanical strength, as compared to specimens activated by a combination of potassium hydroxide and potassium waterglass.

Görhan and Kürklü (2014) investigated the effect of NaOH solution on the 7-day compressive strength of low calcium fly ash geopolymers cured at 65 and 85 °C. The concentrations of NaOH solution were designed at 3, 6 and 9 M, and the sodium

silicate/sodium hydroxide ratio was constantly kept at 2.5. An optimised solution was acquired from the test result, and this 6 M concentration mix design obtained 22 MPa at 7 days.

Somna et al. (2011) reported the test results of ground fly ash geopolymer with NaOH concentration ranged from 4.5 to 16.5 M. The strength increased substantially with the increased concentration of geopolymer with a solution concentration under 9.5 M. The strength of geopolymer paste increased more slowly when the concentration was over 9.5 M. A decrease of compressive strength was observed after the concentration achieved 16.5 M. The excessive hydroxide ions caused the precipitation of N-A-S-H gel at early ages, which resulted in a decrease in compressive strength.

Xu and Van Deventer (2000) confirmed that the use of sodium silicate increases dissolution of raw materials. They studied the alkali-activator with different natural alumina-silicate minerals. The results have shown most natural minerals could not provide enough free Si to initiate the reaction. Fernández-Jiménez and Palomo (2005) studied the geopolymerisation of fly ash, with several activators in which the $Na_2O$ content ranged from 5% to 15%. They concluded that the $SiO_2/Na_2O$ molar ratio and water/binder ratio influenced the mechanical properties. Furthermore, they reported that using a $Na_2O$ content of 5.5% by mass of fly ash led to a very low pH, affecting the reaction development in a negative way, and the $Na_2O$ content increase led to a mechanical strength increase. The use of 14% $Na_2O$ by fly ash mass had optimum mechanical performance.

### 2.2.3 Effect of curing procedures

Attempts have been made to evaluate the effect of different curing regimes on the properties of geopolymer at elevated temperatures. Palomo et al. (1999) studied different curing conditions of alkali activated fly ash-based geopolymer at 65 °C and 85 °C. They proposed the compressive strength of samples ranging from 8–12 M and cured at 85 °C for 24 h was higher than samples cured at 65 °C. The rise of strength was very small when the curing time was longer than 24 h.

Heah et al. (2011) supposed that the curing of Metakaolin-based geopolymers at an ambient temperature was not viable, while an increase in temperature (40 °C, 60 °C, 80 °C and 100 °C) favoured the strength development after 1–3 days. Rovnaník (2010) concluded the curing regime of geopolymer at an elevated temperature (40–80 °C) accelerated the strength development, but the mechanical properties decreased in comparison with results obtained at an ambient temperature within 28 days. In general, adequate curing of geopolymeric materials is required to achieve optimal mechanical and durability performance in order to maintain their structural integrity.

Collins and Sanjayan (1999) noticed a strength decrease following long curing times with high temperature. They suggested that some water may remain in the hardened binder, maintaining the 'gelular' character of geopolymers. Bakharev (2005) also claim the need for isolating the hardened specimens in order to prevent water evaporation, and some of them kept the concrete specimens cured in sealed bags.

However, the heat curing procedure extensively impedes the application of geopolymer in on-site construction. Some researchers have studied different additives

to eliminate the necessity of the heat curing procedure. In this thesis, the main purpose is to study the geopolymer cured at room temperature.

### 2.2.4 Effect of additives

The relative ratio of essential elements (Si, Al, Na and Ca) in raw material plays an important role in the gepolymerisation reaction. Some cements or wastes were added into the raw material to obtain the ideal balance of elements. The additives included calcium hydroxide, aluminium hydroxide, silica fume, nano-$SiO_2$, and nano-$Al_2O_3$ etc. (Mijarsh et al., 2014). Some researchers utilised the "waste to waste" stabilisation technique by incorporating waste materials such as flue gas desulfurisation gypsum (Chindaprasirt et al., 2012) and Al-rich waste sludge (Boonserm et al., 2012) to achieve a more efficient geopolymerisation.

Reuse and recycling of industrial wastes are the ideal solutions for current waste management problems. Chindaprasirt et al. (2012) found a way to utilise Al-rich waste, originated from waste water of a plant, as an additive to make high calcium fly ash based geopolymer mortar. This alumina-rich waste material was dried and grounded into powder at a high temperature. Test results showed the increased strength of geopolymer by adding 2.5 wt.% of Al-rich waste calcined at 1000 °C. However, a further increase in the dosage resulted in a reduced compressive strength because of the excess alumina which acts as non-functional filler in geopolymer matrix. Hanjitsuwan et al. (2017) used calcium carbide residue as an additive to promote the mechanical properties of geopolymer cured at an ambient temperature; the addition ratios were 10%, 20% and 30% by weight of binder. The activator was a mixture of

sodium hydroxide and sodium silicate. The addition of calcium promoter enhances the mechanical properties and also decreases setting time.

Khan et al. (2016c) studied the potential of making geopolymer with a small amount of slag, hydrated lime and ultra-fine fly ash, and found the compressive strength of geopolymer is mainly dependent on the raw material. They observed that geopolymer partially replaced by slag is able to achieve 100 MPa in 28 days. However, the effect of adding a small part of hydrated lime and ultra-fine fly ash is relatively diminutive for geopolymer. Puligilla and Mondal (2013) conducted research on the role of slag in the formation of slag-fly ash geopolymer. The calcium dissolved from slag is the main character on the influence of early strength development of geopolymer; this is due to the fact that free calcium ions prolong fly ash dissolution and enhance geopolymer gel formation. Puligilla and Mondal proposed the hardening process is initiated by the precipitation of C-A-S-H.

The conventional OPC was also investigated to improve the performance of geopolymer by previous researchers. Nath and Sarker (2015) studied the influence of OPC on the mechanical properties of geopolymer. The inclusion of OPC successfully eliminates the requirement of a heat-curing procedure. The results indicated that the inclusion of OPC as a small portion of binder can accelerate the setting time while causing a small decrease in workability. Shehab et al. (2016) investigated the OPC-fly ash geopolymer on the compressive strength, splitting tensile strength, flexural strength and bond strength. The replacement ratios of OPC are 0%, 25%, 75% and 100%, respectively. The strength development rate of geopolymer is different from that of OPC concrete. However, the relationship between compressive strength and flexural, splitting and bond strength of geopolymer have few differences with OPC.

Khan et al. (2016a) investigated geopolymer consisting of 90% low calcium fly ash and 10% GGBFS, and the geopolymer concrete samples were cured in an oven at 75 ℃ for 18 hours after casting. Two geopolymer concrete designs contained 13.3 kg/m$^3$ free water, and both geopolymer concretes achieved more than 200 mm in a slump test. Steel furnace slag aggregate concretes achieved a higher modulus of elasticity, and geopolymer blended with SFS had a slight improvement in 28-day compressive strength.

## 2.3 Properties of GPC at an ambient temperature

### 2.3.1 Workability

Workability indicates the ease which concrete can be transported and consolidated. GPC made with low water content can be very sticky and would not meet the workability requirement.

Previously, a number of superplasticisers were used to improve the flowability in OPC. Nematollahi and Sanjayan (2014) analysed influences of different superplasticisers and activator combinations on the workability and compressive strength of GPC. They tested naphthalene, melamine and modified Polycarboxylate as superplasticiser on geopolymer pastes with two kinds of activator combinations. The result show modified Polycarboxylate based SP was most effective for most activator combinations. Naphthalene based SP is better for sodium hydroxide activator. However, the compressive strength reduced with the addition of SP.

Sathonsaowaphak et al. (2009) reported the sodium silicate/sodium hydroxide ratio and sodium hydroxide concentration were main factors on workability. The increase of these two factors resulted in less water content in geopolymer. The

influence of adding extra water on the workability was also studied. This practice was also used by other researchers (Rickard et al., 2016, Hardjito and Rangan, 2005), and it was proven to be effective. In this thesis, extra water was added into mix to improve the workability of GPC.

### 2.3.2 Compressive stress-strain models

The stress-strain models were studied. Table 2.1 lists typical stress-strain models for unconfined OPC concrete.

Table 2.1. Stress-strain models for unconfined concrete under uniaxial compression

| Source | Stress-strain model |
|---|---|
| Sargin et al. (1971) | $f = k_3 f_c' \frac{AX + (D-1)X^2}{1 + (A-2)X + DX^2}$<br>where: $X = \varepsilon/\varepsilon_0$; $A = \frac{E_{it}\varepsilon_0}{f_c'}$; $D = 0.65 - 7.25 f_c' \times 10^{-3}$;<br>$E_{it} = 5975(f_c')^{1/2}$; $\varepsilon_0 = 0.0024$; $k_3 = 1.0$ |
| Popovics (1973) | $f = \frac{f_c'\beta(\varepsilon/\varepsilon_0)}{\beta - 1 + (\varepsilon/\varepsilon_0)^{\beta}}$<br>where: $\beta = 1.0 + 0.058 f_c'$; $\varepsilon_0 = 735(f_c')^{0.25} \times 10^{-6}$ |
| Carreira and Chu (1985) | $f = \frac{f_c'\beta(\varepsilon/\varepsilon_0)}{\beta - 1 + (\varepsilon/\varepsilon_0)^{\beta}}$<br>where: $\beta = \frac{1}{1 - f_c'/(\varepsilon_c' E_{it})}$; $\varepsilon_c' = (4.88 f_c' + 168) \times 10^{-5}$<br>$E_{it} = 0.0736 \rho^{1.51} (f_c')^{0.3}$ |
| Collins et al. (1993) | $f = f_c' \frac{\varepsilon_c}{\varepsilon_0} \frac{\beta}{\beta - 1 + (\varepsilon/\varepsilon_0)^{\beta k}}$<br>where: $\beta = 0.8 + f_c'/17$;<br>$E_c = \begin{cases} 1.0, & when\ 0 \le \varepsilon \le \varepsilon_0; \\ 0.67 + f_c'/62, & when\ \varepsilon > \varepsilon_0; \end{cases}$ |

Table 2.1. Stress-strain models for unconfined concrete under uniaxial compression (continued)

| Source | Stress-strain model |
|---|---|
| Wee et al. (1996) | $f = \frac{f_c'\beta(\varepsilon/\varepsilon_0)}{\beta - 1 + (\varepsilon/\varepsilon_0)^{\beta}}$ when $0 \le \varepsilon \le \varepsilon_0$;<br>$f = \frac{k_1 f_c'\beta(\varepsilon/\varepsilon_0)}{k_1\beta - 1 + (\varepsilon/\varepsilon_0)^{k_2\beta}}$ when $\varepsilon > \varepsilon_0$;<br>where: $\beta = \frac{1}{1 - f_c'/(\varepsilon_0 E_{it})}$; $\varepsilon_0 = 780(f_c')^{0.25} \times 10^{-6}$;<br>$E_{it} = 10200(f_c')^{1/3}$; $k_1 = (50/f_c')^3$; $k_2 = (50/f_c')^{1.3}$ |
| Samani and Attard (2012) | $\frac{f}{f_c'} = \frac{AX + BX^2}{1 + (A-2)X + (B+1)X^2}$ when $0 \le \varepsilon \le \varepsilon_0$;<br>$\frac{f}{f_c'} = (\frac{f_{ic}}{f_c'})^{(\frac{\varepsilon - \varepsilon_0}{\varepsilon_{ic} - \varepsilon_0})^2}$ when $\varepsilon > \varepsilon_0$;<br>where: $X = \varepsilon/\varepsilon_0$; $A = \frac{E_c\varepsilon_0}{f_c'}$; $B = \frac{(A-1)^2}{0.55} - 1$;<br>$E_c = \begin{cases} 0.043\rho^{1.5}\sqrt{f_c'}, & for\ crushed\ aggregates \\ (3320\sqrt{f_c'} + 6900)\left(\frac{\rho}{2320}\right)^{1.5}, & for\ weaker\ aggregates \end{cases}$<br>$\varepsilon_0 = \begin{cases} \frac{f_c'}{E_c}\frac{4.26}{\sqrt[4]{f_c'}}, & for\ crushed\ aggregates \\ \frac{f_c'}{E_c}\frac{3.78}{\sqrt[4]{f_c'}}, & for\ gravel\ aggregates \end{cases}$<br>$\frac{\varepsilon_{ic}}{\varepsilon_0} = 2.76 - 0.35\ln(f_c')$; $\frac{f_{ic}}{f_c'} = 1.41 - 0.17\ln(f_c')$; $f_c' \ge 20$MPa |
| Lim and Ozbakkaloglu (2014) | $f = \frac{f_c'(\varepsilon/\varepsilon_0)r}{r - 1 + (\varepsilon/\varepsilon_0)^r}$ when $0 \le \varepsilon \le \varepsilon_0$;<br>$f = f_c' - \frac{f_c'}{1 + (\frac{\varepsilon - \varepsilon_0}{\varepsilon_{ci} - \varepsilon_0})^{-2}}$ when $\varepsilon > \varepsilon_0$;<br>where: $r = \frac{E_c}{E_c - f_c'/\varepsilon_0}$; $E_c = 4400\sqrt{f_c'}(\frac{\rho}{2400})^{1.4}$; $\varepsilon_0 = \frac{(f_c')^{0.225}k_d}{1000}k_s k_a$;<br>$k_d = (\frac{2400}{\rho})^{0.45}$; $k_s = (\frac{152}{D})^{0.41}$; $k_a = (\frac{2D}{H})^{0.13}$;<br>$\varepsilon_{ci} = 10\varepsilon_0(f_c')^{-0.47}(\frac{\rho}{2400})^{0.4}$;<br>$D$ and $H$ are the diameter and height of specimen in mm, while $D$ ranged from 50 to 400 mm and $H$ ranged from 100 to 850 mm. |
| Noushini et al. (2016) | $f = \frac{f_c'\beta(\varepsilon/\varepsilon_0)}{\beta - 1 + (\varepsilon/\varepsilon_0)^{\beta}}$<br>$\beta = \begin{cases} [1.02 - 1.17(\frac{f_c'}{\varepsilon_0 E_c})]^{-0.45}, & when\ 0 \le \varepsilon \le \varepsilon_0; \\ [1.02 - 1.17(\frac{f_c'}{\varepsilon_0 E_c})]^{-0.45} + \varpi + 28\xi, & when\ \varepsilon > \varepsilon_0; \end{cases}$<br>$\varpi = C(12.4 - 0.015f_c')^{-0.5}$;<br>$\xi = 0.83 \times e^{-911/f_c'}$;<br>$C = \begin{cases} 15;\ \text{water and internal cruings} \\ 7;\ \text{heat curing} - \text{OPC concrete} \\ 17;\ \text{heat curing} - \text{GPC} \end{cases}$ |

In structural application, an accurate stress-strain curve of concrete is necessary for evaluating the degree of safety and serviceability. Generally, the stress-strain

relationship of concrete can be expressed as a parabolic curve with its vertex at peak stress (Yang et al., 2014). Two major categories of methods were applied to describe the parabolic expression of the stress-strain curve of unconfined concrete. Sargin et al. (1971) proposed a stress-strain relationship expression of unconfined concrete with a quadratic fractional model. Further improvements in the accuracy of ascending and descending phases were achieved by revising some parameters. Attard and Setunge (1996) improved the quadratic fractional function by alternating two sets of parameters, and the model was widely adopted. The model was further improved on the post-peak softening part (Samani and Attard, 2012).

Another widely-accepted method, as proposed by Popvics, used a key parameter $\beta$ in an exponential function to describe the stress-strain curve (Popovics, 1973); such a model was proposed by Carreira and Chu (1985) by considering the influence of Young's modulus to avoid underestimating $\beta$ parameter. In addition, a modified $\beta$ parameter was proposed by Wee et al. (1996) to achieve a better accuracy on the descending branch of high strength concrete. The general trend for the descending branch was the rate of stress drop increases as $f_c'$ increases. Recently, Lim and Ozbakkaloglu (2014) proposed a similar model by updating the strain at peak stress based on a wide range of collected data on unconfined concrete.

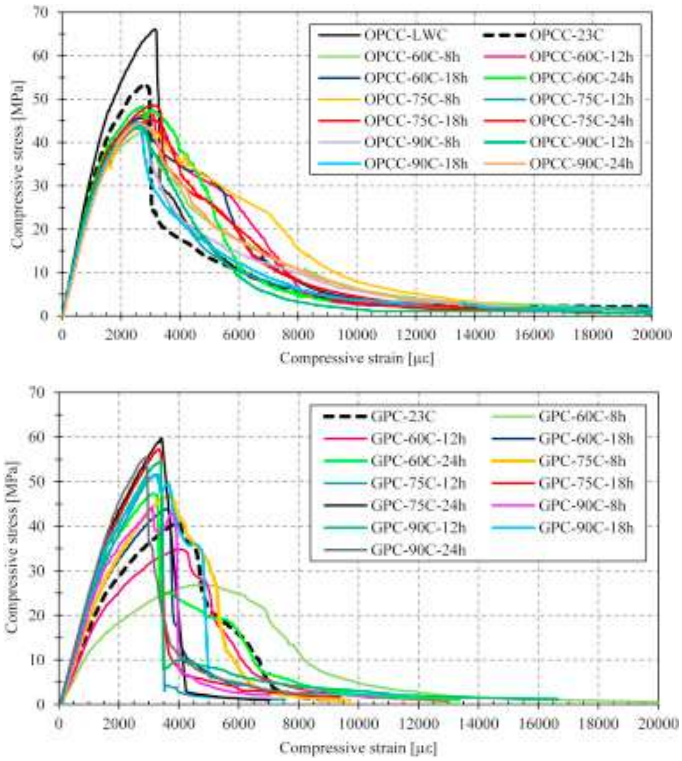


Figure 2.1. Stress-strain curves for OPC and GPC (Noushini et al., 2016)

In contrast to OPC concrete, the research on stress-strain curve of GPC is relatively limited. Previous research was conducted by Hardjito (2005) on heat-cured (60 – 90 °C) GPC. The stress-strain curves of GPC in strength range of 41 - 64 MPa were compared with the constitutive model proposed by Collins et al. (1993) for OPC concrete. The model exhibits good accuracy for predicting the stress-strain relationship of GPC. Noushini et al. (2016) investigated the stress-strain model of geopolymer concrete cured at elevated temperatures, using heat-cured OPC as the control group. Twelve different heat curing conditions were used to study the samples with four curing periods of 8, 12, 18, and 24 hours, and three temperatures of 60, 75 and 90 °C. For geopolymer samples, increasing the curing temperature from 75 °C to 90 °C and the curing duration of up to 18-24 hours results in achieving a higher modulus of

elasticity (increasing the initial slope of curve). As shown in Figure 2.1, OPC and GPC exhibited different strains at peak stress, and the stiffness of GPC was lower than that of conventional OPC concrete. In order to predict the performance of geopolymer concrete, a new stress-strain model was proposed by this literature (Noushini et al., 2016) which considers the parameters of the curing regime.

## 2.4 Properties of GPC at elevated temperatures

### 2.4.1 Hot strength

Geopolymers (Davidovits, 1993) have been reported to possess excellent mechanical properties, fire resistance, and environmental resistant properties. They are produced by synthesising aluminosilicate source materials with alkaline silicate solutions. Due to the ceramic-like properties, geopolymers are believed to possess good fire resistance. By comparison, Sanjayan and Stocks (1993) illustrated chemical and physical properties of OPC concrete degenerating at elevated temperatures. Furthermore, concrete spalling of OPC was commonly reported to occur in fire which causes a rapid layer-by-layer loss of concrete cover, potentially leading to the exposure of the main reinforcements within the concrete to fire.

Research on geopolymer as a fire-resistant binder has been extensive. However, published research on fly ash-based geopolymer is commonly limited to responses at elevated temperatures. Cheng and Chiu (2003) reported that the strength of GGBFS geopolymer binders was enhanced in fire. To further investigate the performance of GPC at elevated temperatures, Pan and Sanjayan (2012) studied the hot strength of geopolymer, and they illustrated all the geopolymer samples tested at high temperature had a lot improvement in the compressive strength. They hypothesised that the

geopolymer with low initial strength has more unreacted materials. At high temperatures, these unreacted materials will be transformed into reaction products by geopolymer reactions. The higher content of unreacted materials the higher strength increase, which is due to the high extent of geopolymer reactions.

Rickard et al. (2016) investigated the in-situ thermo-mechanical properties of geopolymer concretes. A microstructure analysis was employed to explain the mechanism of strength development under fire. The evaporation of capillary water is responsible for the strength loss at temperatures below 300 °C. After higher temperature exposure (higher than 500 °C), GPC exhibited sintering phenomena which led to the strength advantage over OPC concrete. However, geopolymer suffered more strength loss than OPC at 550 °C which was attributed to lower transient thermal creep. The fire performance was also examined on different cellular structures. Rickard and Van Riessen (2014) studied the fire performance of different cellular structures on GPC panels. The fire testing was conducted on 50 mm thick panels with an exposure area of 200 mm × 200 mm. The fire testing lasted for 120 min which complied with the maximum temperature increase limit by Australia Standard 1530.4. The surface cracking condition was inspected and the results showed solid geopolymers exhibited better fire endurance than cellular structure geopolymer.

A parameter analysis on fire performance was conducted by Shaikh and Vimonsatit (2015). The effects of NaOH concentration, aggregate sizes, curing condition and extra water of geopolymer at 200, 400, 600 and 800°C were investigated. Low molarities of NaOH lead to increase in the compressive strength after 800 °C. The addition of extra water adversely affects the compressive strength of geopolymer concrete at all elevated temperatures. However, the extended steam curing regime

improves performance at elevated temperatures. Eurocode EN1994:2005 was used to predict the compressive strength at elevated temperatures, and the predicting equation gives a great agreement with the test results up to 400 °C.

### 2.4.2 Residual strength

Given that geopolymer increases in strength after elevated temperature exposure, the fire resistance of geopolymer is likely to be superior to OPC concrete which loses most of its strength after elevated temperature exposure at about 800°C (Crozier and Sanjayan, 1999). Guerrieri and Sanjayan (2010) studied the fire performance of fly ash-based geopolymer blended with slag. The compressive strength of geopolymer paste tested at ambient temperature ranged from 3 to 83 MPa, and the specimens were tested after exposure to 800 °C for fire performance. They found higher initial strength results in a higher residual strength. Some low initial strength specimens exhibited higher strength after exposure to 800°C. They also found the ductility of specimen decreased as the initial strength increased as observed from the compressive stress versus strain curves.

Rivera et al. (2016) analysed the differences in the elevated temperature performance of geopolymer and OPC concrete. The samples were heated to 650 °C from ambient temperature in 60 seconds, and the temperature was held for 10 minutes without loading. They found fly ash-based geopolymer showed no damage after fire exposure compared to OPC. They explained that despite the chemical composition, the pore size and distribution of geopolymer improved the fire performance. Hussin et al. (2015) studied mass loss, strength and microstructural changes of geopolymer at elevated temperatures. The initial strengths of geopolymer specimens and OPC control were 25

and 26 MPa, respectively. The mass loss of OPC is more severe than that of geopolymer concrete (BAG); especially at 800 °C, the mass loss of OPC is two times more than that of geopolymer. After high temperature exposure, geopolymer concrete maintains an 80% initial strength while the OPC concrete has 50% residual strength.

Kong and Sanjayan (2010) studied the influences of different parameters of geopolymer concrete under fire conditions. The results show specimen size and aggregate size governed the performance of concrete at room temperature and elevated temperatures. They also analysed the influence of different types of aggregates and illustrated slag aggregate geopolymer concrete has the same fire performance and compressive strength as basalt aggregate geopolymer concrete.

GPC with other different aggregates was tested. Junaid et al. (2015) studied the residual strength after exposure of up to 1000 °C of fly ash aggregates with geopolymer binder. GPC has better fire endurance than OPC, they explained, for three reasons: 1. Dehydration of $Ca(OH)_2$ at elevated temperatures; 2. Disparity between thermal expansion of limestone and shrinkage of OPC binder; 3. Aggregate undergoes phase change under elevated temperature. Rickard et al. (2016) investigated the geopolymer concretes with quartz aggregate or expanded clay aggregate exposed to elevated temperatures of up to 750 °C. They found that dehydration of water in a capillary caused cracks which led to strength loss in temperature ranging from 110-300 °C. The condition is even severe for geopolymer concrete with quartz aggregate due to its low permeability. However, the strength of geopolymer concrete will increase in temperatures higher than 500 °C which showed an advantage over conventional OPC concrete.

The residual strength was tested on GPC structural elements. Sarker and Mcbeath (2015) investigated the fire endurance of steel reinforced GPC. The fire performance of geopolymer was tested on 500 mm × 500 mm steel reinforced concrete. One side of the panel was exposed to fire according to heating rate in Australia Standard, and the opposite face was exposed to room temperature, then the panel was cooled to room temperature and tested. The residual strength of GPC was, on average, 30% better than OPC panels.

Shoaib et al. (2001) studied the influence of cooling mode of slag mortars on compressive strength and crack patterns. Three cooling patterns were implemented on samples cured after 7 months: water cooling, furnace cooling and air cooling. Water-cooled mortar retained the best compressive strength. The strength retain ratio of air-cooled mortar is around 50% of a water-cooled specimen. The strength of a furnace-cooled specimen is slightly better than an air-cooled specimen. Shaikh and Vimonsatit (2014) also investigated the effects of different cooling methods on the residual strength of concrete blended with fly ash. Two cooling methods (slow cooling and rapid water cooling) were implemented on specimens exposed to 200, 400, 600 and 800 °C. The test results show the residual compressive strength decreased with the increase in the temperature irrespective of cooling regimes. All concrete exhibited 10% to 35% more reduction in residual strength with the rapid cooling regime. Furthermore, crack development for slowly cooled concrete is smaller than rapid water cooled concrete. The existing Eurocode accurately predicted the compressive strength of fly ash concretes exposed to elevated temperatures.

## 2.5 CFST columns

### 2.5.1 Development of CFST columns

CFST columns offer numerous structural benefits, including high strength and fire resistance, favourable ductility and large energy absorption capacities. There is also no need for the use of formwork during concrete construction, hence the construction cost and time are reduced. These advantages have been widely exploited and have led to the extensive use of CFST columns in civil engineering structures. In CFST columns, steel and concrete are used to combine their advantages. The confinement of concrete is provided by the steel tube, and the local buckling of the steel tube is improved due to the support of the concrete core.

Concrete-filled steel tubes have been used in Australia for many years. They can be used as major compressive components or key members under various loading conditions in buildings, bridges and other structures. Two examples are presented in Figure 2.2.

(a) Brisbane International Terminal (Airport, 1996)

(b) Latitude (Multiplex, 2005)

Figure 2.2 Typical buildings using CFST columns

Brisbane International Terminal was completed in 1996 and is a major international gateway into Australia. The four levels of the 140 m × 100 m building comprise of structural steel columns and floor beams, with a 120 mm thick in-situ concrete slab on steel decking. The steel columns were filled with 40 MPa concrete prior to pouring slab in order to increase the column stiffness. The Latitude Building in Sydney was built in 2005 and exists on George Street on the World Square Site. The building has a total height of 222 m over 45 floors. The twin composite column was used on the perimeter frame and 508 mm diameter steel tubes were filled with 80 MPa concrete.

### 2.5.2 CFST Columns at ambient temperature

In recent years, many researchers have tried to improve the performance of CFST columns. One of the scopes is to use high performance materials in CFST columns. It is known that most of the load-carrying capacity of CFST columns is provided by core concrete. Therefore, the higher the strength of the concrete, the higher the load-carrying capacity of the CFST column.

With the advancements in technology in developing high strength concrete, researchers have tried to fill steel tube with high strength concrete in order to reduce the size of CFST columns. Several experiments were carried out on the CFST columns by employing a concrete strength higher than 100 MPa. Dexin (2012) recently carried out tests on CFST columns with ultra-high strength concrete with a cube strength of filled concrete close to 200 MPa. However, the problem of brittleness might become critical for high strength concrete. One of the methods to solve this problem is to add steel fibres in the high strength concrete. The ductility of concrete could be improved when 1% of steel fibres by volume were added into the concrete (Varma et al., 2002). Another method was to increase the thickness of the steel tube or use high strength steel.

Application of high strength steel in CFST columns is currently being studied. High strength steel with a yield strength of up to 1247 MPa has been used in steel tubes of CFST columns and several experimental investigations have been carried out (Javidan et al., 2016). However, local buckling is the most significant problem and it may limit the usage of high strength steel, due to the fact that the thickness of the steel tube could be reduced when using high strength steel. Stainless steel is another type of high performance steel with high strength and better corrosion resistance and hardness; it has been investigated as outer materials of CFST columns by researchers for nearly a decade (Young and Ellobody, 2006).

Shi et al. (2015) investigated the performance of 12 geopolymer concrete filled square section columns under axial loading. The CFSTs with geopolymer concrete were cured at 80 °C for 24 h in an oven, and they tested the compressive strength at an ambient temperature. Following this, they used an existing theoretical model to

predicted the load-deformation curves of CFST columns with geopolymer concrete. They revised the model to achieve a better correlation between the theoretical model and test results. The results are shown in Figure 2.3.

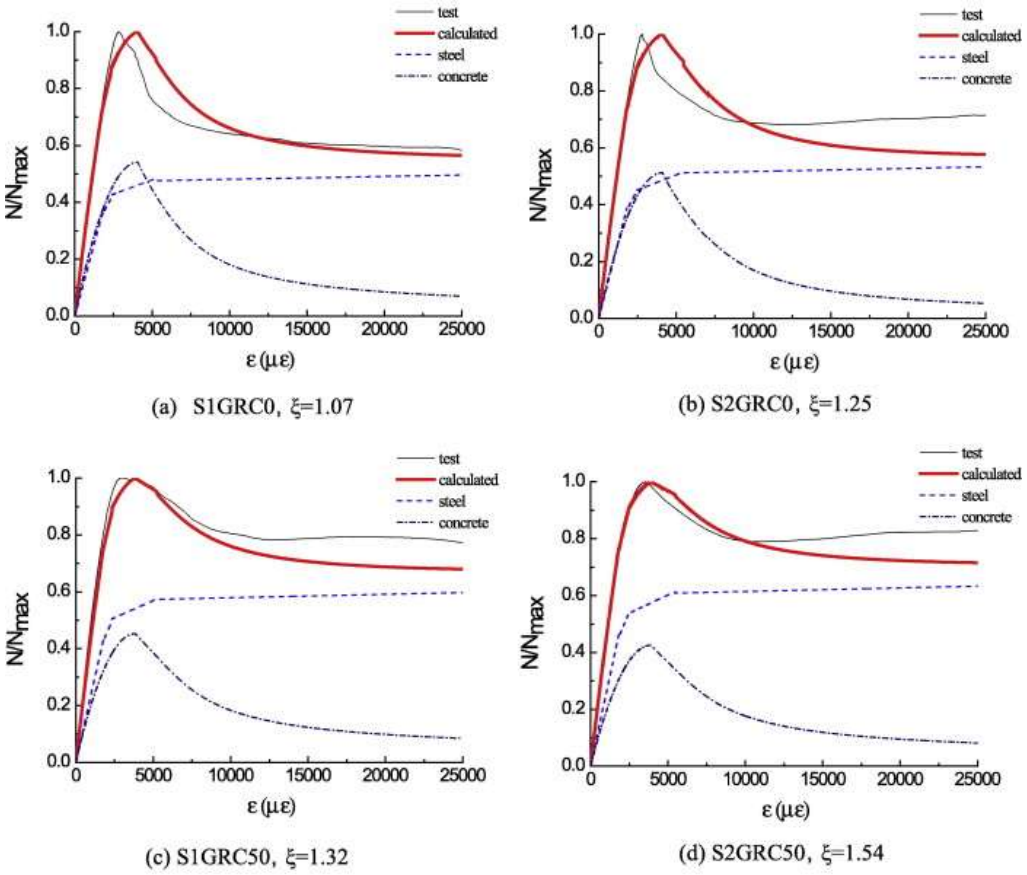


Figure 2.3 Load versus longitudinal strain relation of geopolymer concrete filled columns from a modified model (Shi et al., 2015)

The confinement factor which indicates the constraining effect of the steel tube to the core concrete is defined as $\xi = A_s f_y / A_c f_{ck}$. The square hollow sections of 200 mm × 200 mm × 6 mm and 150 mm × 150 mm × 5 mm specimens were labelled as "S1" and "S2", respectively. GRC0 means all the aggregates are limestone, and GRC50 means 50% of aggregates are recycled aggregates. According to the results, the predictions are more accurate for specimens with a higher $\xi$. However, the elevated temperature-

curing procedure they used limits the implement of geopolymer in construction application. Future research should focus on CFST with geopolymer concrete cured at an ambient temperature.

Geopolymer is a new type of concrete which has the potential to be used in CFST columns. According to former research, the material properties of geopolymer are different from those of OPC concrete. Pan et al. (2011) pointed out that the brittleness of geopolymer is higher than OPC at equivalent compressive strength. Although brittleness could impede the application of geopolymer, the ductility of core concrete will be improved due to the confinement offered by the tube when the CFST column is subjected to axial force.

More work should be undertaken on CFST columns with geopolymer concrete in order to fully understand the behaviour of this new type of composite columns.

### 2.5.3 CFST Columns at elevated temperatures

The fire resistance of unprotected hollow steel tubular columns in high-rise buildings has generally been found to be less than half an hour (Han et al., 2014). For concrete-filled steel tubular columns, the filled concrete can significantly increase the fire resistance. Because the heat is absorbed by the core concrete, the temperature in the steel tube increases much slower than that of the bare hollow steel tubes. Moreover, the outer tube provides a confinement to the core concrete during the fire exposure; the spalling of the core concrete thus can be prevented. Numerous studies (Song et al., 2010) have been conducted on the fire performance of CFST columns, and it has been found that the cross-sectional profile and fire protection thickness had the most significant influence on the temperature distribution in the column.

For the concrete filled steel tube, several parameters could affect its fire resistance, such as the cross-sectional profile, the load eccentricity and the thickness of fire protection. It was found that the cross-sectional profile and the fire protection thickness had the most significant influence on the temperature distribution in the column. It is noted that among some studies (Lu et al., 2011), most experiments were carried out under an ISO 834 standard fire, and the cooling phase was usually not considered. A time-force-temperature path was also proposed to illustrate the fire and the load action during fire exposure. The specimen was loaded at the ambient temperature and heated while the load was kept constant. After the heating, the specimen was once again cooled to an ambient temperature and loaded until failure. Since the mechanical properties of steel and concrete depend on the temperature and loading histories—even when the specimen has survived the heating stage—it would still be possible to fail in the cooling stage. The proposed full range analysis provides a reasonable approach to the evaluation of the structural fire performance.

In practice, the fire exposed CFST column could be strengthened by using fire-resistant coating or internal reinforcement. The measure of using fire-resistant coating is very common in construction, but it still has some problems. Wang (2003) reported that using this method to protect the structures made with steel generally accounted for about 30% of the total cost. In addition, the external coating could be deemed non-functional if it is damaged by the explosion blast in a fire disaster. Another common method is to use reinforcement in columns. For this type of method, typical column reinforcement consists of longitudinal and transverse steel bars tied together at intersections to form a cage; in practice, on-site fabricated cages are lifted and placed in position. Jarkas (2012) illustrated that the complex procedure has significantly

increased the cost of labour by approximately 30%, and the addition of these steel bars further increases the cost of columns. Besides the increase in cost, the installation of steel cages also has side effects, such as insufficient concrete coverage of the reinforcing bars, poor quality of filling concrete due to improper compaction, and restricting the minimum size of the column.

Recently, with the rapid development of high performance materials, the fire performance of CFST columns using innovative steel and concrete has been studied. Experimental investigations on CFST columns coupled with high strength concrete and high strength steel indicate that the use of those high performance materials has a detrimental effect on the fire resistance of CFST columns (Han et al., 2014). This highlights the need to increase the fire performance of CFST columns.

## 2.6 Summary

Based on the above literature review on the development of geopolymer and CFST columns, the following findings can be summarised:

(1) Geopolymer is an emerging fire-resistant concrete. Unlike OPC, geopolymer concrete can retain a large portion of its strength at elevated temperatures and geopolymer has no risk of spalling. Whilst current research is based on mechanical properties of geopolymer cured at elevated temperatures, this research will focus on the fire performance of geopolymer concrete cured at an ambient temperature. Elevated temperature curing regimes will be seen to impede the application of GPC. Simplifying the curing regime is of great importance in order to fully develop the potential of geopolymer in fire-resistant application. Adding some cement into geopolymer allows it to be cured at an ambient temperature (Nath and Sarker, 2015).

Although Kırca et al. (2013) studied the strength development of CAC and GGBFS blends at different temperatures; no studies were found to investigate the potential of using CAC as an additive in fly ash-based geopolymer for ambient curing conditions. CAC is also famous for its high fire performance. Due to the high fire performance and better mechanical properties of geopolymer, it is necessary to carry out study on geopolymer blended with CAC.

(2) CFST columns are increasingly being used in engineering practice, but fire-protection measures need to be implemented to meet the requirement to avoid fire hazards. However, these methods lead to a heavy increase of construction costs or a decrease of the quality of concrete compaction. Filling fire-resistant concrete in tubes will improve the fire performance of CFST columns by absorbing heat from tubes. Geopolymer concrete is a potential fire-resistant concrete. In this case, the CFST column cast with fire-resistant geopolymer concrete is able to improve fire performance without additional fire protection, such as external fire-resistant coating or internal steel bars. Some current questions on the feasibility of the CFST column with geopolymer should also be fully studied for its widely expanded application. However, few researchers (Shi et al., 2015) have investigated the structural behaviour of CFST columns with geopolymer concrete tested at ambient temperatures. Considering geopolymer has a good fire performance, it is worthwhile to carry out investigations to promote the potential applications of fire-resistant geopolymer concretes in CFST columns.

# Chapter 3 Experimental Program

## 3.1 Introduction

This chapter provides a detailed introduction to the experimental program and materials used for this research. Firstly, the properties of concrete raw materials were investigated, if not reported by the suppliers. The second part of this chapter introduces the concrete test method. The last section provides the experimental program for CFST columns. Both GPC and OPC concrete cylinders were cast and tested according to the experiment method discussed in this chapter.

In addition to a workability test of fresh concrete, the main tests for concrete properties include Young's modulus test, the compression test, the indirect tensile strength test and the flexural strength test. An extensometer was used to capture the deformational performance of concrete cylinders at elevated temperatures. The heating regime and microstructure analysis were reported on concrete testing. Additionally introduced is the sample preparation for CFST columns. Fifteen CFST columns were tested in this thesis, five of which at ambient temperature (ultimate loads recorded), while five other columns were heated to failure, exposed to fire at a constant load level (50% of ultimate load). The post-fire loading phases were tested on the remaining five specimens.

## 3.2 Materials

### 3.2.1 Fly ash and calcium aluminate cement (CAC)

As mentioned in Chapter 2, a variety of aluminosilicate source materials such as kaolinite, fly ash, and GGBFS can be utilised to synthesise geopolymer. Fly ash is

exclusively studied in this thesis because the consumption of fly ash can reduce landfill, and it is underutilised in Australia. The fly ash studied was provided by a thermal power plant in Queensland. It is noted that the fly ash has low calcium content, and it can be characterised as dry ASTM type F (low calcium) fly ash (2015). The market brand of CAC used in the geopolymers is Secar 71, which was produced and supplied by Kerneos Inc.

The X-ray fluorescence spectroscopy (XRF) analysis was performed on binding materials of fly ash and CAC, details of which are presented in Table 3.1. Fly ash mainly contains $SiO_2$ (quartz) and $Al_2O_3$ (aluminium oxide). In comparison with fly ash, CAC exhibits higher Aluminium oxide content, while having lower quartz content. The Aluminium content of CAC is much higher than fly ash, while CAC consists of less than 1% quartz. With the addition of CAC, the Al/Si ratio of the geopolymers increases.

Table 3.1 Chemical analysis by X-ray fluorescence of fly ash and CAC

| Constituent (%) | $Al_2O_3$ | $SiO_2$ | $Fe_2O_3$ | CaO | MgO | $SO_3$ | $K_2O$+ $Na_2O$ |
|---|---|---|---|---|---|---|---|
| Fly ash | 30.5 | 48.3 | 12.1 | 2.8 | 1.2 | 0.3 | 0.6 |
| CAC | 68.5 | 0.8 | 0.4 | 31.0 | 0.5 | 0.3 | 0.5 |

The Scanning Electron Microscopy (SEM) analysis was conducted on fly ash and CAC powder, as shown in Figure 3.1. Fly ash particles are a regular round shape, while the body of CAC particles is irregular. The addition of CAC in geopolymer could reduce the workability.

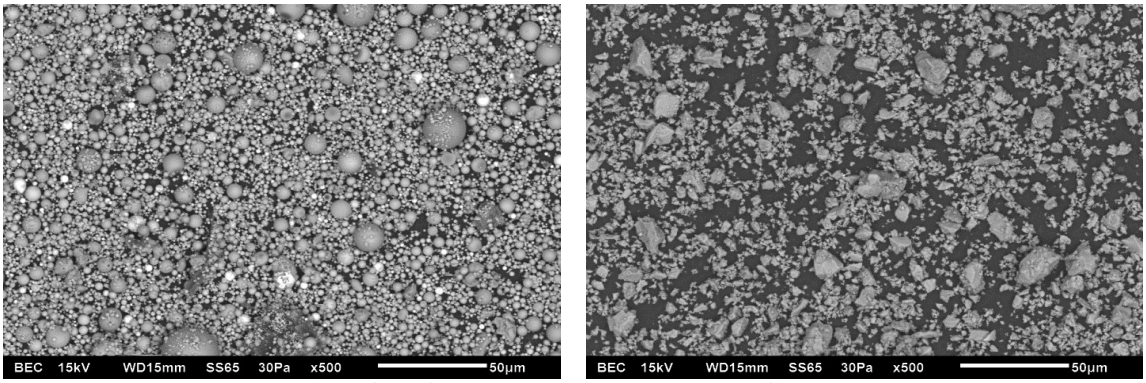


(a) Fly ash (b) CAC

Figure 3.1 SEM images of raw materials

### 3.2.2 Alkaline activators

Throughout this study, alkaline activator was made by mixing sodium hydroxide solution and sodium silicate solution at a constant ratio of 1:2.5. This ratio has a profound effect on the strength of GPC, and the value of 2.5 was recommended by Hardjito (2005). Sodium hydroxide pellets (98% purity) were dissolved in tap water to produce 10, 12 and 14 M concentration solutions for the purpose of optimising the mix design. The amount of sodium hydroxide pellets by weight of the solution is presented by Hardjito (2005), and it is given in Table 3.2.

Table 3.2 Weight of NaOH pellets of solution per kilogram in different molarities

| Molarity of NaOH solution | Weight of NaOH pellets per kilogram solution (g) |
|---|---|
| 10 M | 314 |
| 12 M | 361 |
| 14 M | 444 |

Sodium silicate (grade D) with a modulus silicate ratio (*Ms*) of 2 was used (where *Ms* = $SiO_2/Na_2O$, $SiO_2$ = 29.4%, $Na_2O$ = 14.7%, $H_2O$ = 55.9%). The sodium silicate and sodium hydroxide combined solution was prepared 24 hours prior to the geopolymer mortar or GPC casting.

### 3.2.3 Aggregates

Locally available river sand and limestone were used as fine aggregates and coarse aggregates, respectively; fine aggregates and coarse aggregates (maximum size 20 mm) were used in its saturated surface dry condition. The grading curves of sand and limestone are shown in Figure 3.2. Both fine aggregate grading requirements and coarse aggregate grading requirements were followed, as suggested in ASTM C33 Standard (2003).

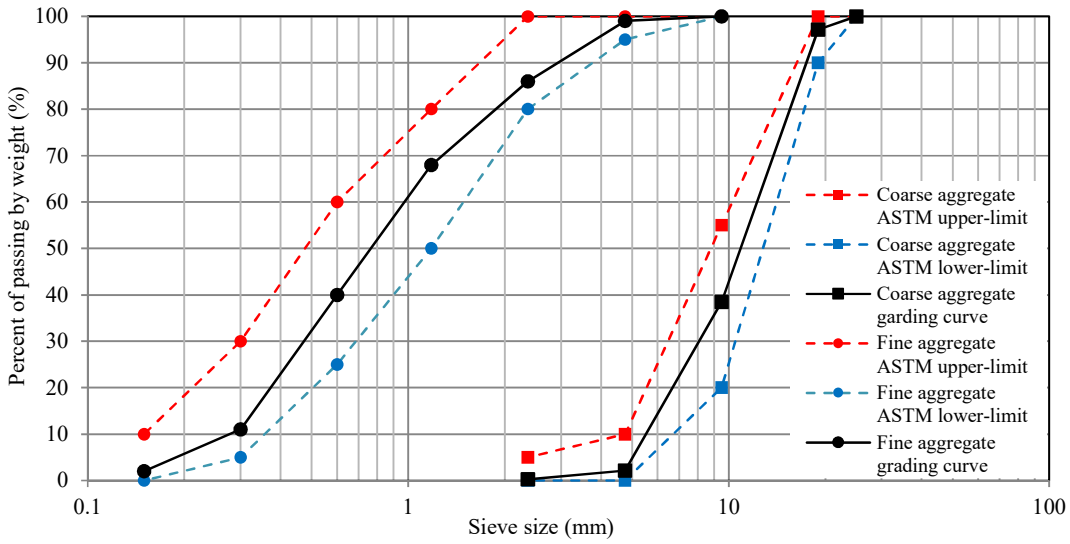


Figure 3.2 Sieve analysis of combined coarse aggregate and fine aggregate.

### 3.2.4 Superplasticiser

High range water reducing admixture in an aqueous solution was used for improving the workability of OPC concrete, which has the product name MasterGlenium SKY 8100. It is a polycarboxylic ether polymer superplasticiser and complies with AS1478.1-2000 Type HWR High Range Water-reducing, which requires 10% water reduction level.

## 3.3 Concrete experiment method

### 3.3.1 Sample preparation

*3.3.1.1 Mixing*

Firstly, the binder (fly ash and CAC) and saturated surface dry aggregates were added into a mixer and dry-mixed for 3 minutes. Extra water, if applied, was added to the dry mix as necessary. Alkaline activator was then added and the wet mixture was stirred for an additional 4-6 mins to form a homogenous state. The mixing procedure for OPC concrete production was similar to that of GPC, except that the water and superplasticiser were added in the mixer after the dry-mixing of aggregate and cement.

Different mixers were used, depending on the volume of raw materials. For geopolymer mortar mixes, a bread mixer was used to mix a small amount of geopolymer mortar which has no aggregates. For GPC and OPC concrete mixes, a pan mixer at Western Sydney University was utilised.

*3.3.1.2 Curing*

After mixing, the mortar or concrete was cast into different moulds. The mortar was transferred into a 50 × 100 mm cylindrical mould. The concrete samples were cast into a 100 × 200 mm cylindrical mould in three equal layers at three time intervals. The concrete was also cast into a 100 × 100 × 300 mm flexural beam mould. A vibrating table was employed to remove air bubbles from the specimens, with each layer being vibrated for 15-30 seconds. The cast specimens were kept in moulds for 24 ± 8 hours at an ambient temperature. The specimens requiring an elevated temperature curing procedure were kept at 80°C in moulds for 24 hours before demoulding. After demoulding, the specimens were sealed in plastic bags until testing.

Both concrete and mortar cylindrical specimens were ground using a CIVILAB core facing grinder to achieve smooth and flat ends before testing.

## 3.3.2 Testing regime

*3.3.2.1 Workability test*

The workability of both fresh GPC and OPC concrete was measured by conventional slump testing. For geopolymer paste, workability was assessed by a mini-slump test. The slump mould, shown in Figure 3.3, had an inner cone, with the top diameter = 19 mm, the end diameter = 38 mm and the height = 57 mm.

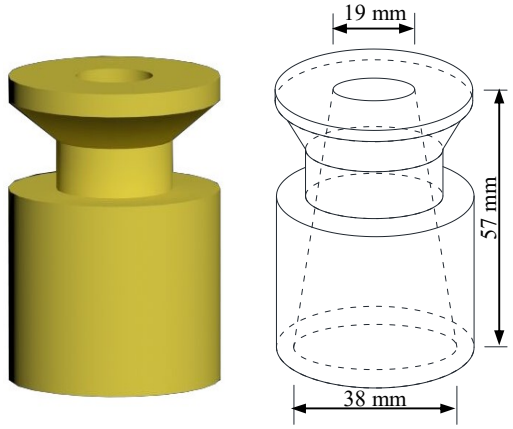


Figure 3.3 Mini-slump mould

During the test, the mould was steadily placed on a plastic sheet on a flat table and filled with paste. The excessive paste was removed and the top surface was levelled after the inner cone was full. The mould was then removed vertically to ensure the paste was laterally undisturbed. The diameter of the spread circle was determined from the mean of two orthogonal direction measurements.

*3.3.2.2 Compression test*

Mortar and concrete cylinders were tested using an INSTRON 8036 universal testing machine which has an uncertainty of 0.45% for loads below 200 kN. The

compression test was conducted in accordance with ASTM C39 Standard (1996). The loading rate was 0.25 ± 0.05 MPa/s. The tests were conducted at an ambient temperature, and the averaged results of three samples were recorded. The diameter and height of cylinders in conjunction with mass were measured before the testing to calculate density.

*3.3.2.3 Young's modulus test*

Young's modulus test was conducted following the ASTM C469 Standard (2002) and the testing results were carried out using an INSTRON 8036 testing machine. The loading and unloading rates were 0.25 ± 0.05 MPa/s. The initial loading and unloading cycle of the test was abandoned. The cylinders were unloaded after loading to 40% of ultimate strength and the whole test cycled three times.

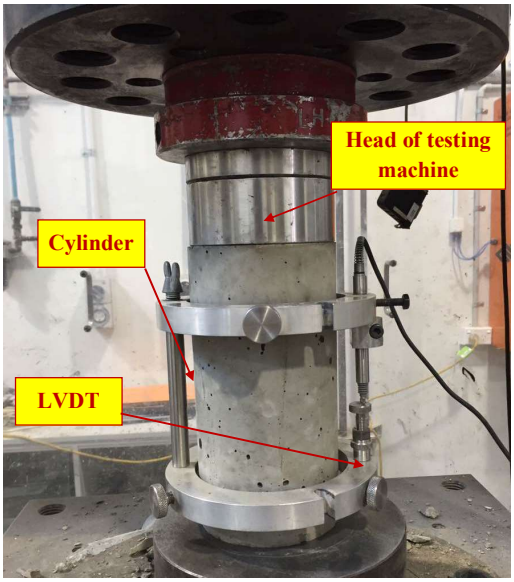


Figure 3.4 Young's modulus test setup

As shown in Figure 3.4, the strain of concrete was measured by two linear variable differential transducers (LVDTs). The two LVDTs were fixed on two rings oppositely.

The relative movements of the concrete cylinder under compression were recorded by LVDTs.

*3.3.2.4 Splitting tensile strength test*

The splitting tensile strength (indirect tensile strength) test was conducted in accordance with procedure prescribed by ASTM C496 Standard (2011). The testing was conducted using the INSTRON 6027 testing machine. Three specimens were tested for each mixing design. The cylinder was subjected to compressive force on either side which caused the splitting of the sample.

*3.3.2.5 Flexural strength test*

The flexural strength was measured according to the ASTM C78 Standard (2010) using the INSTRON 6027 testing machine. As specified in the Standard, two beam specimens were tested for each mix. The specimen was loaded constantly at a rate of 1.0 MPa/min until rupture occurred. The testing setup is shown in Figure 3.5.

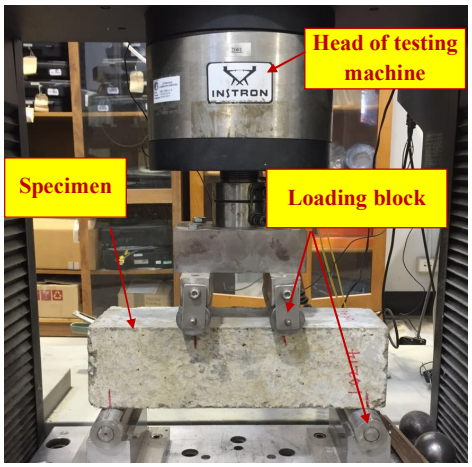


Figure 3.5 Flexural strength test setup

*3.3.2.6 Strain measurement*

There were two strain measurement setups for the concrete experiments. Firstly, Young's modulus was measured under compression using two LVDTs, while the second stain measurement was used to record stress-strain curves of concrete. To obtain complete stress-strain curves, a CM-10H compressometer was employed to measure the strain of concrete cylinders under compression. Two high-sensitivity displacement transducers, with a gauge length of 100 mm, were installed in this compressometer. However, the strain measured by the compressometer became invalid, as extensive cracks developed on the concrete specimen after peak stress. Following this, four LVDTs were used to measure the platen-platen deformation of machine. The LVDTs were fixed on the bottom platen at four sides of the concrete cylinder.

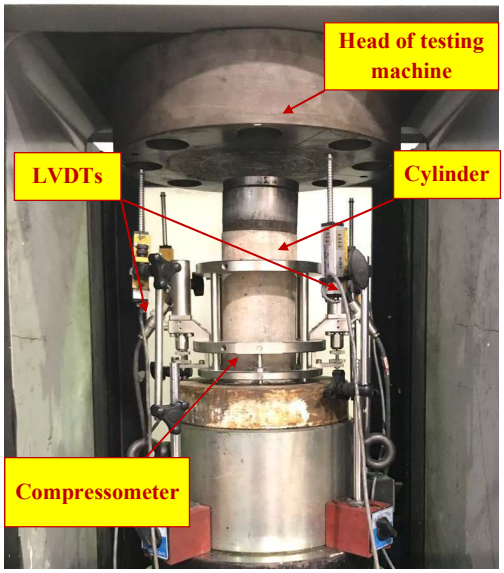


Figure 3.6 Stress-strain relationship experiment setup

The experiment setup is shown in Figure 3.6. The compression load for stress-strain testing was applied by a closed-loop servo controlled hydraulic MTS machine with a

maximum capacity of 5000 kN. A loading rate was kept at 0.05 mm/min for all stress-strain tests of concrete cylindrical specimens.

*3.3.2.7 Heating regime*

Two heating regimes were used in the examination of the fire performance of GPC. Firstly, the slow heating rate was employed to test the post-fire performance of GPC. The specimen was placed in the electrical furnace, see Figure 3.7.

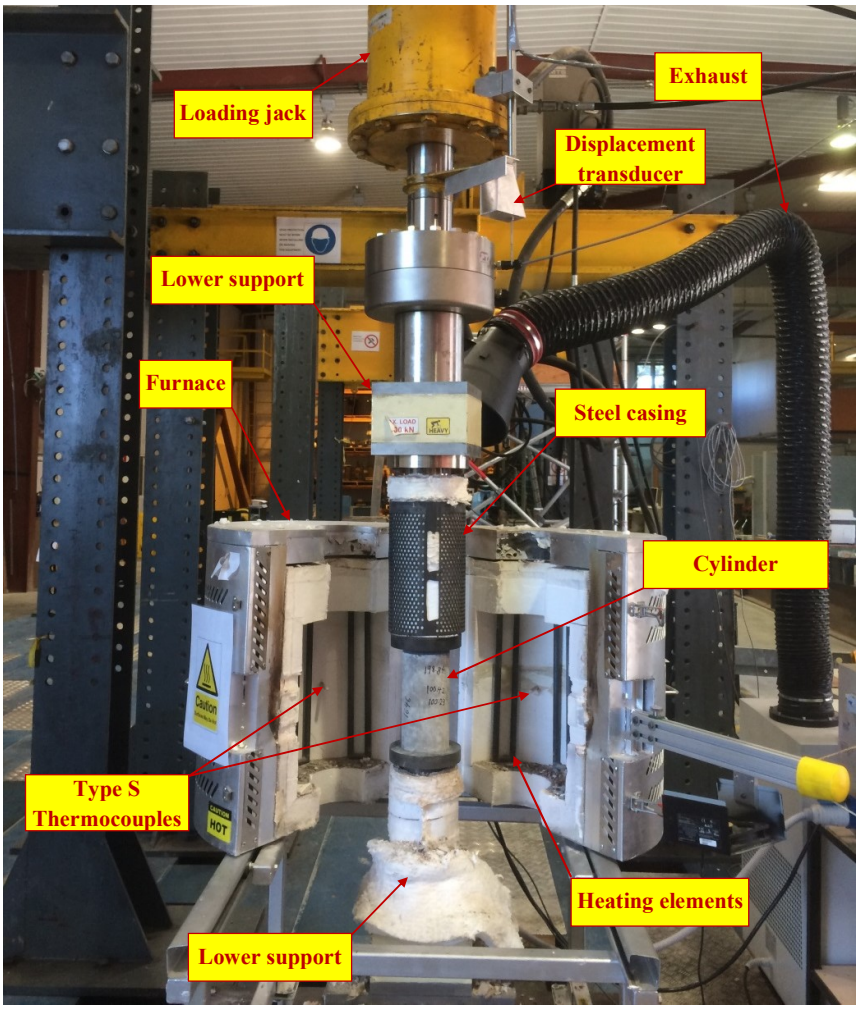


Figure 3.7 Fire test setup of concrete cylinder

The temperature of the furnace was increased to target temperatures (200, 400, 600 and 800°C) at the rate of 5°C/min, and the furnace held this target temperature once

achieved for 3 hours, so as to obtain a state of equilibrium. Afterwards, the furnace was naturally cooled to an ambient temperature. The slow heating regime is shown in Figure 3.8.

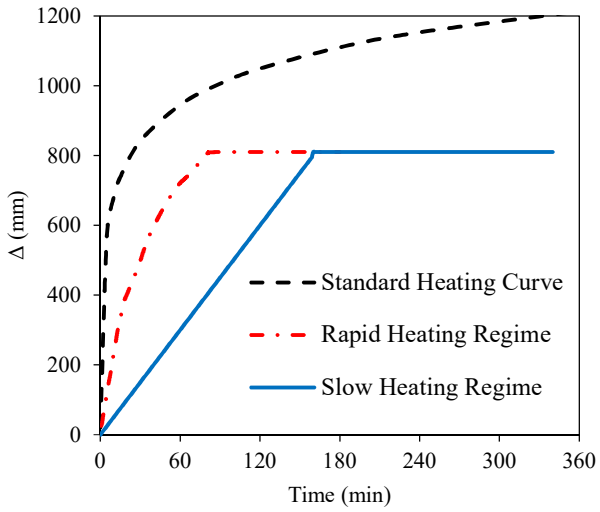


Figure 3.8 Heating regime

The rapid heating was used to test the high temperature performance of a concrete cylinder with constant loading. Firstly, the specimen was loaded by the hydraulic machine to a constant rate of 0.25 ± 0.05 MPa/s. The furnace was closed after keeping the load on specimen for 10 mins. The furnace was ignited and heated the specimen to 800 °C with the maximum capacity. The rapid heating curve, compared to the standard heating curve provided by the Australia Standard 1530.4 (1997), is shown in Figure 3.8. The strength of the specimen decreased in the condition of high temperatures, and once it could no longer bear the constant loading, the test ended. The deformation under high temperatures and high temperature endurance period were recorded.

*3.3.2.8 X-ray diffraction analysis (XRD)*

The X-ray Diffraction Analysis was conducted on a Bruker D8 Advance Powder Diffractometer, as shown in Figure 3.9. The geopolymer paste sample was

crushed and ground into a powder, and the powder was attached to a sample holder. The voltage was 40 kV with a current of 40 mA. The run conditions included Cu-Kα radiation and scanning from 5 to 60° 2θ degrees with a counting time of 5 seconds.

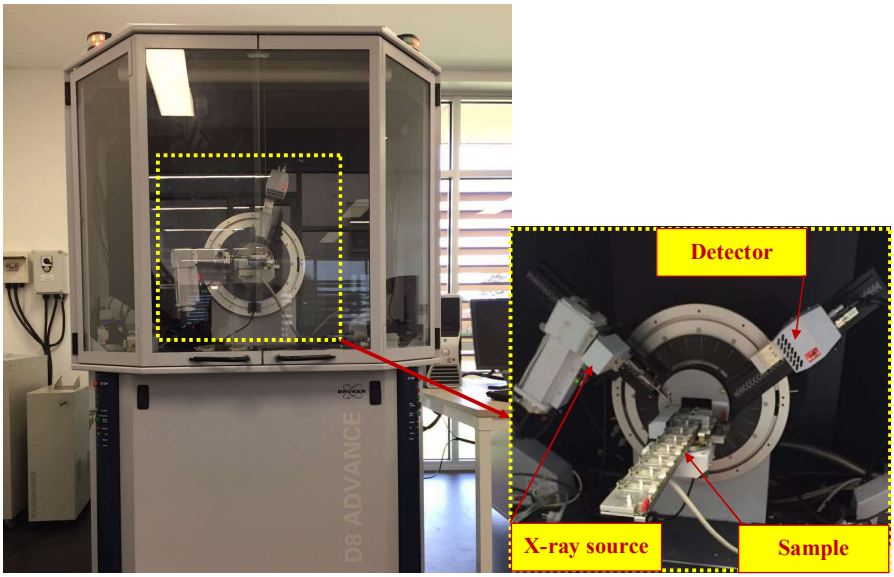


Figure 3.9 Bruker D8 Advance Powder Diffractometer X-ray diffraction

*3.3.2.9 Scanning electron microscopy (SEM)*

The microstructure of paste samples was examined using SEM-EDX (JEOL 6510LV) at 7 and 28 days, and the equipment is shown in Figure 3.10. The SEM specimen was a piece of geopolymer paste fixed on a copper holder. The samples were coated to conduct electron with carbon if necessary. The secondary electron detector was operated at 15 kV.

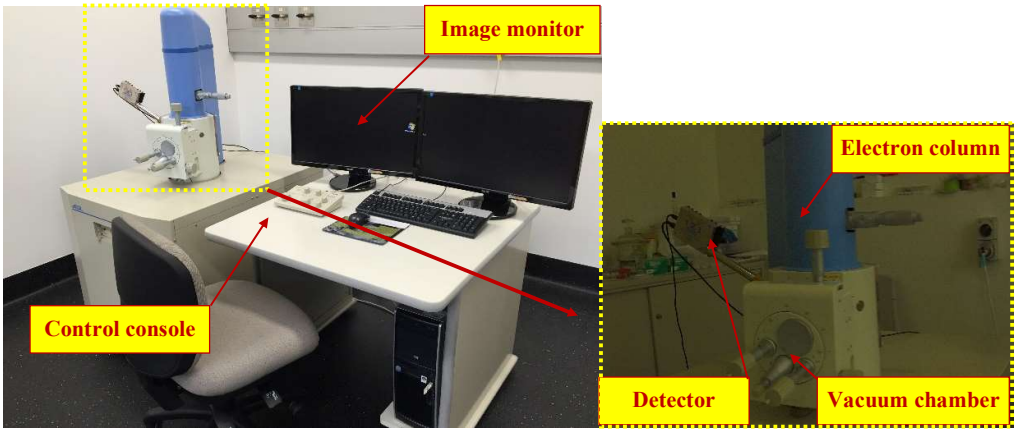


Figure 3.10 JEOL 6510 LV Scanning electron microscope

*3.3.2.10 Thermal gravimetric analysis (TGA)*

The thermal gravimetric analysis was conducted on geopolymer paste by using a Bruker Vertex 70 instrument at 28 days. The samples were heated to 800°C at the rate of 10 °C/min with ultra-high purity nitrogen ($N_2$) as protection gas. The TGA instrument is shown in Figure 3.11.

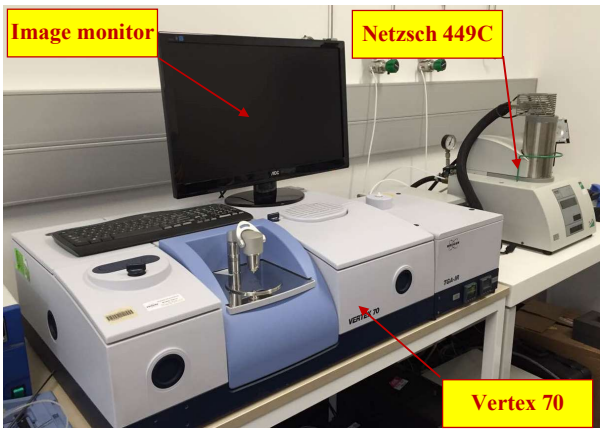


Figure 3.11 Bruker Vertex 70 coupled Netzsch 449C Jupiter DSC-TGA instrument

## 3.4 CFST experiment method

### 3.4.1 Sample preparation

*3.4.1.1 Casting*

As discussed, a total of fifteen circular steel tubes were cast with concrete, and all the tubes were fabricated from the same batch. All specimens had a designed length ($L$) of 340 mm, including two endplates with a thickness of 12 mm. The diameter of the endplate was 200 mm, and a 120 mm hole was cut on the top of the endplate to pour concrete into. The nominal external diameter ($D$) of the steel tube was 150 mm, and the nominal thickness ($t$) was 3 mm.

The concrete was mixed in a uniform state according to Section 3.3.1.1, and then the concrete was cast into the steel tube in three equal layers at three time intervals. At the same time, a concrete vibrator was utilised to compact the concrete and expel the internal air bubbles.

*3.4.1.2 Curing*

After casting, the top ends of all fifteen steel tubes were wrapped by polyethylene films. The ten fresh OPC concrete and GPC filled steel tubes were left at ambient temperature. The rest of GPC filled steel tubes were firstly cured at 80°C in an oven for 24 h, and then the GCFSTs were cured at an ambient temperature until the test was carried out.

## 3.4.2 Testing regime

*3.4.2.1 Material properties test*

Tensile tests, performed by the INSTRON 6027, were conducted on three steel coupons cut from one of the original steel tubes; all steel tubes came from one batch of fabricating. The material properties were recorded, including Young's modulus, the yield stress, yield strain and ultimate strength of the steel tube. The residual strength of steel was also tested with the same machine. The material test setup is show in Figure 3.12, and the heating rate is identical to that recorded in Figure 3.8.

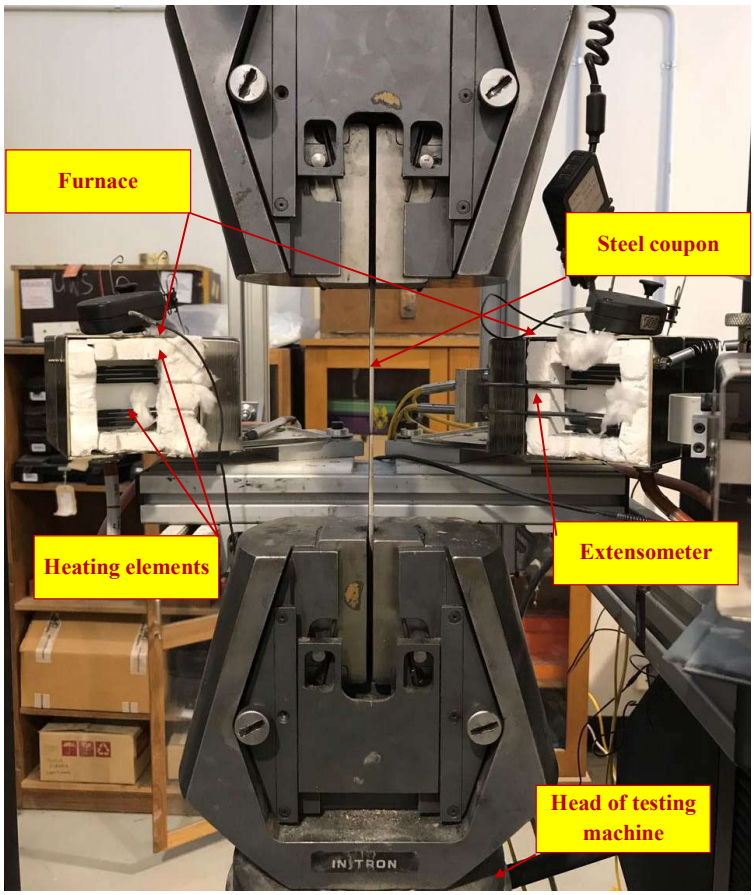


Figure 3.12 Fire test setup of steel coupon

*3.4.2.2 Compression test*

The compression test of CFST columns was performed by a closed-loop servo controlled hydraulic MTS machine with a maximum capacity of 5000 kN. Firstly, a 10 kN preload was applied to the specimen, and the load was maintained for 2 minutes. Secondly, the specimen was loaded until the peak load was reached, with the loading rate of 0.12 mm/min. In the post-peak range, the loading rate was increased to 0.6 mm/min until the test stopped when severe failure occurred.

*3.4.2.3 Strain measurement*

Four bidirectional strain gauges, with a gauge length of 3 mm, were attached at the mid-height of the steel tube to measure the longitudinal and lateral strains; the strain gauge has a limited measuring range. Four LVDTs were installed against the top platen to measure the displacement of the machine after the failure of stain gauges. The details of the setup and location are shown in Figure 3.13.

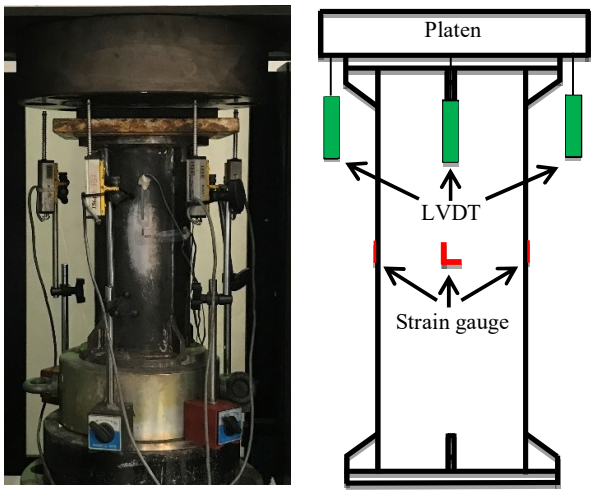


Figure 3.13 Setup and location of strain gauges and LVDTs

*3.4.2.4 Heating regime*

Two heating regimes were used to evaluate the fire performance of CFST columns, as seen in Figure 3.14. The first one was a slow heating regime used to study the post-fire performance of CFST columns. The CFST column was put in the electrical furnace, and the temperature of the furnace was increased to 800°C at the rate of 5°C/min. The furnace maintained the target temperature for 3 hours to achieve a state of equilibrium. Lastly, the furnace was naturally cooled to room temperature.

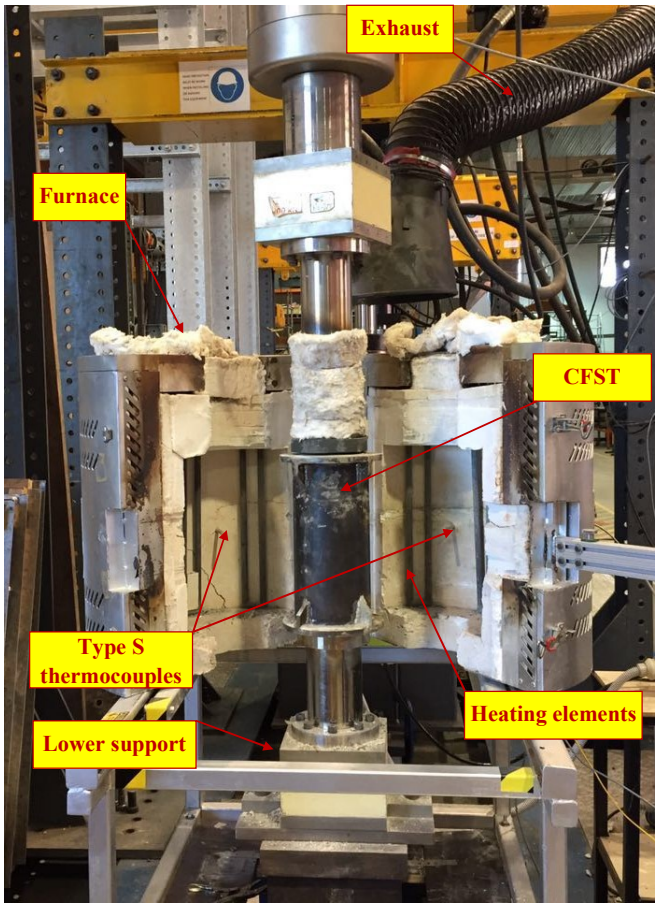


Figure 3.14 Fire test setup of CFST

The rapid heating regime was used to test the response of CFST columns to fire when holding a constant load. The control model of the compression machine was set to load control for the whole testing process. The CFST column was firstly loaded to 50% of

its ultimate load. The furnace was then started and the heating rate was the same as noted in Figure 3.8. The load bearing capacity of a CFST column decreased after sufficient fire exposure, which caused deformation to the column. When the deformation exceeded 40 mm, the experiment was stopped.

## 3.5 Summary

This chapter presented a detailed description of raw materials and the experimental methods adopted in this thesis. The results are reported of tests on raw material properties in the laboratory, which were not provided by suppliers. The preparation process of both concrete and CFST specimens were introduced in detail. Following this, standard test methods and microstructure characterisation methods on the mechanical properties of concrete were explained. The testing regimes of CFST columns were also summarised in this chapter.

# Chapter 4 Development of Optimised Mix Design for Geopolymer Concrete

## 4.1 Introduction

Several factors of GPC were considered to develop successful GPC mixing designs with optimised mechanical properties and workability. In a conventional experimental study, changing one factor at a time and keeping other factors constantly is a common approach. However, this approach requires extensive experimental work as the mechanical properties of GPC depend on various mixing parameters. In addition to different factors of mixing design, each factor has several values, for example, the alkaline solution concentration has four levels commonly used by former researchers: 8, 10, 12 and 14 M (Hardjito, 2005). Therefore, employing an effective strategy to design the salient parameter experiment of GPC is of great importance.

To save the cost and time of doing experiments, the Taguchi method will be implemented to determine the optimal mixtures of geopolymer with high strength and good workability. The Taguchi experimental design method has been widely applied in determining concrete mix design through experiments. Instead of the "one-variable-one-value" experimental method, the Taguchi method changes one variable and its level once, whilst keeping others fixed. The Taguchi method efficiently optimises the experiment with multi-variables and multi-levels, whilst ensuring satisfactory and reliable results (Wu and Naik, 2003).

## 4.2 Background of Taguchi method

The influence of using CAC as a supplementary material to simplify the curing procedure of geopolymer was analysed with the Taguchi method. This method is an

effective approach to designing multifactor experiments, with the advantage of selecting an optimal test scheme and salient parameters.

The five-step parameter analysing method was carried out as follows (Ross, 1988):

(1) The influencing factors and ranges of factors were chosen, based on former experimental research (Cao et al., 2016a). Tests were conducted on the workability and compressive strength of nine geopolymer mixtures.

(2) To investigate the significance of all factors, the range analysis was analysed on flow ability and compressive strength. The results of an orthogonal test were analysed with the direct-viewing analysis method (means $k$ and maximal range $R$) (Li et al., 2015), by taking the mini-slump test results of the orthogonal experiment shown in Table 4.3, as an example, so as to demonstrate the data processing of $K$, $k$ and $R$ in Table 4.4. For each factor in the $K_{w1}$ row, the test results of level 1 of this factor were summed. For instance, A factor at $K_{w1}$ row is $K_{w1}$ = 100 + 114 + 120. The $K_{w1}$ was divided by 3 which gave the mean values of level ($k_{w1}$), and so on. For each factor, the minimum value (among $k_{w1}$, $k_{w2}$, $k_{w3}$) was subtracted by the corresponding maximum value to get the range value $R$ of each factor. For example, $R_w$ for A factor is $R_w = k_{w1} - k_{w2}$ = 111.3 – 107.7.

(3) The bigger mean value $R$ equates to a better response. The factor order was sorted by the mean values and then the optimum level was determined to be the maximum value among $k_{w1}$, $k_{w2}$, $k_{w3}$.

(4) Two optimal mixture designs based on compressive strength and workability were proposed. Another mixture design was also proposed which considered economic factors.

(5) Three confirmation experiments were conducted on optimised GPC mixing designs.

## 4.3 Controlling ratios in GPC

The chemical components of GPC binders were presented in Chapter 2. The properties of GPC mainly depend on the composition of binding materials and other factors. Investigations were carried out on three main factors related to compressive strength and workability such as alkaline solution concentration, CAC replacement ratio, and activator to binder ratio. Each factor has three levels. The number of factors and levels of those factors were selected based on the results obtained in our previous study (Cao et al., 2016a). The selected factors and levels are shown in Table 4.1.

Table 4.1 Orthogonal experimental factors

| Level | Experimental factor | | |
|---|---|---|---|
| | A | B | C |
| | Alkaline solution concentration | CAC replacement ratio | A/B ratio |
| 1 | 10 M | 5% | 35% |
| 2 | 12 M | 10% | 40% |
| 3 | 14 M | 20% | 45% |

### 4.3.1 Alkaline solution concentration

To achieve a better fire-resistant geopolymer, the sodium alkaline solution was used in synthesising the geopolymer. Sodium hydroxide pellets were dissolved into water to form an alkaline solution. Based on the literature review in Chapter 2, three concentrations were chosen: 10, 12, 14 M. Considering the cost of sodium hydroxide, the maximum concentration was capped at 14 M. GPCs made with these concentration levels were able to achieve a sufficient compressive strength at a reasonable cost.

### 4.3.2 Calcium aluminate cement replacement ratio

CAC is well known for its high temperature resistance, and it has also been found to have rapid hardening properties (Hewlett, 2003). Therefore, part of the fly ash was replaced by CAC to achieve better mechanical properties and eliminate the heat-curing procedure. The CAC replacement ratio was selected as 5%, 10% and 20% of fly ash by mass. The maximum amount of CAC was controlled below 20% for the following reasons:

(1) First, a process called 'conversion' occurs in hydrated CAC over time (Fernández-Jiménez and Puertas, 1997), whereby metastable hydrates convert to stable hydrates, leading to an increase in porosity and a subsequent decrease in strength. It is not clear if the same problem would occur if excessive CAC is used in making GPC.

(2) Secondly, CAC is more expensive than Portland cement, with the cost related directly to the limited supply of bauxite, which is the main source of alumina in CAC production.

### 4.3.3 Activator to binder ratio

The activator was a mixed solution—from a sodium silicate and sodium hydroxide solution at the ratio of 2.5—and the binder was a mix of fly ash and CAC. The activator to binder ratio had three levels: 35%, 40%, 45%. Since the amount of binder was relatively similar, the activator to binder ratio directly indicated the amount of alkaline solution, which was an indication of the workability.

## 4.4 Salient parameter analysis and optimised mixing design

The full factorial experiment requires 27 mixing designs if a conventional method is implemented. The experiment can be designed more efficiently using an orthogonal array ($3^3$) developed by Taguchi. As shown in Table 4.2, nine geopolymer mortar mixtures were implemented to analyse the significance of three factors.

Table 4.2 Mixture proportions of geopolymer mortar (kg/m$^3$)

| Trial No. | Activator | | | Sand | Binder | |
|---|---|---|---|---|---|---|
| | NaOH pellet | Water | Sodium silicate | | Fly ash | CAC |
| 1 | 40.7 | 89.0 | 324.3 | 648.6 | 1232.4 | 64.9 |
| 2 | 45.3 | 99.0 | 360.9 | 631.6 | 1136.8 | 126.3 |
| 3 | 49.7 | 108.6 | 395.6 | 615.4 | 984.6 | 246.2 |
| 4 | 52.1 | 92.2 | 360.9 | 631.6 | 1200.0 | 63.2 |
| 5 | 57.1 | 101.1 | 395.6 | 615.4 | 1107.7 | 123.1 |
| 6 | 46.8 | 82.9 | 324.3 | 648.6 | 1037.8 | 259.5 |
| 7 | 63.9 | 94.3 | 395.6 | 615.4 | 1169.2 | 61.5 |
| 8 | 52.4 | 77.3 | 324.3 | 648.6 | 1167.6 | 129.7 |
| 9 | 58.3 | 86.0 | 360.9 | 631.6 | 1010.5 | 252.6 |

In this experiment design, every combination of levels appears in the same repetitions. This method provided an opportunity for all variables to be tested to obtain the optimum mixture. The mini-slump tests were conducted on geopolymer pastes. Compression tests on geopolymer mortars were conducted after casting on the following days: 3, 7, 28, 56, 150. The test results of nine mortar mixtures designed by orthogonal array are presented in Table 4.3.

Table 4.3 Results of nine geopolymer mortar mixtures

| Trial No. | Factor | | | Mini-slump diameter /mm | Strength at 3 days /MPa | Strength at 7 days /MPa | Strength at 28 days /MPa | Strength at 56 days /MPa | Strength at 150 days /MPa |
|---|---|---|---|---|---|---|---|---|---|
| | A /M | B /% | C /% | | | | | | |
| 1 | 10 | 5 | 35 | 100.0 | 18.7 | 34.4 | 62.5 | 73.3 | 81.2 |
| 2 | 10 | 10 | 40 | 114.0 | 32.9 | 51.7 | 107.6 | 99.4 | 87.6 |
| 3 | 10 | 20 | 45 | 120.0 | 39.1 | 50.8 | 50.4 | 61.4 | 105.4 |
| 4 | 12 | 5 | 40 | 113.0 | 33.4 | 47.5 | 63.5 | 83.7 | 79.3 |
| 5 | 12 | 10 | 45 | 115.0 | 39.5 | 71.8 | 101.1 | 108.0 | 83.4 |
| 6 | 12 | 20 | 35 | 95.0 | 57.1 | 54.8 | 80.0 | 80.0 | 91.2 |
| 7 | 14 | 5 | 45 | 122.0 | 21.2 | 47.4 | 75.1 | 80.1 | 64.7 |
| 8 | 14 | 10 | 35 | 92.5 | 48.0 | 73.4 | 118.9 | 118.0 | 112.4 |
| 9 | 14 | 20 | 40 | 115.0 | 48.0 | 51.5 | 55.7 | 53.2 | 56.9 |

### 4.4.1 Salient parameter analysis on workability

In general, the effects of an NaOH solution and CAC replacement ratio on workability are negligible. As shown in Table 4.4, the mean ranges $R_w$ are 3.7 and 4.5, respectively. The best concentration of alkali solution is 10 M, and the best replacement ratio of CAC is 5%. Figure 4.1 indicates the NaOH concentration and CAC replacement ratio have the same influence on workability.

Table 4.4 Range analysis on workability.

| Factor | Mini-slump diameter /mm | | |
|---|---|---|---|
| | A | B | C |
| $K_{w1}$ | 334.0 | 335.0 | 287.5 |
| $K_{w2}$ | 323.0 | 321.5 | 342.0 |
| $K_{w3}$ | 329.5 | 330.0 | 357.0 |
| $k_{w1}$ | 111.3 | 111.7 | 95.8 |
| $k_{w2}$ | 107.7 | 107.2 | 114.0 |
| $k_{w3}$ | 109.8 | 110.0 | 119.0 |
| $R_w$ | 3.7 | 4.5 | 23.2 |
| Factor order | C > B > A | | |
| Optimisation level | $A_1$ | $B_1$ | $C_3$ |
| Optimum combination | $A_1B_1C_3$ | | |

The mini-slump analysis of orthogonal array testing in this study has shown that the concentration of A/B ratio plays the most important role on the workability of geopolymer paste. More specifically, $R_w$ = 23.2 mm, which means the workability of geopolymer is mainly determined by this single factor. On average, a 23.2 mm improvement is expected by increasing the A/B ratio from 35 to 45%. However, the influence of improving the activator to binder ratio from 35% to 40% is four times higher than improving the activator/binder ratio from 40% to 45%.

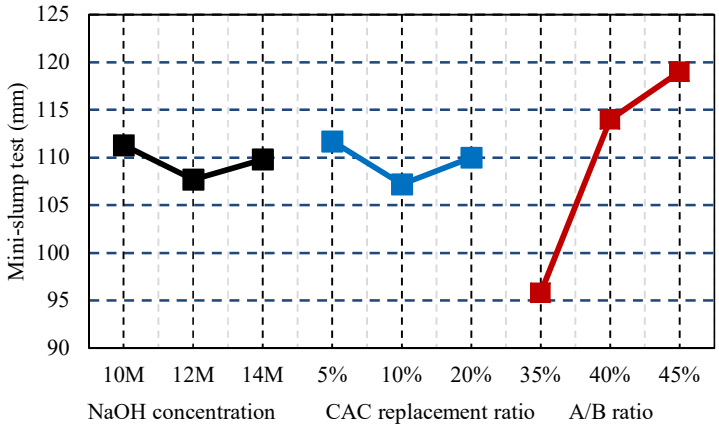


Figure 4.1 Average effect of factors on the workability of fresh geopolymer paste.

Activator to binder ratio is the most salient factor for workability, of which 45% has the best results. CAC replacement ratio is the second important factor, and the NaOH concentration is the least important factor. The optimised design based on workability is $A_1B_1C_3$.

### 4.4.2 Salient parameter analysis on compressive strength

Nine trial mixtures were implemented to analyse the significance of three factors. Compression tests on GPM were conducted at the following days after casting: 3, 7, 28, 56, 150. Table 4.4 provides the compressive strength of GPM cylinders at 3, 7, 28, 56 and 150 days. Three mix designs had higher compressive strengths than 100 MPa after being cured for 28 days, while the weakest mixture design was 50.4 MPa. The factor has a distinct influence on the compressive strength of geopolymer. As shown in Table 4.5, the range analysis of strength at early ages was reported. With the addition of CAC, the strength of geopolymer develops very fast at early ages.

Table 4.5 Range analysis on early-age strength

| Factor | 3 day compressive strength | | | 7 day compressive strength | | |
|---|---|---|---|---|---|---|
| | A | B | C | A | B | C |
| $K_{s1}$ | 90.7 | 73.3 | 123.8 | 136.9 | 129.3 | 162.6 |
| $K_{s2}$ | 130.0 | 120.4 | 114.3 | 174.1 | 196.9 | 150.7 |
| $K_{s3}$ | 117.2 | 144.2 | 99.8 | 172.3 | 157.1 | 170.0 |
| $k_{s1}$ | 30.2 | 24.4 | 41.3 | 45.6 | 43.1 | 54.2 |
| $k_{s2}$ | 43.3 | 40.1 | 38.1 | 58.0 | 65.6 | 50.2 |
| $k_{s3}$ | 39.1 | 48.1 | 33.3 | 57.4 | 52.4 | 56.7 |
| $R_s$ | 13.1 | 23.6 | 8.0 | 12.4 | 22.5 | 6.5 |
| Factor order | B > A > C | | | B > A > C | | |
| Optimisation level | $A_2$ | $B_3$ | $C_1$ | $A_2$ | $B_2$ | $C_3$ |
| Optimum combination | $A_2B_3C_1$ | | | $A_2B_2C_3$ | | |

As shown in Table 4.6, the range analysis was conducted on compressive strength of geopolymer mortar at 28 days. The influence of three factors is different with the early age strength. The results offered information for the design of GPC mixtures. The mechanical properties of GPC were also tested and reported at 28 days in Chapter 5.

Table 4.6 Range analysis on strength at 28 days

| Factor | 28 day compressive strength | | |
|---|---|---|---|
| | A | B | C |
| $K_{s1}$ | 220.5 | 201.1 | 261.4 |
| $K_{s2}$ | 244.6 | 327.6 | 226.8 |
| $K_{s3}$ | 249.7 | 186.1 | 226.6 |
| $k_{s1}$ | 73.5 | 67.0 | 87.1 |
| $k_{s2}$ | 81.5 | 109.2 | 75.6 |
| $k_{s3}$ | 83.2 | 62.0 | 75.5 |
| $R_s$ | 9.7 | 47.2 | 11.6 |
| Factor order | B > C > A | | |
| Optimisation level | $A_3$ | $B_2$ | $C_1$ |
| Optimum combination | $A_3B_2C_1$ | | |

The range analysis of long-term strength was reported in Table 4.7. The strength of some geopolymer mortar cylinders increases steadily from the 3 days to 150 days,

while the strength of some mixtures decreased slightly after 28 days. Further experiments were conducted in Chapter 6 to investigate whether or not conversion happened in the GPC.

Table 4.7 Range analysis on long-term strength

| Factor | 56 day compressive strength | | | 150 day compressive strength | | |
|---|---|---|---|---|---|---|
| | A | B | C | A | B | C |
| $K_{s1}$ | 234.1 | 237.1 | 272.2 | 274.2 | 225.2 | 284.8 |
| $K_{s2}$ | 271.7 | 326.3 | 236.3 | 253.9 | 283.4 | 223.8 |
| $K_{s3}$ | 252.2 | 194.6 | 249.5 | 234.0 | 253.5 | 253.5 |
| $k_{s1}$ | 78.0 | 79.0 | 90.7 | 91.4 | 75.1 | 94.9 |
| $k_{s2}$ | 90.6 | 108.8 | 78.8 | 84.6 | 94.5 | 74.6 |
| $k_{s3}$ | 84.1 | 64.9 | 83.2 | 78.0 | 84.5 | 84.5 |
| $R_s$ | 12.5 | 43.9 | 12.0 | 13.4 | 19.4 | 20.3 |
| Factor order | B > A > C | | | C > B > A | | |
| Optimisation level | $A_2$ | $B_2$ | $C_1$ | $A_1$ | $B_2$ | $C_1$ |
| Optimum combination | $A_2B_2C_1$ | | | $A_1B_2C_1$ | | |

*4.4.2.1 Effect of alkaline solution concentration*

The effect of three parameters on compressive strength has been illustrated in Figure 4.2. In general, high NaOH concentration leads to high average compressive strength at both 7 and 28 days. However, the influence of high NaOH concentration became insignificant as the age increased. The range R reduced by 2.7 MPa as the age increased from 7 to 28 days.

In terms of a 7 day compressive strength, the GPM is very weak when the NaOH concentration is lower than 12 M. Improving NaOH concentration from 10 M to 12 M is able to increase the compressive strength by 27.2%. Strength decreases slightly after the concentration exceeds 14 M. 12 M concentration is the optimum level for compressive strength at 7 days.

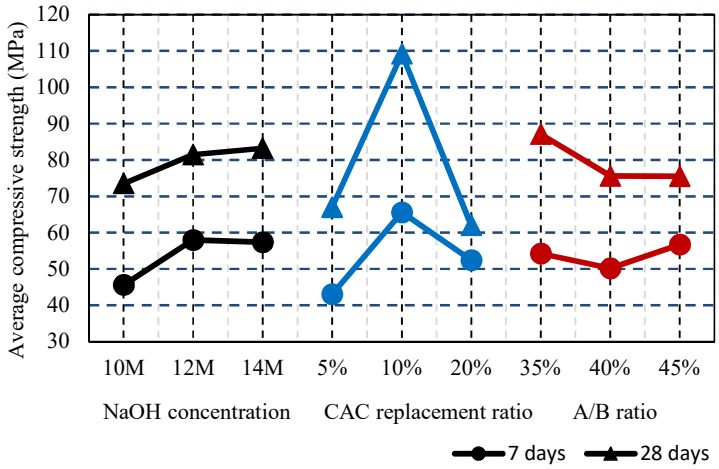


Figure 4.2 Average effect of factors on the compressive strength of geopolymer mortar.

The strength of GPM at 28 days developed with the increase of the NaOH concentration. The average compressive strength of GPM at 28 days is 83.2 MPa when the concentration is 14 M. The optimised level of NaOH concentration for 28 days compressive strength is 14 M.

*4.4.2.2 Effect of calcium aluminate cement replacement ratio*

In general, the CAC replacement ratio is the most important factor for strength development of geopolymer mortar. According to the *k* value, 5% and 20% are not optimal CAC addition ratios. The optimal CAC addition for GPM is 10% for both 7 day and 28 day compressive strength.

In regards to a 7 day compressive strength, 5% and 20% CAC addition contributed to 43.1 MPa and 52.4 MPa of GPM, respectively. However, the average strength of 10% CAC addition geopolymer is 65.6 MPa.

On the 28th day, the level two has the highest compressive strength of 109.2 MPa, while level 1 and level 3 have a strength of 67 MPa and 62 MPa, respectively. The optimised level is 10% CAC addition.

*4.4.2.3 Effect of activator to binder ratio*

Based on the R value, the influence of A/B ratio for 7 day compressive strength of GPM is comparatively small. The optimum level is 45%, which has an averaged result of 56.7 MPa.

The influence of A/B ratio on 28 day compressive strength is different to the influence on 7 day compressive strength. The optimised averaged strength is 87.1 MPa, and its activator to binder ratio is 35%. When the A/B ratio increased to 40% and 45%, the average strength decreased to 75.6 MPa and 75.5 MPa.

### 4.4.3 Optimised mixing design

Table 4.4 provides the factor order for workability, which is in sequence A/B ratio, CAC replacement ratio and NaOH concentration. The optimum combination for workability is $A_1B_1C_3$.

Tables 4.5 - 4.7 contain the range analysis on compressive strength. The factor order for early compressive strength is CAC replacement ratio, NaOH concentration and A/B ratio. However, the factor order for a 28 day result is different, being CAC replacement ratio, A/B ratio and NaOH concentration. The factor order for long term compressive strength is also different. The sequence for 56 day compressive strength is CAC replacement ratio, NaOH concentration and A/B ratio. The sequence for 150 day compressive strength is A/B ratio, CAC replacement ratio and NaOH

concentration. The optimum combinations for 3, 7, 28, 56 and 150 day compressive strengths are $A_2B_3C_1$, $A_2B_2C_3$, $A_3B_2C_1$, $A_2B_2C_1$ and $A_1B_2C_1$, respectively.

The design based on workability is $A_1B_1C_3$ i.e. alkali solution concentration = 10 M, CAC replacement ratio = 5% and activator to binder ratio = 45%. The GPC mixed by this design should have the best workability.

The optimised design which has good workability and good mechanical property is $A_3B_2C_1$ (alkali solution = 14M, CAC replacement ratio = 10% and activator to binder ratio = 35%) with extra water. Alkali solution concentration and CAC replacement ratio are chosen based on compressive strength. The liquid phase of concrete mixture was increased to improve workability, which decreases compressive strength. Considering the cost of the alkaline solution, extra water was added into the aggregate to improve workability.

The design to achieve high compressive strength is concentration of alkali solution = 14M, CAC replacement ratio = 10% and activator to binder ratio = 35% ($A_3B_2C_1$). This concrete mixture will exhibit better compressive strength than others on 28 days.

## 4.5 Summary

This chapter details the study of the influence of CAC on fly ash based geopolymers cured at ambient temperature. Three factors were studied using the Taguchi method. The results of the experiments are summarised below:

1. The presence of CAC is able to help the geopolymerisation reaction at ambient temperature. The mechanical properties of the alkali-activated fly ash blended with CAC are very good. By adding 10% of CAC in fly ash, it is reasonable to

expect a compressive strength of 100 MPa for mortar after being cured for 28 days.

2. Optimisation of geopolymer mixture design can be conducted by the Taguchi method. Alkali solution concentration plays a complex role. Increasing the concentration will improve compressive strength while it will decrease the workability. CAC replacement ratio is the most important factor for the mechanical property. The mechanical property on 28 days is strengthened by adding 10% CAC. Activator to binder ratio is crucial for workability. However, too much activator will diminish the compressive strength. Considering both compressive strength and flowability, the optimal design is 10M alkali solution concentration, 10% CAC replacement and 45% activator to binder ratio.

The Taguchi method is a good tool for analysing the influence of different parameters. In Chapter 5, the three optimal designs will be made to further study the mechanical property of concrete.

# Chapter 5 Behaviour of GPC at Ambient Temperature

## 5.1 Introduction

Using Taguchi method, three optimised geopolymer mix designs were proposed in the preliminary study of Chapter 4. To fully understand the properties of GPC, the performances of three proposed GPCs at ambient temperature are studied in this chapter. Firstly, the workability of fresh GPC is reported, then the mechanical properties such as density, Young's modulus, compressive strength, splitting tensile strength, and flexural strength are investigated. The experimental method of Chapter 3 is followed. Further, the material microstructure characterisations of three geopolymer pastes were conducted to confirm GPC has no risk of conversion. Lastly, the mechanical properties of GPC including Young's modulus, splitting tensile strength and flexural strength were compared with predictions from existing models and a standard prediction equation.

## 5.2 Test results and discussion of GPC

The development of concrete mixtures using the Taguchi method resulted in three mix designs, as shown in Table 5.1. GPC1 is the first optimised design which results in the best workability performance. The alkali solution concentration used in GPC1 is 10 M, and activator to binder ratio is 45% which provides more solution for GPC. The CAC replacement ratio is 5% which decreases the strength of concrete made by GPC1.

The parameters of the second optimised design (GPC2) are $A_1B_2C_3$, which has good workability and mechanical property. The alkali solution, CAC replacement ratio and activator to binder ratio are 14 M, 10% and 35%, respectively. Considering the

cost of alkaline solution, extra water was added to the aggregate to improve the workability. GPC2 achieved a balance between workability and compressive strength.

Table 5.1 GPC mixing proportions

| Label | NaOH pellet (kg) | Water (kg) | Sodium silicate (kg) | Fly ash (kg) | Cement (kg) | CAC (kg) | 20 mm coarse aggregate (kg) | 10 mm coarse aggregate (kg) | Fine aggregate (kg) | Extra water (kg) |
|---|---|---|---|---|---|---|---|---|---|---|
| GPC1 | 0.380 | 0.833 | 3.022 | 8.924 | _ | 0.460 | 9.430 | 11.546 | 11.385 | _ |
| GPC2 | 0.409 | 0.603 | 2.530 | 9.085 | _ | 1.012 | 9.430 | 11.546 | 11.385 | 0.603 |
| GPC3 | 0.488 | 0.722 | 3.022 | 8.464 | _ | 0.943 | 9.430 | 11.546 | 11.385 | _ |

The design to achieve the highest compressive strength is GPC3. The concentration of alkali solution = 14M, CAC replacement ratio = 10% and activator to binder ratio = 35% ($A_3B_2C_1$). This concrete mixture is expected to exhibit better compressive strength than GPC1 and GPC2.

### 5.2.1 Workability of fresh concrete

To justify GPC1 having the best performance in workability, mini-slump tests were conducted on pastes following the same method in Chapter 4. The slump tests on concrete were conducted on mixes of three optimised designs. The slump test method is recommended in ASTM C143, as shown in Figure 5.1.

Figure 5.1 Slump test of fresh GPC

The test results are illustrated in Table 5.2. GPC1 has 210 mm slump test result which is much better than GPC2 and GPC3 on workability. The activator to binder of GPC1 is 45%; by contrast, activator to binder ratio of GPC2 and GPC3 is 35%. However, the slump test of GPC2 is 120 mm because it has extra water compared to GPC3. The test results are compared to results reported by Hardjito and Rangan (2005), and their test results agree well with the current test results.

Table 5.2 Workability test of fresh GPC

| Label | **Workability Test (mm)** | | **Hardjito and Rangan (2005)** |
|---|---|---|---|
| | Mini-slump test for geopolymer paste | Slump test for fresh GPC | Slump test results (mm) |
| GPC1 | 127.5 | 210 | Maximum 215 |
| GPC2 | 122.0 | 120 | Average 135 |
| GPC3 | 95.0 | 55 | Minimum 39 |

### 5.2.2 Density of hardened concrete

The average density of GPC at 28 days is presented in Table 5.3. GPC3 exhibits higher density than GPC1 and GPC2, as the mixture with higher liquid content loses more moisture during the curing process. GPC3 has the highest density because it has the least liquid content. Compared to the results reported by Olivia (2011), the average density tested in this study is higher for 3.1%. The density of GPC is close to a density of conventional concrete in practice, which ranges from 2200-2600 kg / $m^3$.

Table 5.3 Density of hardened GPC

| Label | **Density of GPC at 28 days (kg / $m^3$)** | **Density of GPC (kg / $m^3$) (Olivia, 2011)** |
|---|---|---|
| GPC1 | 2363.4 | Maximum 2336.0 |
| GPC2 | 2368.5 | Average 2291.4 |
| GPC3 | 2371.7 | Minimum 2248.5 |

### 5.2.3 Young's modulus

The measured static elastic modulus was calculated as the secant modulus measured at a stress value corresponding to 40% of the average compressive strength of concrete cylinder specimens. The test data is shown in Table 5.4. The Young's modulus increases as the age increases. GPC2 and GPC3 exhibit similar Young's modulus test results with 10% higher than GPC1. The results obtained are also higher than the results reported by Hardjito and Rangan (2005).

Table 5.4 Young's modulus test results

| Label | Young's modulus (MPa) | | Hardjito and Rangan (2005) |
|---|---|---|---|
| | Test at 7 days | Test at 28 days | Young modulus results (MPa) |
| GPC 1 | 23096 | 30271 | Maximum 30800 |
| GPC 2 | 20138 | 33015 | Average 26800 |
| GPC 3 | 22837 | 32820 | Minimum 23000 |

### 5.2.4 Compressive strength

Compressive strength tests were conducted to justify that the GPC3 mixing design has the best compressive strength. The compressive strengths of GPC are tested after being cured for 7 and 28 days, as shown in Table 5.5. The strength tested at 7 days was around 30 MPa for all three mixtures. After being cured for 28 days, GPC3 reached 61.3 MPa, which is the highest among the three GPC mixtures. Compared with the results tested by Olivia (2011), GPCs cured at elevated temperature in this research are stronger at 28 days, while the early strengths are inferior.

Table 5.5 Compressive strength

| Label | Compressive strength (MPa) | | Olivia (2011) (MPa) | |
|---|---|---|---|---|
| | Test at 7 days | Test at 28 days | Test at 7 days | Test at 28 days |
| GPC 1 | 27.4 | 42.4 | Maximum 52.3 | 54.9 |
| GPC 2 | 30.4 | 55.0 | Average 38.4 | 39.6 |
| GPC 3 | 30.5 | 61.3 | Minimum 27.2 | 29.7 |

The mix design for geopolymer mortar Trial No. 8 had an activator to binder ratio = 35%, concentration of alkali solution = 14 M and CAC replacement ratio = 10%. As can be seen, the mix design was the same as the mix design for GPC3 except the addition of coarse aggregate in GPC3. The compressive strengths of geopolymer mortar Trial No. 8 tested at 7 and 28 days were 73.4 and 118.9 MPa, respectively. In

contrast, the strengths of GPC3 tested at 7 and 28 days were 30.5 and 61.3 MPa. The strength ratios of geopolymer concrete and geopolymer mortar were 41.6% and 51.6% at 7 and 28 days, respectively.

### 5.2.5 Splitting tensile strength

To measure the splitting tensile strength, at least two specimens were tested for each mix at each age, as shown in Table 5.6. GPC3 gained a significant splitting tensile strength increase after being cured for 28 days. GPC1 and GPC2 have gradual increases on the splitting tensile strength with age. Lee and Van Deventer (2004) suggests that high splitting tensile strength is assumed from the improved bonding at the interface of geopolymer paste and aggregate. Pacheco-Torgal et al. (2007) explained that this phenomenon was caused by a chemical interaction between an aggregate and alkaline solution.

Table 5.6 Splitting tensile strength

| Label | **Splitting tensile strength (MPa)** | |
|---|---|---|
| | Test at 7 days | Test at 28 days |
| GPC 1 | 2.59 | 3.64 |
| GPC 2 | 2.66 | 4.25 |
| GPC 3 | 2.52 | 5.78 |

### 5.2.6 Flexural strength

The flexural strengths of GPC were measured using at least two moulded flexural test beams for each mix design. Table 5.7 presents the averaged flexural strengths of GPC compared with the previously considered research (Olivia, 2011).

Table 5.7 Flexural strength

| Label | **Flexural Strength of GPC at 28 days (MPa)** | **Flexural Strength Olivia (2011) (MPa)** |
|---|---|---|
| GPC1 | 4.78 | Maximum 9.91 |
| GPC2 | 5.78 | Average 8.47 |
| GPC3 | 6.02 | Minimum 7.02 |

Similar to splitting strength, GPC3 has a higher flexural strength than the other two GPC mixtures. The flexural strength tested in this research is lower than the strength reported by Olivia (2011). A trend similar to splitting tensile strength can be observed, as high compressive strength leads to a high flexural strength. In contrast to OPC, Lee and Van Deventer reported higher bonding at the interface of geopolymer paste and aggregate, which contributes to the improvement of flexural strength (Lee and Van Deventer, 2004).

## 5.3 Microstructure characterisation of geopolymer pastes

A microstructure study was conducted on geopolymer paste samples. As mentioned in Chapter 3, SEM and TGA experiments were tested using the JEOL 6510LV and a Bruker Vertex 70 coupled with a Netzsch 449C Jupiter DSC-TGA instrument. Three pastes were prepared using the geopolymer paste mixing proportions presented in Table 5.8, which were the same as the three optimised GPC proportions, except for the aggregates.

Table 5.8 Geopolymer paste mixing proportions

| Label | NaOH pellet (kg) | Water (kg) | Sodium silicate (kg) | Fly ash (kg) | CAC (kg) | Extra water (kg) |
|---|---|---|---|---|---|---|

| | | | | | | |
|---|---|---|---|---|---|---|
| GPP1 | 0.380 | 0.833 | 3.022 | 8.924 | 0.460 | _ |
| GPP2 | 0.409 | 0.603 | 2.530 | 9.085 | 1.012 | 0.603 |
| GPP3 | 0.488 | 0.722 | 3.022 | 8.464 | 0.943 | _ |

Firstly, the conversion phenomenon of a CAC structure was explained. A test recommended by Jambunathan et al. (2013a) was conducted on a geopolymer specimen to determine if there was any conversion affecting the compressive strength. Secondly, TGA and differential scanning calorimeter (DSC) experiments were conducted on three geopolymer pastes to further prove three optimised GPC has no risk of conversion. Lastly, the SEM images of some freshly-fractured geopolymer paste samples were examined at the ages of 3 days, 7 days and 28 days.

## 5.3.1 Conversion of CAC

*5.3.1.1 Literature Review*

Conversion is the reaction of unstable hexagonal calcium aluminate hydrates ($CAH_{10}$ or $C_2AH_8$ or $C_4AH_{13}$) converting into stable cubic hydrogarnet ($C_3AH_6$); this reaction is mainly determined by a reaction to temperature. Conversion destructs the material because of increasing porosity. Talabér (1993) concluded the transformation accelerating factors are temperature, water content (high w/c ratio), $CO_2$ content and the presence of alkaline. Ding et al. (1996a) studied the reacting mechanism in a HAC-$Na_2SiO_3$ system and found a small addition of $Na_2SiO_3$ is able to delay $C_3AH_6$ formation, but that inhibition is not able to prevent a conversion reaction.

Puertas et al. (2000) revealed the products of carbonation in the form of CAC is predominantly $CaCO_3$, which leads to a reduction of porosity. Following this, the hydration process of CAC is retarded (or even stopped) when specimens are simultaneously subjected to an accelerated carbonation process. In a nutshell, alkali accelerates carbonation and conversion but it retards hydration, therefore little material is available for the conversion reaction. Ding et al. (1996b) found inorganic salt or alkali is able to inhibit hydrogarnet ($C_3AH_6$): for example, sodium salts, sodium nitrate, sodium chloride, sodium sulphate, and sodium metaphosphate. If conversion happened in CAC concrete, inorganic salt or alkali can be added to restrain the conversion reaction.

In this study, a small portion of CAC was added into GPC binder. Further studies need to be undertaken to ascertain whether or not the conversion phenomenon will occur, by microstructure characterisation.

*5.3.1.2 Conversion Test*

To study the influence of potential conversion of CAC to geopolymer, four geopolymer mortar specimens were cast and two of them were cured at 50°C with 26% humidity for 24 hours before the test, as shown in Figure 5.2. According to Jambunathan et al. (2013a), after exposure to 50°C, some hydration products of alkali-activated ground-granulated blast-furnace slag pastes convert to $C_3AH_6$, leading to a rapid deterioration in the strength of the paste.


Figure 5.2 Conversion curing temperature and humidity

The compressive strength test results, before and after the conversion processing, are presented in Table 5.9. The geopolymer specimens after conversion processing lose 0.9% of the original compressive strength, which illustrates that conversion, if any, is insignificant for GPC.

Table 5.9 Conversion test

| **Compressive strength(MPa)** | | | | **Degradation percentage** |
|---|---|---|---|---|
| Control group (56-day-curing) | | Conversion test (56-day-curing) | | |
| 84.7 | 79.8 | 80.1 | 83.0 | 0.9% |

In conclusion, the material may not degrade, however, if it does, the impact can be disregarded for the following reasons: the $Na_2SiO_3$ in reaction environment of CAC will postpone the conversion reaction (Ding et al., 1996a), and from the GPC mixing design recorded, CAC contributes small proportion to the GPC raw materials. The GPC using CAC could act just like alloy, which displays only the best property of the constituents.

### 5.3.2 Thermal gravimetric analysis (TGA)

After a conversion test, the result of TGA was reported. The samples were heated to 800°C at the rate of 10 °C/min with ultra-high purity nitrogen ($N_2$) as protection gas. As mentioned, conversion is the reaction of unstable hexagonal calcium aluminate hydrates ($CAH_{10}$ or $C_2AH_8$ or $C_4AH_{13}$) converting into stable cubic hydrogarnet ($C_3AH_6$).

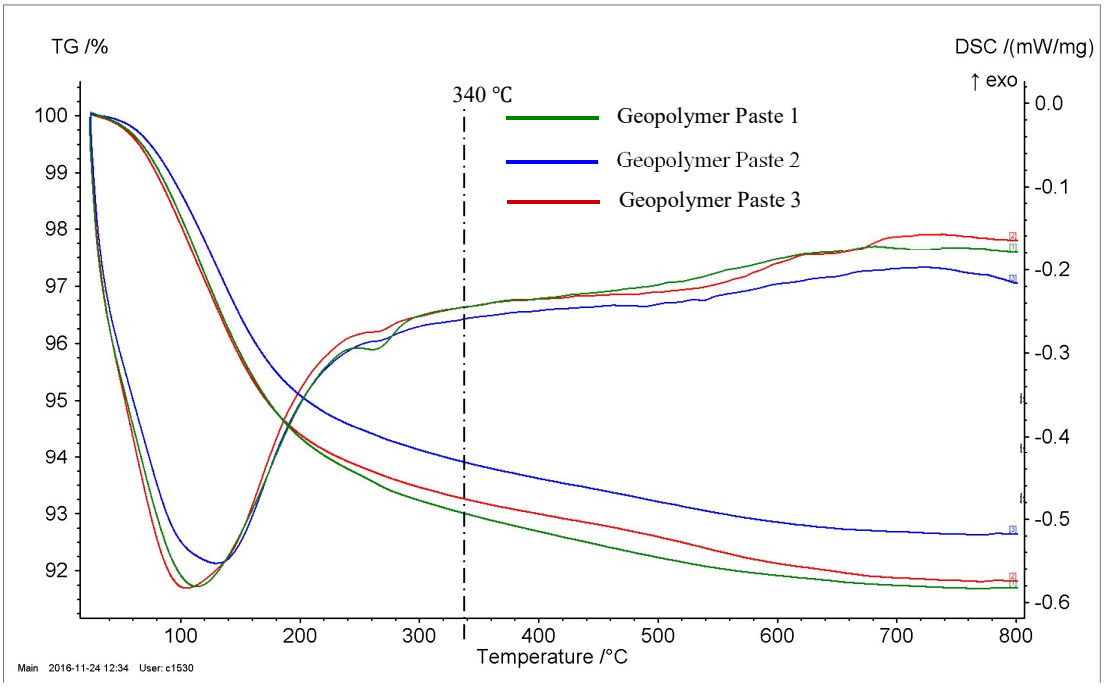


Figure 5.3 TGA results of geopolymer pastes

According to the research conducted by Reig et al. (2016) and Pacewska et al. (2011), the signal of $C_3AH_6$ cubic compounds will appear at around 340 °C. The test results are shown in Figure 5.3. However, no signal appeared in all three of our test results which indicates negligible or no $C_3AH_6$ was detected. Cubic katoite ($C_3AH_6$) is a hexagonal hydrate and it contributes to the conversion of CAC material.

The test results are in accordance with research findings reported by Fernández‐Jiménez et al. (2008b), who proposed the alkali-activated CAC blended with metakaolin does not contain a normal CAC hydration product. Further, Shi et al. (2011) pointed out that alkali-activated CAC blended with other cement does not undergo a normal hydrating process; the product is (N,C)-A-S-H or C-A-S-H which is derived from N-A-S-H taken Al or Ca.

### 5.3.3 Scanning electron microscopy (SEM) analysis

*5.3.3.1 Sample Preparation*

In order to study the microcracks of geopolymer paste, some freshly-fractured samples were broken into small pieces for observation in SEM, as shown in Figure 5.4. There was a carbon conductive tab between the bottom of the sample and surface of the holder, which was used to reduce the vibration of the sample under observation.

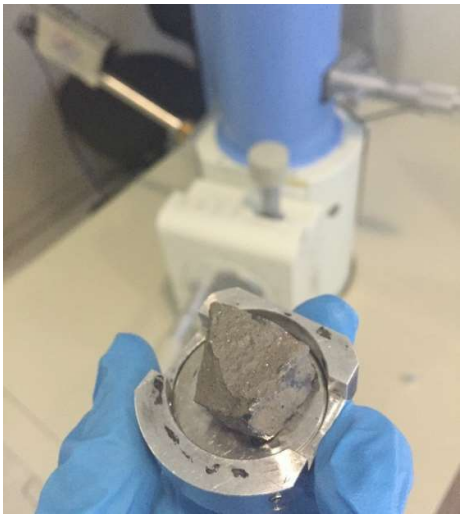

Figure 5.4 Geopolymer paste sample for SEM

*5.3.3.2 Microstructure at Early Ages*

Early age SEM results of paste at 3 days and 7 days are shown in Figure 5.5. GPP1 demonstrates that the section of geopolymer paste is very loose at 3 days, which could be caused by the low NaOH concentration. After being cured for 7 days, the matrix became solid, but it was still looser than GPP2 and GPP3. GPP2 and GPP3 are very similar to each other; however, a sizeable amount of part-solved fly ash can be found in GPP3 at 3 days. GPP2 is more solid than GPP3, and the 3-day compressive strength of GPP2 could be stronger than GPP3. At the age of 7 days, fewer unsolved fly ash can be found in the GPP2 and GPP3 matrix. However, minor cracks appeared on the surface because the matrix used up the solution.

As previously discussed, GPP1 has more activator solution than GPP2 and GPP3 after casting. No major crack was observed in GPP1 after 3 days. Minor cracks were observed in GPP2 after 3 days. By comparison, several cracks—including a major crack—was observed in GPP3 after 3 days. The SEM images illustrate the liquid content of GPP1 was still more than GPP2 and GPP3 after being cured for 7 days. By comparing GPP2 and GPP3, more unreacted fly ashes can be found in GPP2 which means the matrix of GPP2 is weaker than GPP3. The mechanical properties of GPC have proven the assumption.

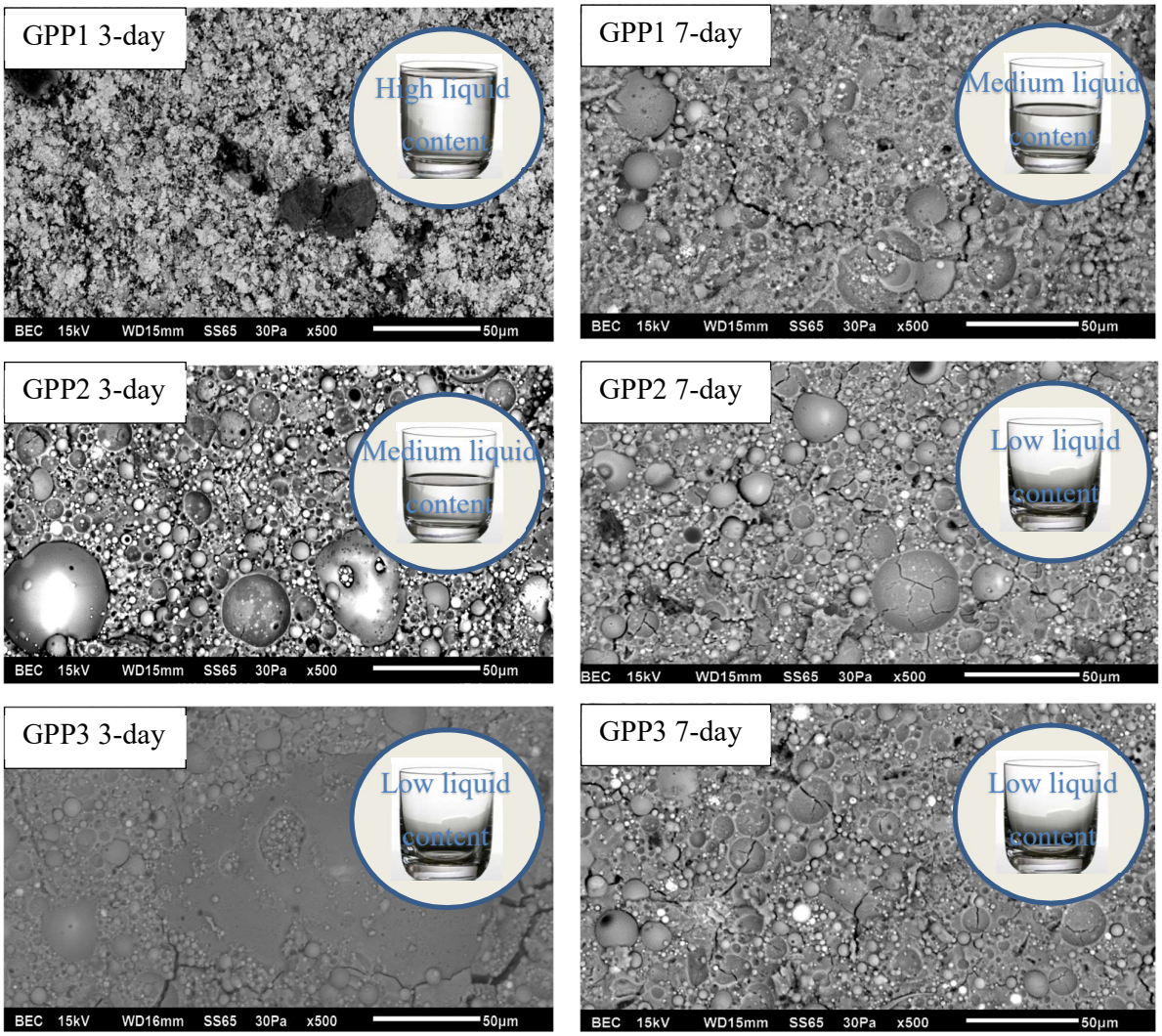


a) 3 day SEM results b) 7 day SEM results

Figure 5.5 SEM images of pastes at a) 3 days and b) 7 days

*5.3.3.3 Microstructure at 28 days*

The SEM images of geopolymer pastes at 28 days are reported in Figure 5.6, showing after 28 days of curing, GPP1 lost more liquid content and a major crack formed. The microcracks in GPP1 caused the decrease in strength of GPC1. On the contrary, GPP2 and GPP3 contained very low liquid content after being cured for 7 days, and fewer cracks were observed after 28 days. The liquid content determines the

strength development of GPC; this assumption is able to explain why GPC2 and GPC3 are stronger at 28 days, while GPC1 has the same strength at 7 days.

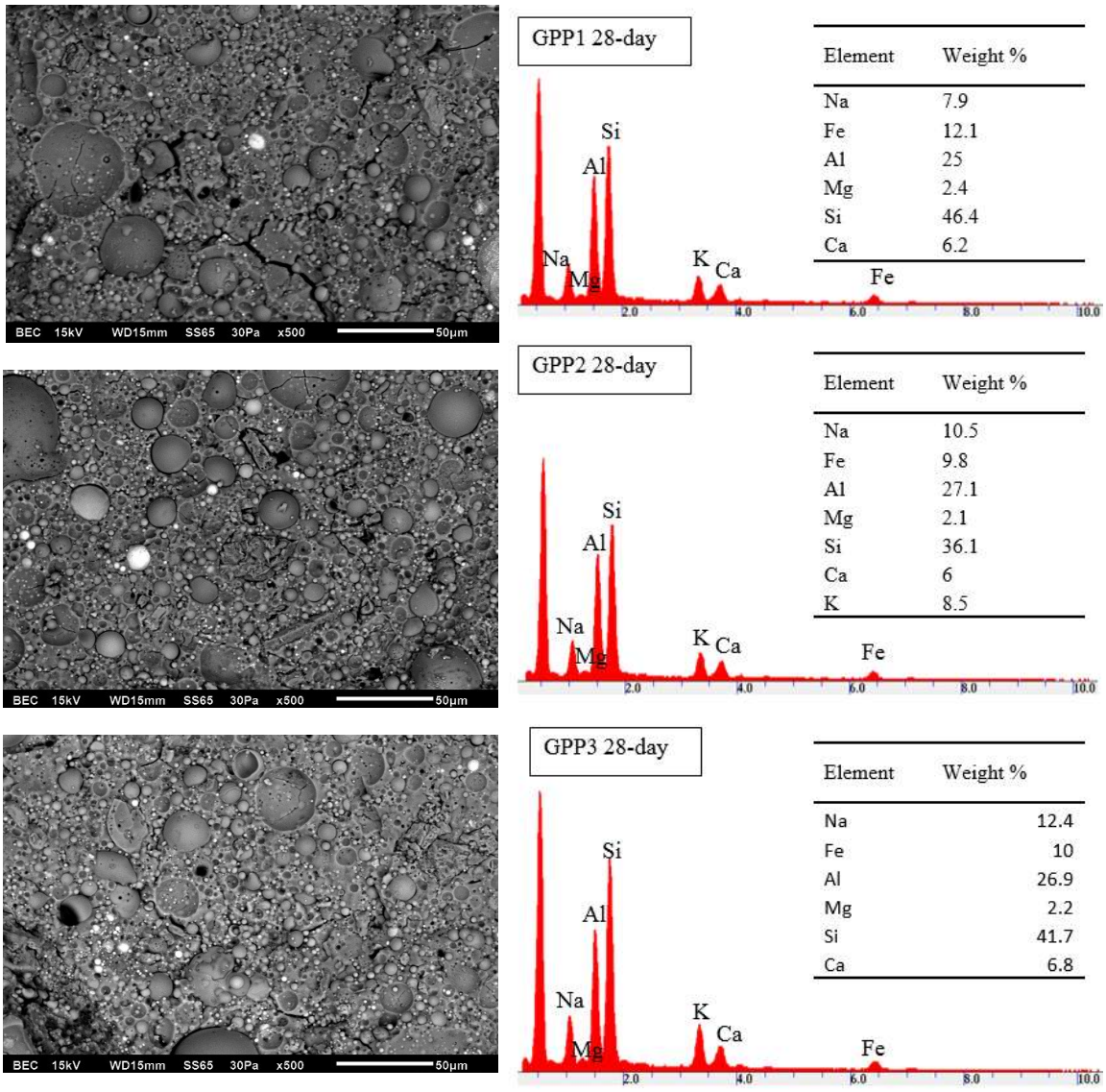


Figure 5.6 SEM images and EDS results of pastes at 28 days

The Energy-dispersive X-ray spectroscopy (EDS) result shows a similar composition of the geopolymer pastes. However, a slight change in the composition can lead to different mechanical properties of GPC. GPP3 has more Na, Si and Ca than GPP1 and GPP2. The high content of Na is caused by the high concentration of alkaline solution.

GPP1 has smaller unreacted fly ash and major cracks. GPP2 and GPP3 have a denser microstructure than GPP1 and less unreacted fly ash. A large amount of unreacted fly ash is responsible for the inferior strength of GPC1.

## 5.4 Comparison of experimental results with existing models

### 5.4.1 Comparison of Young's modulus

The elastic modulus is commonly expressed in terms of compressive strength for OPC using empirical equations. The elastic modulus was compared with the prediction of OPC concrete empirical equations provided by AS 3600-2009 (2009) and ACI 318-14 (2015). The comparison between existing models and test data are shown in Figure 5.7, where the data points are shown as solid triangles.

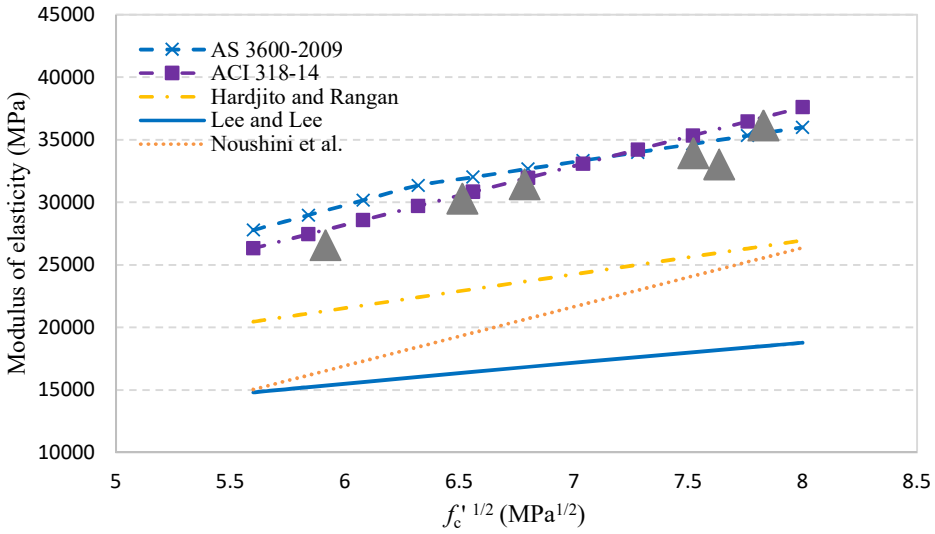


Figure 5.7 Relationship of modulus of elasticity with compressive strength

For concrete strength up to 65 MPa, the Australia standard 3600-2001 recommends:

$$E_c = 0.043 \times \rho^{1.5} \times \sqrt{f_c'}\ (\text{MPa}) \quad (5.1)$$

to calculate the elasticity, where $\rho$ is the density of concrete which is 2370 kg / m$^3$ on average for GPC. The $f_c'$ is the mean value of compressive strength. The predicted result of $E_c$ has an error of plus or minus 20%. The prediction usually overestimates the elastic modulus of concrete. AS 3600-2009 proposed another model for strength, higher than 40 MPa, as shown in Eq. (5.2). In this research, Eq.(5.1) is used for $f_c' \leq 40$ MPa, and Eq. (5.2) is used when $f_c' \geq 40$ MPa

$$E_c = \left[0.024 \times \sqrt{f_c'} + 0.12\right] \times \rho^{1.5} \text{ (MPa)} \tag{5.2}$$

According to the ACI 318-14 building code, the elastic modulus of concrete (normal weight) stronger than 21 MPa at 28 days can be calculated from the following expression:

$$E_c = 4700 \times \sqrt{f_c'} \text{ (MPa)} \tag{5.3}$$

Hardjito and Rangan (2005) proposed the following equation to calculate the elastic modulus for GPC:

$$E_c = 2707 \times \sqrt{f_c'} + 5300 \text{ (MPa)} \tag{5.4}$$

Lee and Lee (2013) summarised the results of GPC from Sofi et al. (2007) and Fernandez-Jimenez et al. (2006); the following prediction equation was proposed based on these results:

$$E_c = 4700 \times \sqrt[3]{f_c'} \tag{5.5}$$

Noushini et al. (2016) tested 195 GPC concrete cylinders and proposed an expression to predict the elastic modulus of GPC.

$$E_c = 2707 \times \sqrt{f_c'} - 11400 \text{ (MPa)} \tag{5.6}$$

The elastic modulus for geopolymer is commonly lower than its OPC counterpart which has been reported in the studies (Pan et al., 2011). The prediction equation of GPC on elastic modulus is also lower than code prediction; however, it cannot be concluded that alkali activated fly ash reduced the strength, because the elastic modulus of concrete is mainly affected by the amount and type of coarse aggregate (Lee and Lee, 2013). According to the comparison of predictions from Eq. (5.1-5.6), the prediction made by ACI 318-14 (2015) is more accurate for the current GPC samples. The most accurate prediction among former research on the elastic modulus was made by Hardjito and Rangan (2005), which is very close to the prediction in ACI 318-14 (2015).

### 5.4.2 Comparison of splitting tensile strength

Measured splitting tensile strengths were compared with the predictions of AS 3600-2009 (2009), ACI 318-14 (2015) and Eurocode 2 (2004). The comparison is plotted in Figure 5.8.

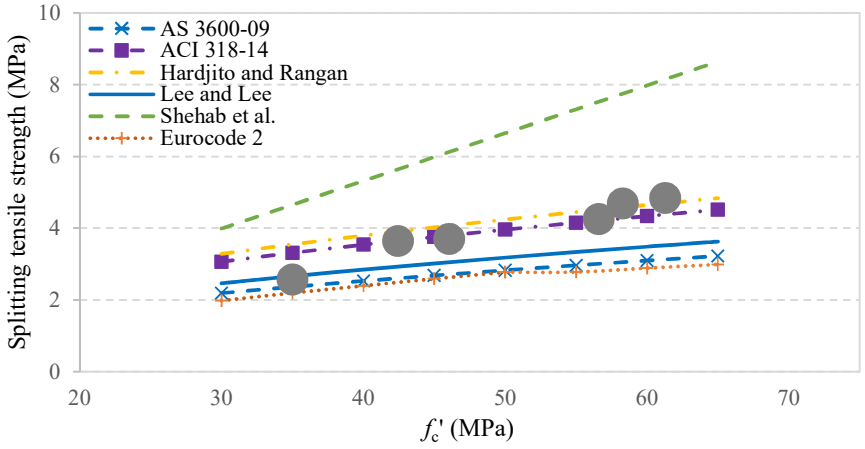


Figure 5.8 Relationship of splitting tensile strength with compressive strength

Tensile strength is also expressed as a function of compressive strength using empirical relations in codes. In AS 3600-2009 (2009), the relationship between compressive strength and splitting tensile strength is expressed as follows:

$$f_{ct} = 0.4 \times \sqrt{f_c'}, f_c' \leq 65\text{MPa} \tag{5.7}$$

The average splitting tensile strength $f_{ct}$ is predicted in ACI 318-14 (2015) as:

$$f_{ct} = 0.56 \times \sqrt{f_c'} \tag{5.8}$$

$f_c'$ is specified compressive strength of concrete. According to Eurocode 2, the relationship between the tensile strength $f_{ct}$ can be expressed in the following:

$$f_{ct,0.05} = 0.7 \times 0.3 \times f_c'^{2/3} \text{ 5\% fractile, } f_c \leq 50\text{MPa} \tag{5.9}$$

And

$$f_{ct,0.05} = 0.7 \times 2.12 \times \ln(1 + f_c'/10) \text{ 5\% fractile, } f_c > 50\text{MPa} \tag{5.10}$$

Hardjito and Rangan (2005) proposed a formula to predict the splitting tensile strength of GPC:

$$f_{ct} = 0.6 \times \sqrt{f_c'} \tag{5.11}$$

where $f_c'$ is the averaged compressive strength of concrete. Lee and Lee (2013) tested six mixing designs of GPCs and proposed a new model.

$$f_{ct} = 0.45 \times \sqrt{f_c'} \tag{5.12}$$

Shehab et al. (2016) reported results from 54 GPC cylinders. A new relation between the average compressive strength and splitting tensile strength was proposed:

$$f_{ct} = 0.133 \times f_c' \tag{5.13}$$

It is observed in Figure 5.7 that all the measured strengths are constantly higher than the prediction by AS 3600-2009 (2009) and Eurocode 2 (2004), while ACI 318-14 (2015) demonstrated better accuracy than AS 3600-2009 (2009) and Eurocode 2 (2004). Hardjito and Rangan (2005) proposed an accurate expression to predict the splitting tensile strength of GPC. The prediction made by Shehab et al. (2016) severely overestimates the splitting tensile strength of GPC. Lee and Lee (2013) reported most measured splitting tensile strengths are lower than the predictions by the codes, while the predictions made by Lee and Lee (2013) underestimates splitting tensile strength. The higher tensile strength can be explained due to the stronger connection between aggregate and geopolymer binder Nguyen et al. (2016).

### 5.4.3 Comparison of flexural strength

The average flexural strengths were reported in Figure 5.9 with respect to the square roots of their compressive strengths.

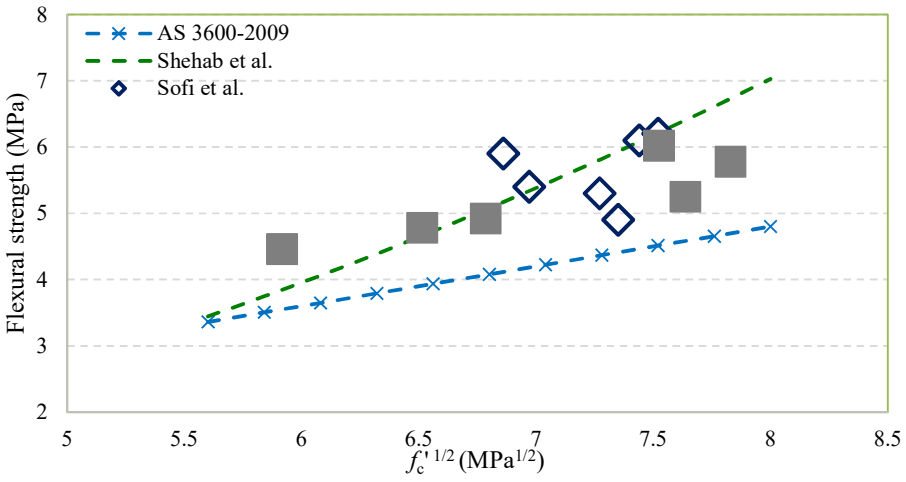


Figure 5.9 Relationship of flexural strength with compressive strength

The Australia standard AS 3600-2009 (2009) provides the estimation of the flexural strength of OPC concrete using the following equation:

$$f'_{cf} = 0.6 \times \sqrt{f'_c} \quad (5.14)$$

Shehab et al. (2016) reported a new relation between average compressive strength and flexural strength for GPC concrete, which is proposed as the following:

$$f_t = 0.1098 \times f_c' \quad (5.15)$$

The measured flexural—along with the previous study on flexural strength of inorganic polymer concrete conducted by Sofi et al. (2007)—are compared to AS 3600-2009 (2009) and the expression provided by Shehab et al. (2016). Similarity can be found between splitting tensile strength and flexural strength. As the flexural strength results show in Figure 5.9, GPC exhibits considerably better performance than OPC, which is attributed to the supreme structural strength of geopolymer matrix (Sofi et al., 2007). On average the flexural strengths of GPC are 1MPa higher than the standard model line for OPC. The predicting expression proposed by Shehab et al. (2016) exhibits good accuracy compared to the test results.

## 5.5 Summary

This chapter details the studies of the mechanical properties of three proposed GPCs at ambient temperature. These properties include density, Young's modulus, compressive strength, splitting tensile strength, and flexural strength. To justify that GPC has no risk of conversion, the material microstructure characterisations and compressive strength test of three geopolymer pastes were conducted. Lastly, the mechanical properties of GPC, including Young's modulus, splitting tensile strength and flexural strength, were compared with existing models and standard prediction equations. A good agreement was found between the test results and ACI 318-14 (2015)

prediction expressions for Young's modulus and splitting tensile strength, while Shehab et al. (2016) reported an accurate expression to calculate flexural strength.

# Chapter 6 Performance of GPC at elevated temperatures

## 6.1 Introduction

Concrete is known to be a fire-resistant material; however, while conventional concrete uses OPC as a binding material, the binder suffers severe damage under fire conditions. Due to increasing populations, high rise buildings have become prevalent in megacities. Extremely high residential density has increased the probability of fire outbreaks, as well as the severity of the aftermath. The threat of fire has raised researchers' interest in studying fire-resistant binders, as such geopolymer has been considered as a promising alternative to OPC in construction applications.

GPC has better fire performance than OPC because of the ceramic-like properties of alkali aluminosilicate binding materials. The properties of geopolymers are dependent on compositions of raw material. Regarding compositions, $Al_2O_3$, $SiO_2$, and the calcium content have an important role in determining the mechanical properties and fire performance. Some researchers have found the addition of CAC (Cao et al., 2016b), OPC (Nath and Sarker, 2015) or GGBFS (Khan et al., 2016b) is able to improve the mechanical properties at an ambient temperature. These three additions are considered as a solution for curing geopolymers at an ambient temperature. However, the addition of OPC introduces the hazard of spalling into geopolymer under high temperatures, while the GGBFS blended geopolymer was reported to have a strength decrease when exposed to temperatures of 50 °C and above (Jambunathan et al., 2013b). In contrast, CAC is known for its high early strength and fire performance. While the mechanical properties of geopolymer blended with CAC

at an ambient temperature were studied in Chapter 5, this chapter will focus on the study of elevated temperature performance of GPC.

Hot strengths of nine geopolymer mortars (GPM) tested at 600 and 800 °C are reported and analysed firstly. The crack patterns of GPMs under fire are compared to typical failure patterns proposed by ASTM C39 (ASTM, 1996). Analysis is undertaken of the influence of three different factors, including activator concentration, CAC replacement ratio, and activator to binder ratio, on the hot strength of GPM.

In order to investigate the fire performance of GPC, the hot strength of GPC under high temperatures is reported, using the slow heating rate. The hot strengths of GPC after exposed to different high temperatures are compared with those of OPC, including 23, 200, 400, 600 and 800 °C. The deformation of GPC under combined loading and a high temperature is studied, while the rapid heating rate has been implemented. Lastly, the residual properties of GPC—such as residual density and stress-strain relationship after exposed to 800 °C—are reported and compared with those of OPC concrete.

## 6.2 Performance of geopolymer mortar at elevated temperatures

### 6.2.1 Specimen preparation

Raw materials (fly ash and CAC) and sand were dry-mixed in a mixer for 3 minutes before the alkali activator was added. The mixing proceeded for 4-6 minutes until the mixture formed a homogenous slurry. The fresh mortar was cast into 60 × 180 mm cylinder moulds in three layers. A vibrating table was working all the process of casting fresh mortar into moulds. Each layer was kept vibrating for 15 to 30 seconds to chase the bubbles out. The specimens were demoulded after one day and cured at a

constant room temperature with vacuum bags. A CIVILAB core facing grinder was employed to grind both ends of each cylinder to achieve smooth and flat surfaces.

Three factors (activator concentration, CAC replacement ratio, activator to binder ratio) at three levels were investigated with nine mixture designs. These three factors were designed from the knowledge of preliminary experiments. The sodium silicate to sodium hydroxide ratio was kept constantly at 2.5, similarly to the activator discussed in Chapter 4. The key factors of the nine mixture designs are shown in Table 6.1.

Table 6.1 Orthogonal experimental factors

| Level | Experimental factor | | |
|---|---|---|---|
| | A | B | C |
| | Alkaline solution concentration | CAC replacement ratio | A/B ratio |
| 1 | 10 M | 5% | 35% |
| 2 | 12 M | 10% | 40% |
| 3 | 14 M | 20% | 45% |

### 6.2.2 Test method

After 28 days of curing, compression and fire performance tests were conducted. The mortar cylinders (GPM) were tested by an hydraulic loading jack with a vertical tube furnace testing machine, in accordance with the requirement in ASTM C39 (ASTM, 1996). The loading rate was 0.25 ± 0.05 MPa/s. The testing was conducted in the Structural Research and Testing Laboratory at Western Sydney University. The cross-sectional area of each cylinder was measured to calculate the stress before the test.

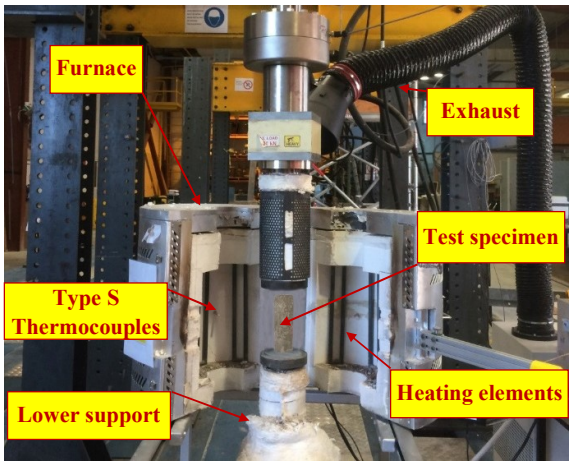


Figure 6.1 Setup of GPM fire test

As shown in Figure 6.1, a hydraulic loading jack, which had 1000 kN capacity, was located at the top of the vertical tube furnace. The steel casing was installed after the cylinder sample was steadily put on the lower holder. Following this, the furnace temperature was increased to the target temperature of 600 or 800 °C with a heating rate of 5 °C/min. To investigate the ultimate strength of GPMs in a hot state, the hydraulic jack started loading when the furnace had held the target temperature for 2 hours. Two specimens were conducted in the same condition to get an average compressive strength. The furnace was cooled naturally to an ambient temperature to avoid thermal shock.

## 6.2.3 Test results

*6.2.3.1 Visual appearance*

After 28 days of curing, the GPM specimen was dark grey in appearance. Once heated at 600 °C for 2 hours, the colour turned light grey, whereas at 800 °C the sample turned yellow ochre. After the target temperature was maintained for 2 hours, the GPM specimens were loaded during an elevated temperature exposure.

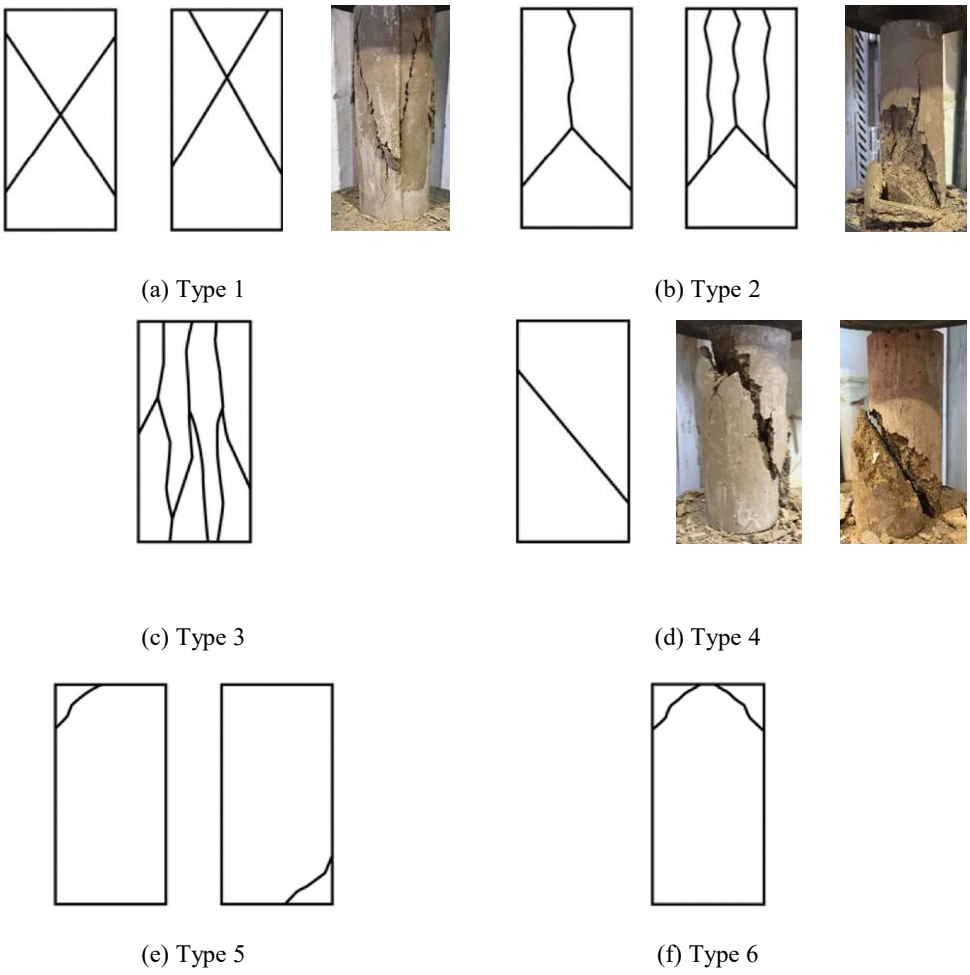

(a) Type 1 (b) Type 2

(c) Type 3 (d) Type 4

(e) Type 5 (f) Type 6

Figure 6.2 Typical fracture patterns of specimens during elevated temperature exposure

Figure 6.2 presents the crack patterns of the specimens after compressive strength testing for high temperature exposure. The crack patterns are compared with typical fracture patterns defined in ASTM C39 (ASTM, 1996). Type 1 was discovered to be very common in GPMs: reasonably well-formed cones on both ends, less than 25 mm cracking through caps. Type 2 was least common among the three fracture patterns that appeared: well-formed cone on one end, no well-defined cone on the other end, vertical cracks running through caps. Type 4 was the most common fracture pattern in GPM specimens exposed to high temperature: diagonal fracture with no cracking through ends (tap with a hammer to distinguish from Type 1). No Type 3 fracture pattern was observed among all the specimens recorded: columnar vertical cracking through both ends, no well-formed cones. Neither Type 5 or Type 6 fracture patterns were observed in GPM samples. In conclusion, GPM was easier to form cones or diagonal fracture. Vertical cracks were observed less than shear failure cracks.

*6.2.3.2 Hot strength*

The results were calculated based on at least two samples after being cured for 28 days. A third specimen was tested if the deviation exceeded 5%, which was a rare condition. Table 6.2 shows the compression testing results of different GPM mixes at 23, 600 and 800 °C. The average strength at ambient temperature was 79.4 MPa, while the strength tested at 600 and 800 °C were 33.0 MPa and 48.1 MPa, respectively. The compressive strength of geopolymer blended with CAC tested at a high temperature was lower than its ambient temperature strength.

In general, GPM exhibited ideal mechanical properties and fire resistance. After being exposed to 600 °C for two hours, the strength of OPC mortar specimens decreased by 58.4% on average, while geopolymer subjected to 800 °C decreased only

39.4% of ambient compressive strength. In a temperature range of 600 to 800 °C, the geopolymer samples regained their strength, indicating a phase transformation took place in this temperature range; further research is required to provide evidence for such transformations.

Table 6.2 Compressive strengths of GPMs at different temperatures

| Mixture No. | Mixture factors | | | Compressive strength (MPa) | | | | |
|---|---|---|---|---|---|---|---|---|
| | Activator concentration | CAC replacement ratio | Activator/binder ratio | 23 °C | 600 °C | | 800 °C | |
| 1 | 10 M | 5% | 35% | 62.5 | 26.4 | 42% | 52.9 | 85% |
| 2 | 10 M | 10% | 40% | 107.6 | 25.8 | 24% | 58.5 | 54% |
| 3 | 10 M | 20% | 45% | 50.4 | 40.9 | 81% | 23.1 | 46% |
| 4 | 12 M | 5% | 40% | 63.5 | 23.1 | 36% | 58.1 | 91% |
| 5 | 12 M | 10% | 45% | 101.1 | 26.2 | 26% | 41.1 | 41% |
| 6 | 12 M | 20% | 35% | 80.0 | 49.5 | 62% | 38.5 | 48% |
| 7 | 14 M | 5% | 45% | 75.1 | 25.6 | 34% | 55.4 | 74% |
| 8 | 14 M | 10% | 35% | 118.9 | 31.2 | 26% | 67.7 | 57% |
| 9 | 14 M | 20% | 40% | 55.7 | 48.6 | 87% | 38.0 | 68% |

At an ambient temperature, the highest compressive strength achieved was 118.9 MPa in Mix 8, which was two times more than Mix 3, the weakest mixture. At 600 °C, the highest compressive strength was 49.5 MPa (Mix 6), while the highest strength retention ratio was 87.3% (Mix 9). The highest strength of specimens tested at 800 °C was 67.7 MPa (Mix 8), and the best strength retention ratio was 91.5% (Mix 4).

### 6.2.4 Parameter analysis on hot strength

The variations of compression results regarding the three key factors are shown in Figures 6.3-6.5. Most of the samples exhibit lower strength at 600 °C than at 800

°C. However, GPM with 5% CAC at 600 °C had a higher strength than at 800 °C. The following parameter analysis is conducted by changing one factor while keeping two other factors consistent; the compressive strength of heated geopolymer is normalised by its ambient temperature strength. The test result of one level is the averaged compressive strength of three results, and three levels of other two parameters all appear once. For example, the compressive strength result of 12 M is calculated from mixing design numbers 4, 5 and 6, while 14 M parameter is the averaged value of mixing design numbers 7, 8 and 9.

*6.2.4.1 Activator concentration*

As shown in Figure 6.3 (a), the compressive strength of geopolymer mortar increased as the alkali activator concentration increased before fire exposure. Geopolymer specimens with 14 M concentration had higher compressive strength than other specimens. At 800 °C, the strength increase of 14 M geopolymer was as high as 18.6%, compared with 10 M and 12 M geopolymers.

Strength ratios of different geopolymer samples at specific temperatures were almost identical. The results in Figure 6.3 (b) show the strength of geopolymer decreased by 60% when heated to 600 °C, while the strength decrease was only about 40% for geopolymers heated at 800 °C.

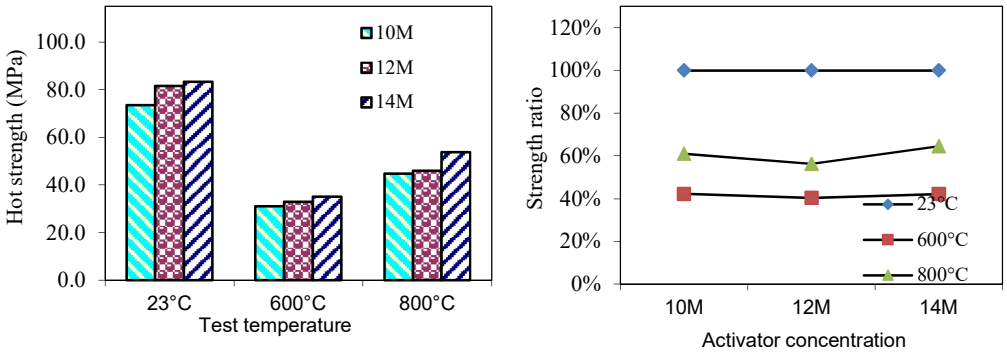


(a) Compressive strength vs. activator concentration

(b) Strength ratio vs. activator concentration

Figure 6.3 Influence of activator concentration

*6.2.4.2 CAC replacement ratio*

CAC replacement ratio is the most important parameter on the fire performance of geopolymer mortar, as shown in Figure 6.4 (a). The geopolymer mortar with 10% CAC exhibited the highest compressive strength at an ambient temperature. Geopolymer with 5% CAC had the lowest compressive strength of 25 MPa when under fire conditions. The compressive strength of geopolymer at 800 °C was higher than the strength at 600 °C when the CAC addition was 5%.

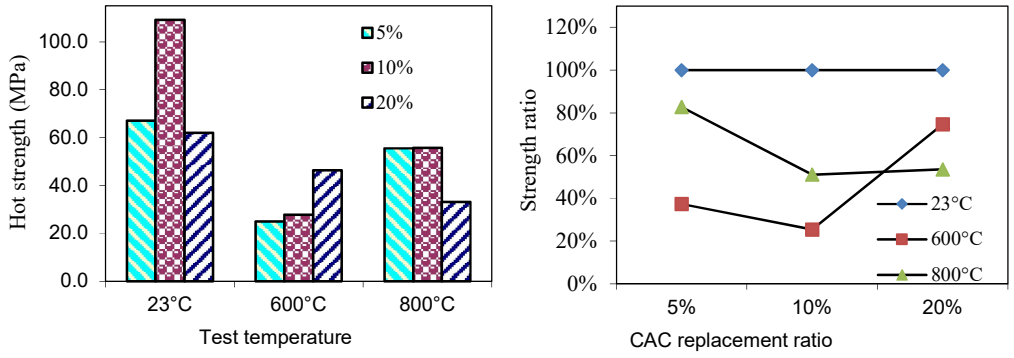


(a) Compressive strength vs. CAC replacement ratio

(b) Strength ratio vs. CAC replacement ratio

Figure 6.4 Influence of CAC replacement ratio

As can be seen from the results in Figure 6.4 (b), geopolymer with 20% CAC only decreased 15.3% in compressive strength at 600 °C, while 46.5% of strength was lost

at 800 °C. The addition of 5% CAC improved the fire performance of geopolymer at 800 °C, as it maintained an 82.7% compressive strength in contrast to the strength results tested at room temperature.

*6.2.4.3 Activator to binder ratio*

Increasing liquid content in geopolymer mortar caused the decrease of strength at all temperatures. For specimens tested at 23 and 600 °C, the average strengths dropped 15.4% and 15.5%, respectively, when the activator content was increased from 35% to 45%. Meanwhile, the strength loss increased 33.0% for geopolymer exposed to 800 °C, as shown in Figure 6.5 (a).

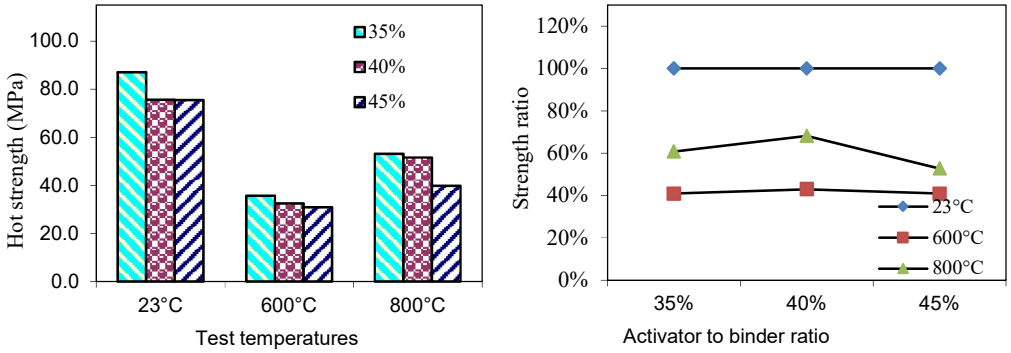


(a) Compressive strength vs. activator to binder ratio

(b) Strength ratio vs. activator to binder ratio

Figure 6.5 Influence of activator to binder ratio

Changing the activator to binder ratio had a negligible influence on the strength ratio of geopolymers at 600 °C, which was around 41% of that at ambient temperature, see Figure 6.5 (b). At 800 °C, the relative changes of strength—for geopolymers with activator contents ranging from 35% to 45%, were 60.7%, 68.2% and 52.8%, respectively.

## 6.3 Performance of GPC at elevated temperatures

### 6.3.1 Hot strength

In this section investigations are conducted on the hot strength of GPC at temperatures ranging from 23 to 800 °C. Furthermore, reference OPC samples with similar strength are tested under the same conditions. The GPC and OPC mixing designs are shown in Table 6.3. Extra water was added into the GPC mixture to improve workability.

Table 6.3 Concrete mixing proportions (kg/m$^3$)

| Label | NaOH pellet | Water | Sodium silicate | Fly ash | Cement | CAC | 20 mm coarse aggregate | 10 mm coarse aggregate | Fine aggregate | Extra water |
|---|---|---|---|---|---|---|---|---|---|---|
| GPC | 19.6 | 29.0 | 121.6 | 437.8 | _ | 48.6 | 501.4 | 612.8 | 600.0 | 29.0 |
| OPC | _ | 220.0 | _ | _ | 400.0 | _ | 459.0 | 561.0 | 680.0 | _ |

As shown in Figure 6.6, CAC geopolymer concrete exhibited a better fire performance than the OPC at all temperatures. The strength reduction of concrete was calculated by dividing the strength at the elevated temperature to the initial strength (at ambient temperature).

By comparing the relative changes in strength, it was found that geopolymer had much higher strength than OPC at 200 and 800 °C. The strength decrease at 200 °C was accounted for an increase in porosity caused by water evaporation. The geopolymer also had a mild drop of strength at 400 °C which was possibly caused by the evaporation. At the temperature of 800 °C, the strength of geopolymer dropped

slowly because of the ceramic-like property of matrix. Some researchers even reported strength gain of geopolymers at high temperatures (Pan et al., 2009). However, OPC exposed to 800 °C suffered a severe decrease in the mechanical properties which was likely due to the chemical decomposition of its matrix. OPC and GPC have similar performance at 400 °C. The hot strength of GPC increased slight after 400°C. By comparison, the hot strength of OPC decreased severely at 600 and 800 °C.

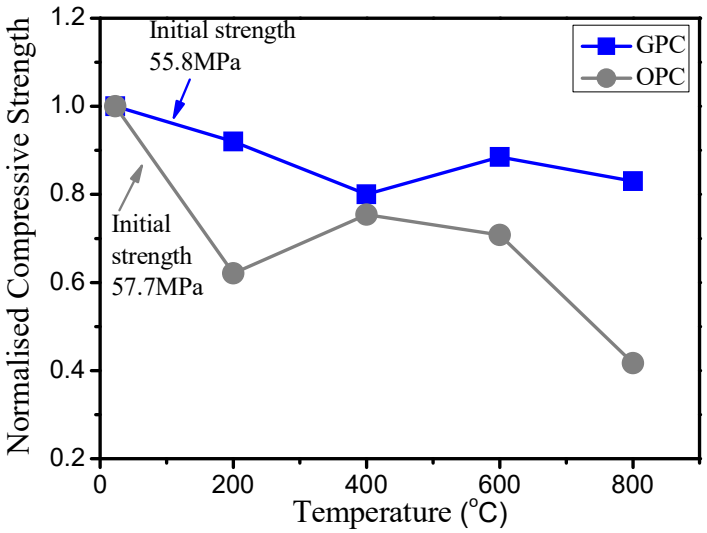


Figure 6.6 Hot strength of concrete

In general, GPC exhibited better fire performance than OPC among the whole range of temperatures, owing to the matrix of geopolymer which was much more stable and durable than OPC.

## 6.3.2 Deformation of GPC at high temperature under constant load

*6.3.2.1 Test result*

A rapid heating regime was implemented to study the deformation of GPC under combined loading and high temperature. A constant axial load was applied (40% of ultimate strength) on the cylinder for the first stage. In the second stage, the

temperature was increased to 800 ℃ according to the rapid heating rate, then the oven was kept at this temperature until failure of the sample. Results are shown in Figure 6.7.

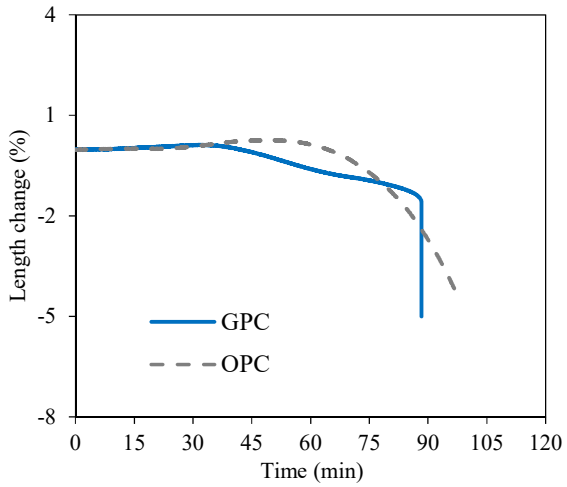


Figure 6.7 Deformation of concrete under constant load and high temperature

Since the GPC deformed too large before fracturing under a high temperature state, the testing machine stopped when the deformation of GPC increased too fast. In contrast to the geopolymer sample, OPC failed within 10 mins in a brittle failure mode. The thermal properties of these two concretes are different: e.g. thermal extension of geopolymer occurred later and more severely than OPC.

*6.3.2.2 Failure mode*

As presented in Figure 6.8, two different typical fracture patterns were observed for GPC and OPC specimens tested under combined loading and high temperature. The failure surfaces of OPC are “neat surfaces” which pass through the broken aggregate; this phenomenon was also observed by Cheng et al. (2004). The end portion of the failed specimen resembled a double-cone pattern. GPC exhibited a different failure mode compared with OPC, for with the increase of temperature the

specimen deformed gradually. Several vertical cracks developed at the mid-height of the specimen where large expansion happened. The deformation rate accelerated after 100 mins due to the propagation of vertical cracks in the GPC.

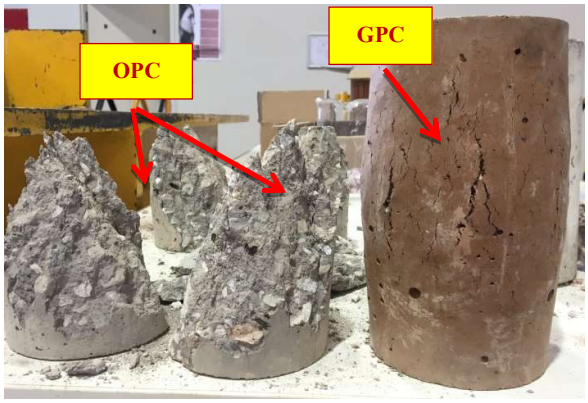


Figure 6.8 Deformation of concrete under constant load and high temperature

The brittle failure mode was observed in OPC specimens; in contrast, ductile failure mode occurred in GPC specimens. Large deformation in both lateral and longitudinal directions was observed on GPC specimen before it lost load carrying capacity. During elevated temperature exposure, the GPC structure had more obvious signs of failure, which is a critical consideration in structural design when attempting to target the collapse of buildings.

The performance of GPC is also better than OPC under a rapid heating rate and loading. As studied in Figure 6.6, by replacing OPC with GPC in a structure, a 40-50% improvement was expected on the hot strength at 800 °C. During the test at elevated temperatures and constant loading, GPC lasted for 98 mins, which is 11.4% better than OPC which only maintained its integrity for 88 mins. However, the failure mode of GPC is much more ductile than OPC. The improved ductility makes the GPC safer than OPC to be used in the building with fire hazards.

## 6.4 Residual properties of GPC after exposure to elevated temperatures

### 6.4.1 Experimental setup

As mentioned in Chapter 3, there were two strain measurement setups for the concrete experiments. The setup of the experiment is presented in Figure 6.9 (a), where the first part of the stress-strain curve (before peak stress) was measured by a CM-10H compressometer. The second part of the stress-stain curve was recorded by four LVDTs.

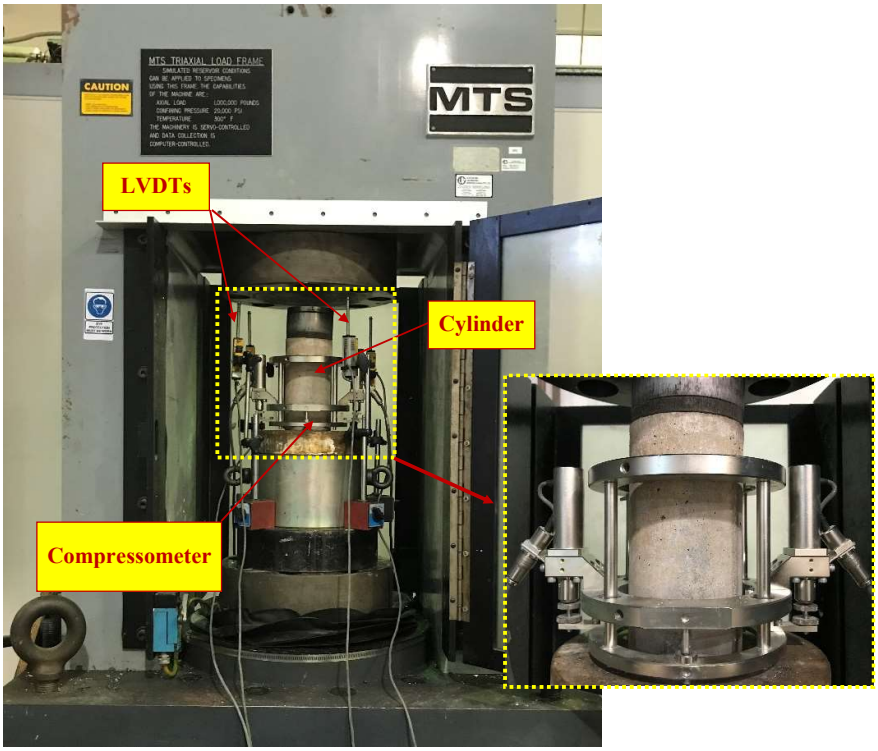


Figure 6.9 Experimental setup of GPC residual properties

The concrete specimen was placed in an oven, and the temperature of the oven was increased to 800 °C under the slow heating regime (5 °C per min). The oven kept the target temperature for 2 hours after the target temperature was reached, and then the

oven was naturally cooled to an ambient temperature for seven days until the test. The comparison of GPC specimens before and after the heat process is shown in Figure 6.9 (b). The concrete specimen was sealed with a vacuum bag and kept for 1 week until the testing.

The concrete mixing proportions tested in this section are shown in Table 6.4. The GPC was cured at an ambient temperature, while the heat cured GPC (HGPC) was cured at an elevated temperature. The OPC reference specimens were also cast and cured at an ambient temperature.

Table 6.4 Concrete mixing proportions (kg/m$^3$)

| Label | NaOH pellet (kg) | Water (kg) | Sodium silicate (kg) | Fly ash (kg) | Cement (kg) | CAC (kg) | Coarse aggregate (kg) | Fine aggregate (kg) | Extra water (kg) | Water reducer (L) |
|---|---|---|---|---|---|---|---|---|---|---|
| GPC | 25.6 | 37.6 | 157.6 | 441.4 | – | 49.0 | 1094.6 | 594.3 | _ | – |
| HGPC | 21.1 | 30.9 | 130.3 | 520.1 | – | – | 1080.3 | 586.5 | 30.9 | – |
| OPC | _ | 186.6 | _ | _ | 466.4 | _ | 1131.3 | 614.2 | – | 1.6 |

## 6.4.2 Density

The GPC specimen before and after the heating process is shown in Figure 6.10. Due to the iron content of fly ash (12.1%), the surface of GPC turned to a yellow ochre colour. The limestone of GPC maintained the same colour after elevated temperature exposure.

The measured density before and after exposure to elevated temperatures is shown in Table 6.5. Chapter 5 revealed that the density of GPC is close to the density of OPC in practice, ranging from 2200-2600 kg / m$^3$. Compared with GPC cured at an ambient temperature, HGPC is denser because the heat curing regime leads to severer evaporation.


Figure 6.10 GPC specimens before and after heat process

Among three types of concretes, HGPC has the smallest density and OPC has the highest density before elevated temperature exposure. However, the density of OPC decreased by 8.62% after exposure to 800°C, and the averaged densities of all three concretes was 2195.0 kg/m$^3$ after elevated temperature exposure.

Table 6.5 Density of different concrete

| Concrete type | Density (kg/m$^3$) | |
|---|---|---|
| | Before exposure to 800°C | After exposure to high temperatures |
| GPC | 2371.7 | 2186.1 (-7.82%) |
| HGPC | 2343.4 | 2190.9 (-6.51%) |
| OPC | 2416.5 | 2208.0 (-8.62%) |

### 6.4.3 Stress-strain relationship curve

Normally, a complete stress-strain curve of concrete consists of two branches: the ascending branch before peak strength and descending branch until the concrete is crushed. As previously mentioned, the strain measured by the compressometer will be affected by the contact points between the compressometer and surface of a specimen. The strain recorded by the compressometer was used for the ascending branch of stress-strain curve. The platen-to-platen deformation of the machine was calibrated and used for the descending branch.

The comparison of stress-strain curves of GPC tested at elevated temperatures and after elevated temperature exposure is shown in Figure 6.11. Junaid et al. (2017) tested the stress-strain curve of low calcium fly ash geopolymer at elevated temperatures. A significant softening phenomenon of HGPC (cured at 80 °C) after being heated to 800 °C was observed, as shown in Figure 6.11 (a). The strain of the peak load increased severely and the ultimate strain also increased.

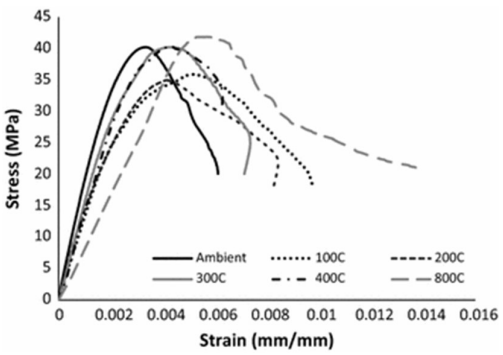


(a) Stress-strain relationship of GPC samples at high temperatures (Junaid et al., 2017)

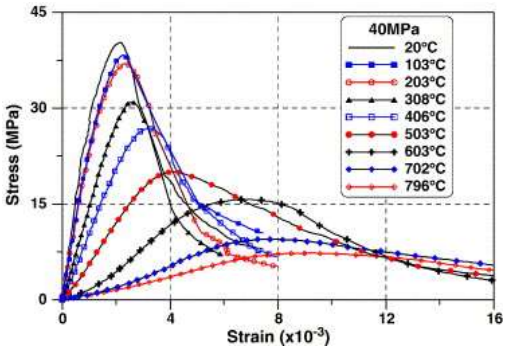


(b) Stress-strain relationship of OPC after exposure to high temperatures (Chang et al., 2006)

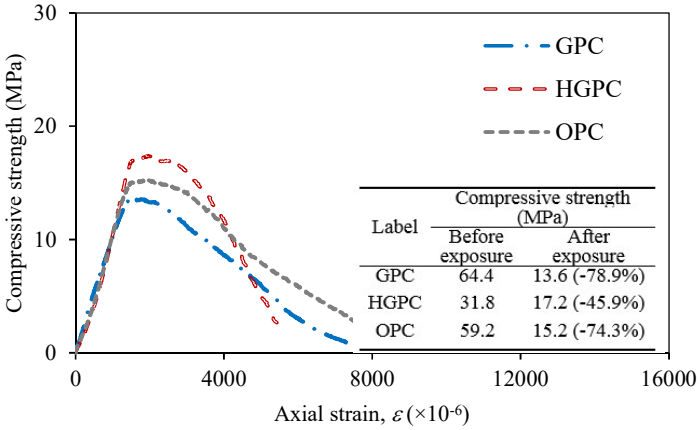


| Label | Compressive strength (MPa) | |
|---|---|---|
| | Before exposure | After exposure |
| GPC | 64.4 | 13.6 (-78.9%) |
| HGPC | 31.8 | 17.2 (-45.9%) |
| OPC | 59.2 | 15.2 (-74.3%) |

(c) Test results of concretes after exposure to 800°C

Figure 6.11 Stress-strain relationship curve of concretes

According to the results reported by Chang et al. (2006), after exposure to 800°C the ultimate strain of OPC is higher than GPC. As presented in Figure 6.11 (b), the strain of peak strength and the ultimate strain increased with the temperature increase. The test result in Figure 6.11 (c) further prove that the ductility of GPC is higher than OPC after exposure to 800 °C; performance reported in Section 6.3.2, little influence was found for HGPC after exposure to elevated temperatures, which was attributed to its denser matrix. After exposure to elevated temperatures and seven days cooling, GPC and OPC suffered a severe load carrying capacity loss, in contrast to HGPC. By comparison, HGPC kept more than half of its strength after elevated temperature exposure. According to the density loss proposed in Table 6.5, GPC and OPC lost more density than HGPC. The severe mass losses lead to a loose matrix of GPC and OPC, and these loose matrixes were responsible for the low strength of the samples.

## 6.5 Summary

This chapter reported the hot strengths of nine GPM mixtures tested at 600 and 800 °C, and the influence of three factors on the hot strength of geopolymer was analysed. A GPC mixture was chosen based on the results of a salient parameter analysis. The hot strength of this GPC was tested at temperatures ranging from 23, 200, 400, 600 and 800 °C. In contrast to OPC, GPC exhibited a similar performance at 400°C, and a higher fire endurance at 200, 600 and 800°C.

To evaluate the performance of a loaded GPC specimen under the condition of a fire, the deformation of GPC under combined loading and temperature was analysed. The GPC cylinder maintained its integrity for 10 mins longer than the OPC cylinder under the same condition. The failure modes of these two concretes are also different:

GPC exhibited large deformation before failure, while a brittle failure mode was observed in OPC.

Lastly investigated were the residual properties of GPC after exposure to 800 °C. The density of three types of concretes was studied and it was found that heat cured GPC exhibited a higher density than the other concretes. The stress-strain relationships of GPC after exposure to 800 °C were reported and compared with current research work.

# Chapter 7 Performance of GCFST columns at ambient and elevated temperatures

## 7.1 Introduction

Fire disasters have been frequently reported worldwide in recent years, seriously threatening personal and public safety. Exposure of concrete and steel to fire leads to serious structural deterioration and possible failure of columns, thus resulting in the local or global collapse of a building (Han et al., 2010). However, in most cases, unprotected CFST columns are not able to maintain structural integrity for sufficient time under fire conditions. External insulating coating or internal reinforcing steel are required to improve the fire resistance of CFST columns, but these two methods tremendously increase the cost of CFST columns and heighten the difficulty of construction.

Despite the fact that using industry by-product in concrete can achieve significant economic and environmental benefits, the supreme fire endurance of GPC and its application in structures has not been fully explored. Furthermore, to the best knowledge of the authors, very little research has been conducted to investigate the behaviour of GCFST columns. In addition to detailing the background of GCFST columns, the mechanical properties and fire performance of these columns are investigated in this chapter. Reference specimens made from OPC concrete were tested and compared with GPC specimens. A finite element (FE) model is employed to predict the behaviour of GCFST columns and the model is verified by experimental results.

## 7.2 Experimental investigation

### 7.2.1 Specimen preparation

*7.2.1.1 Concrete sample*

Firstly, the binder (fly ash and CAC) and saturated surface dry aggregates were added into a mixer and dry-mixed for 3 minutes. Afterwards, extra water was added to the dry-mix for GPC-2 and GPC-4 to ensure there was adequate slump. The alkaline activator was then added, and the wet mixture was stirred for an additional 4-6 minutes to form a homogenous state. The mixing procedure for OPC concrete production was similar to that of the GPC. Superplasticiser was added in the mixer, after the dry-mix of aggregate and cement; extra water was added into GPC, after dry-mix of aggregate and fly ash. A vibrating table was employed to remove air bubbles from the specimens. Each layer was vibrated for 15-30 seconds. The cast specimens were kept in moulds for 24 ± 8 hours. After demolding, all specimens were cured in an ambient temperature until compressive strength testing. Before demolding specimen GPC-4, this specimen was cured at 80 ℃ in moulds for 24 hours to check the effect of the elevated temperature curing method. After demolding, all specimens were sealed in plastic bags until being tested. Both concrete and mortar cylindrical specimens were ground using a CIVILAB core facing grinder to get smooth and flat ends before the testing.

Five types of concrete were mixed to fill the steel tubes. During casting, a concrete vibrator was utilised to compact the concrete to expel the internal air bubbles. After casting, the specimens were stored in a laboratory at an ambient temperature. The specimens requiring a heat curing regime were firstly cured at 80 ℃ for 24 hours before being stored in the laboratory.

*7.2.1.2 CFST column specimens*

A total of fifteen steel columns were cast and tested. The mixture proportions are shown in Table 7.1.

Table 7.1. Proportions of concrete mixes (kg/m$^3$)

| Label | NaOH pellet (kg) | Water (kg) | Sodium silicate (kg) | Fly ash (kg) | Cement (kg) | CAC (kg) | Coarse aggregate (kg) | Fine aggregate (kg) | Extra water (kg) | Water reducer (L) |
|---|---|---|---|---|---|---|---|---|---|---|
| OPC | – | 186.6 | – | – | 466.4 | – | 1131.3 | 614.2 | – | 1.6 |
| GPC-1 | 19.8 | 43.3 | 157.6 | 465.6 | – | 24.0 | 1095.1 | 594.5 | – | – |
| GPC-2 | 21.1 | 30.9 | 130.3 | 468.1 | – | 52.0 | 1080.3 | 586.5 | 30.9 | – |
| GPC-3 | 25.6 | 37.6 | 157.6 | 441.4 | – | 49.0 | 1094.6 | 594.3 | – | – |
| GPC-4 (Heat cured) | 21.1 | 30.9 | 130.3 | 520.1 | – | – | 1080.3 | 586.5 | 30.9 | – |

All specimens had a designed length ($L$) of 340 mm which was intended to fit in the furnace. The $L/D$ is 2.26, which is lower than the normal value of 3. However, when the $L/D$ ratios lie in the range 2-5, very close load-strain relationships were reported (Tao et al., 2013). The nominal external diameter ($D$) of the steel tube was 150 mm, and the nominal thickness ($t$) was 3 mm. Mild steel sheets were used to cold form circular tubes, and two circular endplates were then welded together with the tube to form a whole circular tube. The diameter and thickness of the endplates were 200 mm and 12 mm, respectively. A 120 mm hole was cut on the top endplate to pour concrete. A Vernier calliper was used to measure the cross-sectional dimensions of the hollow tubes.

The parameters of the CFST columns include: (a) concrete type, (b) concrete strength, (c) curing condition of geopolymer concrete. Fifteen labels are made for fifteen CFST columns. Label details are listed in Table 7.2, where GPC1, GPC2, GPC3, GPC4 and OPC refer to specimens cast by ambient cured GPC-1, GPC-2, GPC-

3, heat cured GPC and OPC, respectively. In order to designate specimens with different test methods, prefixes were added. The prefixes CFT, RES and HOT refer to a test at an ambient temperature, a test after a slow heating regime, and a test at a rapid heating regime, respectively.

Table 7.2. Summary of CFST stub column specimens

| Test method | Label | $D$ (mm) | $t$ (mm) | $f_c'$ (MPa) | $f_y$ (MPa) | $E_s$ (GPa) | $N_{ue}$ ($N_{u,r}$) | $N_0$ (kN) | Time (min) | Concrete type |
|---|---|---|---|---|---|---|---|---|---|---|
| Ambient strength test | CFT-OPC | 150.0 | 3.01 | 59.2 | 326.0 | 206.4 | 1681.0 | 0 | – | OPC |
| | CFT-GPC1 | 150.4 | 3.01 | 37.4 | 326.0 | 206.4 | 1207.5 | 0 | – | GPC-1 |
| | CFT-GPC2 | 149.6 | 3.01 | 58.6 | 326.0 | 206.4 | 1479.7 | 0 | – | GPC-2 |
| | CFT-GPC3 | 150.3 | 3.01 | 64.4 | 326.0 | 206.4 | 1649.9 | 0 | – | GPC-3 |
| | CFT-GPC4 | 150.2 | 3.01 | 31.8 | 326.0 | 206.4 | 1196.2 | 0 | – | GPC-4 |
| Residual strength test | RES-OPC | 150.6 | 3.01 | 15.2 | 314.3 | 202.1 | 788.0 | 0 | – | OPC |
| | RES-GPC1 | 149.6 | 3.01 | 18.9 | 314.3 | 202.1 | 507.9 | 0 | – | GPC1 |
| | RES-GPC2 | 150.3 | 3.01 | 20.3 | 314.3 | 202.1 | 555.6 | 0 | – | GPC2 |
| | RES-GPC3 | 150.8 | 3.01 | 13.6 | 314.3 | 202.1 | 553.0 | 0 | – | GPC3 |
| | RES-GPC4 | 149.3 | 3.01 | 17.2 | 314.3 | 202.1 | 643.6 | 0 | – | GPC-4 |
| Combined loading and temperature test | HOT-OPC | 150.6 | 3.01 | 59.2 | 326.0 | – | – | 840.5 | 36.7 | OPC |
| | HOT-GPC1 | 150.2 | 3.01 | 37.4 | 326.0 | – | – | 603.8 | 60.1 | GPC1 |
| | HOT-GPC2 | 150.8 | 3.01 | 58.6 | 326.0 | – | – | 739.9 | 44.3 | GPC2 |
| | HOT-GPC3 | 149.5 | 3.01 | 64.4 | 326.0 | – | – | 825.0 | 37.5 | GPC3 |
| | HOT-GPC4 | 149.9 | 3.01 | 31.8 | 326.0 | – | – | 598.1 | 85.4 | GPC-4 |

### 7.2.2 Test setup

The compressive strength and Young's modulus tests on concrete cylinders were conducted according to ASTM C39 (1996) and ASTM C469 (Standard, 2002), respectively. The compression test of CFST columns was performed by a closed-loop servo controlled hydraulic MTS machine with a maximum capacity of 5000 kN. Firstly, a 10 kN preload was applied to the specimen, and the load was held for 2 minutes. Secondly, the specimen was loaded until the reaching of peak load with the loading rate of 0.12 mm/min. In the post-peak range, the loading rate was increased to 0.6 mm/min until the test was stopped when severe failure occurred. A total of four bidirectional strain gauges, with a gauge length of 3 mm, were used for each specimen

to measure the longitudinal and transverse strains of the steel tube at mid-height. Four LVDTs were used to measure the column's axial deformation.

Two heating rates were used in the examination of CFST columns, as shown in Figure 7.1. The first rate is a slow heating regime which was used to study the post-fire performance of CFST columns. The CFST column, aged 28 days, was put in the electrical furnace, and the temperature of the furnace was increased to 800 ℃ at the rate of 5 ℃/min, without loading. The furnace kept the target temperature for 3 hours to achieve an equilibrium state of temperature distribution. Lastly, the furnace was naturally cooled to room temperature. The post-fire testing was conducted on the specimen after 7 days of cooling.

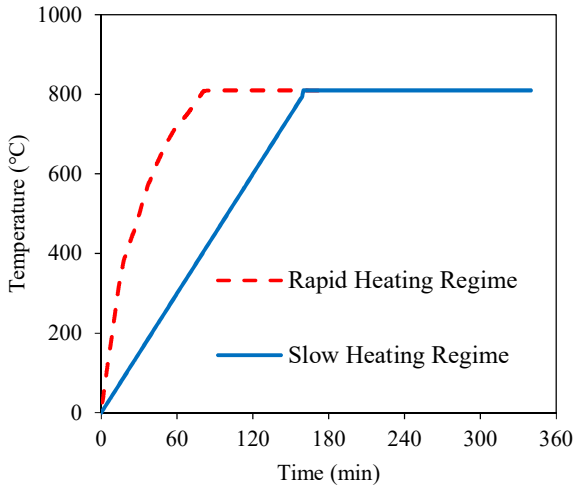


Figure 7.1. Heating regime

A rapid heating regime was used to test the response of CFST columns to fire with a constant load. The control mode of the compression machine was set to load control for the whole testing process. The CFST column was firstly loaded to 50% of the ultimate load measured at ambient temperature. The actually applied axial load ($N_0$) is shown in Table 7.2. Following this, the temperature was rapidly increased to 800 ℃,

and 800 ℃ was maintained until the failure of specimens. Due to the maximum capacity of the furnace, the rapid heating regime is slower than the standard heating curve provided by the Australian Standard (1997).

## 7.3 Experimental results and discussion

### 7.3.1 Performance of CFST columns at ambient temperature

*7.3.1.1 Axial load versus axial strain curves*

The specimens tested at ambient temperature are shown in Figure 7.2. Figures 7.3-7.5 present the effects of different concrete strength levels, the heating regime, and concrete types on the measured axial load ($N$) versus axial strain curves, respectively. In the figures, the strain values were obtained from the measurements of strain gauges and LVDTs. The values from four strain gauges were implemented before the steel tube buckled. After the steel tube buckled, the axial strain $\varepsilon$ was calculated from average readings of the four LVDTs divided by the overall length of the specimen. Each figure indicates the steel yield point.


Figure 7.2. Tested specimens at ambient temperature

Figure 7.3 presents a comparison between GCFST columns with different strength levels on the $N$-$\varepsilon$ curves. The concrete strengths for CFT-GPC1, CFT-GPC2 and CFT-

GPC3 are 37.4 MPa, 58.6 MPa and 64.4 MPa, respectively. A typical *N*-*ε* curve can be found in high strength GCFST, and has an ascending branch, a descending branch and a stable branch. However, GCFST made with low strength CFT-GPC1 was seen to have no obvious descending branch before the curve reached a stable condition.

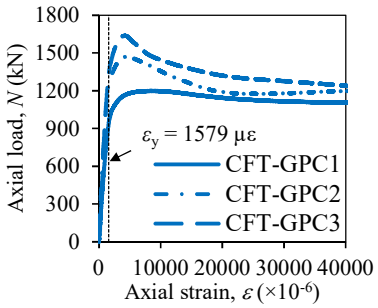


Figure 7.3. Comparison between *N*-*ε* curves of GCFST columns with different strength levels

As can be seen in Figure 7.4, the influence of different heating regimes on the *N*-*ε* performance of GCFST is illustrated. The curing regimes for CFT-GPC1, CFT-GPC2 and CFT-GPC4 GCFST columns are ambient curing, ambient curing and elevated temperature curing, respectively. The CFT-GPC4 GCFST column was firstly cured at 80 ℃ in an oven for 24 hours, then it was cured at ambient temperature. The mixing design for CFT-GPC2 and CFT-GPC4 were the same, except for the CAC addition in CFT-GPC2. With the addition of CAC, the strength of GPC in CFT-GPC2 could be developed at an ambient temperature. By comparison, the CFT-GPC4, which was cured at an elevated temperature, exhibited a lower load-bearing capacity than CFT-GPC2.

Also conducted was a comparison of *N*-*ε* performance on two columns with similar GPC compressive strengths (CFT-GPC1 and CFT-GPC). The curves of CFT-GPC1 and CFT-GPC4 GCFST columns almost superpose each other. The behaviours

of GCFST columns are similar if the GPC strengths are relatively similar under two curing conditions.

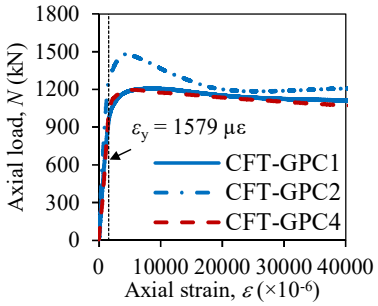


Figure 7.4. Comparison between *N*-*ε* curves of GCFST columns with different heating regimes

Figure 7.5 presents the differences found when comparing *N*-*ε* curves of GCFST (CFT-GPC3) and conventional CFST (CFT-OPC) columns. The descending branch of the *N*-*ε* curve is very steep for GCFST columns. The CFT-OPC CFST column has a slow descending part once it reaches peak strength.

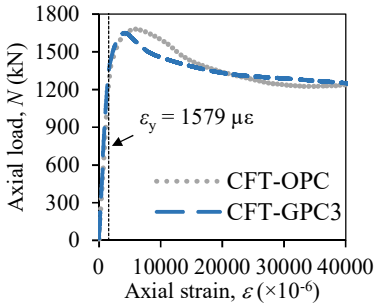


Figure 7.5. Comparison between *N*-*ε* curves of GCFST and conventional CFST columns

Furthermore, the load carrying capacity of CFT-OPC increased slightly after 34000 με, while the CFT-GPC3 GCFST column reached a relatively stable residual strength. The residual strength of the CFT-GPC1 GCFST column was observed to be generally close to the minimum strength of CFT-OPC CFST column.

*7.3.1.2 Ultimate strength*

The measured ultimate strengths ($N_{ue}$) for all OPC CFST and GCFST columns are provided in Table 7.2. Following the definition proposed by Tao et al. (2013), the $N_{ue}$ is defined as the peak load corresponding to the axial strain of less than 0.01 if the load-strain curve has a descending branch. Otherwise, the ultimate strength is defined as the load at the strain of 0.01. Different concrete types have significant influences on ultimate strength, since 50-70% of the load carrying capacity of CFST is provided by concrete. To quantify the strength improvement of CFST with different concrete types, a strength index (*SI*) (Wang et al., 2014) was used as shown in Eq. (7.1):

$$SI = \frac{N_{ue}}{N_0} \tag{7.1}$$

where $N_0 = f_y A_s + f_c' A_c$; and $f_y$ is the yield strength of steel; $f_c'$ is the compressive strength of concrete; $A_s$ and $A_c$ are cross-sectional areas of steel and concrete, respectively. The comparison between different CFST columns on the strength index is shown in Figure 7.6.

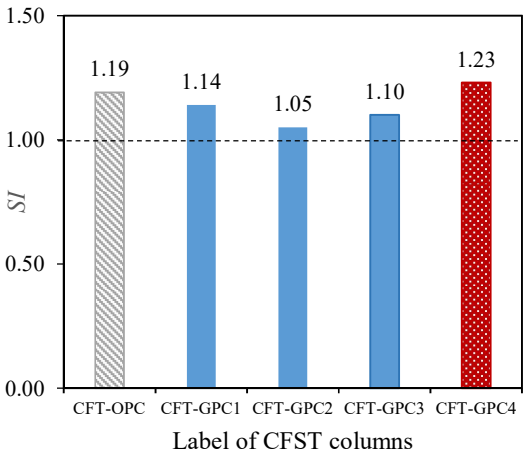


Figure 7.6. Comparison of different strength indexes

The *SI* values for GCFST columns ranged from 1.05 to 1.23, while the value for a OPC CFST column reference specimen is 1.19. Once GCFST undergoes a heat-curing process it exhibits higher *SI* value than GCFST column cured at ambient temperature. The higher *SI* value means a higher concrete confinement. In conclusion, the GCFST column with initial 24 hours heat-curing process presented better confinement than both OPC CFST and GCFST columns cured at ambient temperature.

*7.3.1.3 Compressive stiffness*

Steel tubes of CFST columns exhibit a linear stress-strain relation before yielding. The previous study proves that microcracks in concrete leads to a decrease in Young's modulus (Neville, 1995). The secant modulus of CFST columns will also decrease after cracks develop in the concrete core under compression. The compressive stiffness (*EA*) was defined as the secant stiffness corresponding to $0.4N_{ue}$. This definition was widely adopted by previous researchers (Yang et al., 2013, Wang et al., 2017, Huo et al., 2013).

According to the previous study by Wang et al. (2017), the compressive stiffness of circular CFST columns under axial compression can be calculated by Eq. (7.2) and Eq. (7.3). The results of the experiment and empirical prediction of compressive stiffness are shown in Table 7.3.

$$EA = E_s A_s + \kappa_c E_c A_c \tag{7.2}$$

$$\kappa_c = \left(\frac{D}{t}\right)^{0.004} + \left(\frac{tf_y}{Df_c'}\right)\left[56.8 - 56.3\left(\frac{D}{t}\right)^{0.004}\right] \leq 1 \tag{7.3}$$

Table 7.3. Compressive stiffness (kN)

| Label | Experiment | Wang et al. (2017) | Prediction error |
|---|---|---|---|
| CFT-OPC | 809258 | 881911 | +9.0% |
| CFT-GPC1 | 717908 | 757661 | +5.5% |
| CFT-GPC2 | 1089054 | 874576 | -19.7% |
| CFT-GPC3 | 1050119 | 911313 | -13.2% |
| CFT-GPC4 | 574550 | 716433 | +24.7% |

The values of compressive stiffness derived from $N$-$\varepsilon$ curves are plotted in Figure 7.7; also plotted is the comparison of test results and equation predictions. The CFT-GPC4 exhibits the least compressive stiffness, which might be due to the lower Young's modulus and compressive strength of heat cured GPC. In general, the equation proposed by Wang et al. (2017) gives a reasonable prediction close to the test result.

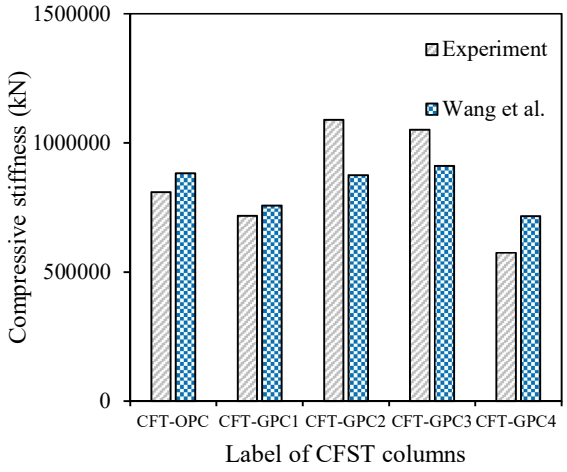


Figure 7.7. Comparison of compressive stiffness

The *EA* of CFT-GPC1 is also relatively low compared to those of CFT-GPC2 and CFT-GPC3. GPC-1 has more liquid content which is due to the gap caused by liquid evaporation during curing. By comparing CFST columns cured at ambient temperature, the CFT-GPC3 exhibits higher compressive stiffness than CFT-OPC.

*7.3.1.4 Ductility*

A ductile structure design was recommended by the Eurocode (2004) to drastically reduce the seismic force. The ductile structure design can also mitigate the influence of extreme events, such as blasts and high-impact. The ductility of CFST columns was studied to estimate the difference in the ability to sustain deformation beyond the elastic limit, while maintaining a sufficient load-bearing capacity until failure. The ductility index (Yu et al., 2016) was defined in Eq. (7.4) to evaluate the ductility of CFST columns:

$$DI = \frac{\varepsilon_{90\%}}{\varepsilon_y} \tag{7.4}$$

where $\varepsilon_{90\%}$ is axial strain when the load decreased to 90% of the ultimate strength; $\varepsilon_y = \varepsilon_{75\%}/0.75$, $\varepsilon_{75\%}$ is axial strain when the load attained 75% of the ultimate strength in the pre-peak stage.

Figure 7.8 presents the ductility index of CFST stub columns. In general, low strength CFST columns exhibit better ductility. The ultimate strengths for CFT-GPC1 and CFT-GPC4 GCFST columns are 1207.5 kN and 1196.2 kN, respectively. The peak strength for CFT-GPC3 GCFST column is 1649.9 kN, and it had the worst ductility. The ductility index of conventional CFST columns is 7.1 which is relatively high. By comparing *DI* of GPCs with different curing methods, it is concluded that the curing methods have little relationship with ductility. The ductility index of CFST columns was mainly determined by the strength of core concrete.

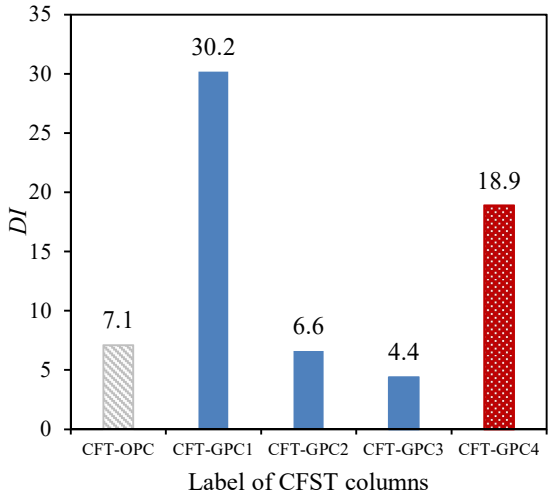


Figure 7.8. Comparison of different ductility indexes

*7.3.1.5 Lateral and axial strain curves*

The axial load versus axial and lateral stain relationships are shown in Figure 7.9. The steel yield strain obtained from a steel coupon test is also plotted in the figures. The figure indicates that the steel tube yielded before the CFST column achieved its ultimate load, and the steel strength, was fully developed in the CFST columns.

It can be seen that the high strength CFST columns (CFT-GPC2, CFT-GPC3, CFT-OPC) exhibit a descending branch after peak strength, while low strength GCFST columns (CFT-GPC1, CFT-GPC4) have no obvious descending branch. The difference between low and high strength CFST columns agrees with the axial load versus strain curve test result. The descending branch of a conventional CFST column (CFT-OPC) is slower than GCFST columns after peak strength, due to the OPC CFST column exhibiting better ductility than GCFST columns at the high strength level.

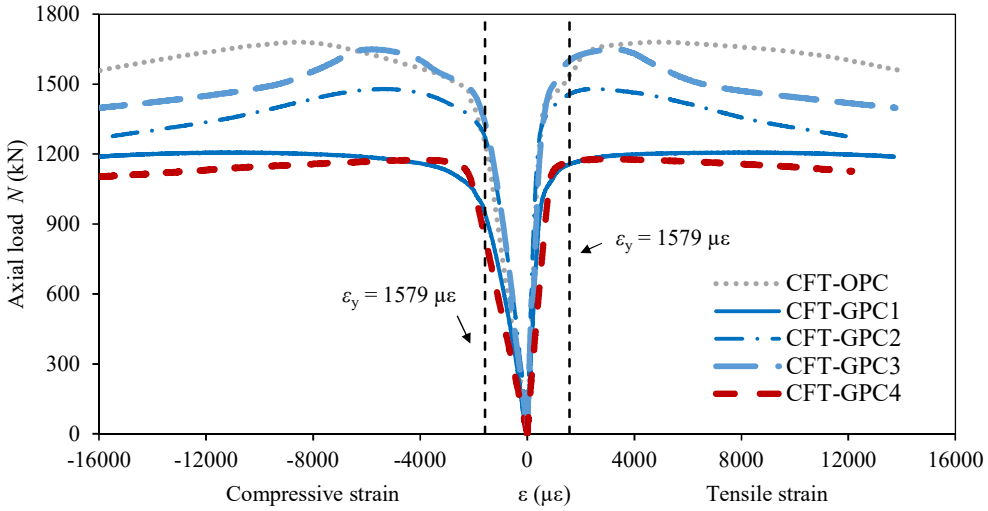


Figure 7.9. Axial load versus strains at mid-height of test specimens

In Figure 7.10, the normalised axial load ratio ($N/N_{ue}$) of CFST columns is depited and the development of lateral-to-axial strain ratio (ν) is compared. The ratio is calculated by the strain readings from corresponding strain gauges, and is used to evaluate the concrete confinement of steel tube. The axial loads $N$ was normalised with respect to the corresponding peak loads $N_{ue}$ for a meaningful comparison. The initial ν values of all specimens are around 0.3, which is the normal Possion's ratio for mild steel before yield. The lateral expansion of the steel tube is higher than the concrete core which has a Possion's ratio of 0.2. Due to the incongruous deformation, a gap between the steel tube and concrete appeared, and no confinement effect on the concrete was provided by the steel tube. After the nominalised axial load reached 90% of its peak strength, the interaction of the steel tube and core concrete occurred. The lateral-to-axial stain ratios ν quickly increased to around 0.6, while load-bearing capacities were kept constant. The same lateral-to-axial strain ratio development curves indicate the same volumetric expansion of different core concretes, despite different curing methods, strength levels and concrete types.

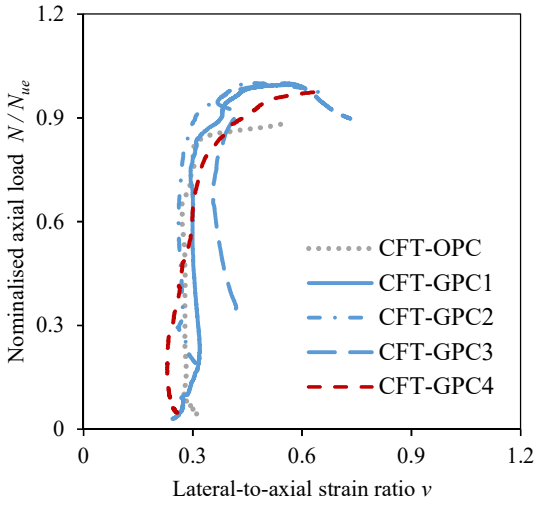


Figure 7.10. Development of lateral-to-axial strain ratio for CFST columns

The lateral-to-axial strain ratio of CFT-OPC increased earlier than GCFST columns, which means GCFST columns developed interaction later than CFT-OPC. The early interaction can be explained by the fact that the Young's modulus of GPC is smaller than OPC. The lateral-to-axial strain ratio of OPC increases sharply at the normalised axial load ratio of 0.85; Yu et al. (2016) reported the normalised axial load ratio of 0.95. Compared to CFT-OPC, the lateral-to-axial ratio of GCFST columns have no sharp increase, as most of GCFST columns have a higher *DI* value than OPC, and a part of the load was transferred to the GPC core after the steel failed.

## 7.3.2 Comparison between test results and FE predictions

*7.3.2.1 Introduction to FE model*

The model proposed by Tao et al. (2013) was implemented in this thesis. A typical 3D FE model built in ABAQUS 6.12 is shown in Figure 7.11. After meshing the model, 3744 8-node solid (C3D8R) elements were generated for concrete and 792 4-node shell (S4R) elements for the steel tube. Surface-to-surface contact was used to

simulate the interaction between the steel tube and concrete, and the friction coefficient was specified as 0.6.

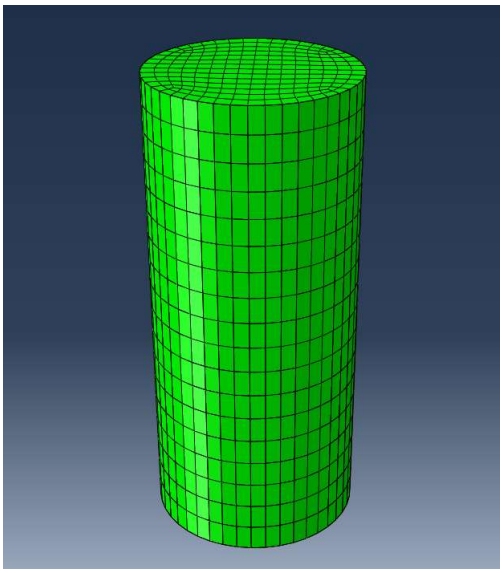

Figure 7.11. 3D FE model of CFST column

As mentioned in previous literature, the confinement of steel increased the compressive strength and ductility of concrete. To accurately simulate the performance of concrete in CFST, a damaged concrete plasticity material model was implemented in ABAQUS. The key parameters are: dilation angle ($\psi$), flow potential eccentricity ($e$), Young's modulus ($E_c$), the ratio of the second stress invariant on the tensile meridian to that on the compressive meridian ($K_c$), ratio of the compressive strength under bi-axial loading to uniaxial compressive strength ($f_{b0}/f_c'$), and the tensile behaviour of concrete. The calculation methods proposed by Tao et al. (2013) for different parameters are summarised as follows:

Young's modulus was calculated using Eq. (7.5), where $f_c'$ is the compressive strength of concrete (MPa).

$$E_c = 4700\sqrt{f_c'} \tag{7.5}$$

Dilation angle was determined by Eq. (7.6).

$$\psi = \begin{cases} 56.3(1-\xi_c) & \text{for } \xi_c \le 0.5 \\ 6.672e^{\frac{7.4}{6.64+\xi_c}} & \text{for } \xi_c > 0.5 \end{cases} \tag{7.6}$$

in which,

$$\xi_c = \frac{A_s f_y}{A_c f_c'} \tag{7.7}$$

$A_s$ = cross-sectional area of steel

$A_c$ = cross-sectional area of concrete

$f_y$ = yield strength of steel, MPa

$f_c'$ = compressive strength of concrete, MPa

The ratio of the second stress invariant on the tensile meridian to that on the compressive meridian ($K_c$) was calculated using Eq. (7.8).

$$K_c = \frac{5.5}{5+2(f_c')^{0.075}} \tag{7.8}$$

Ratio of the compressive strength under bi-axial loading to uniaxial compressive strength ($f_{b0}/f_c'$) was calculated using Eq. (7.9).

$$f_{b0}/f_c' = 1.5(f_c')^{-0.075} \tag{7.9}$$

The assumption of tensile behaviour of concrete is: tensile strength is linear until $0.1f_c'$; tensile softening was characterised by facture energy ($G_F$) beyond $0.1f_c'$, as illustrated in Eq. (7.10).

$$G_F = (0.0469d_{max}^2 - d_{max} + 26)(\frac{f_c'}{10})^{0.7} \tag{7.10}$$

where $d_{max}$ is the maximum size of coarse aggregate (mm), the unit for $G_F$ is N/m. The strain hardening and softening of confined concrete in a CFST column was illustrated in three stages, as shown in Figure 7.12.

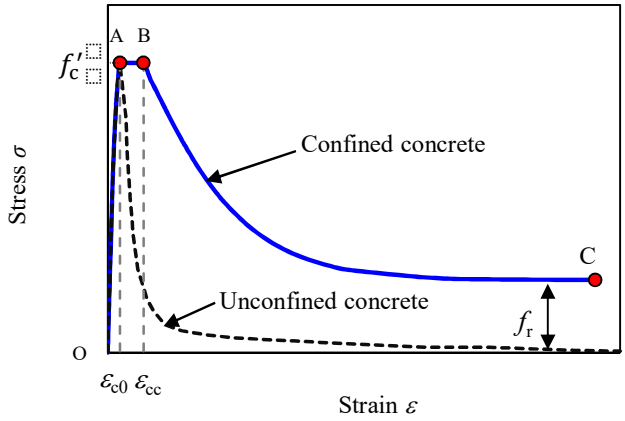


Figure 7.12. Model of confined concrete in CFST column

The ascending branch of confined concrete was defined in Eq. (7.11), as shown in stage OA of Figure 7.12.

$$\frac{\sigma}{f_c'} = \frac{AX+B\,X^2}{1+(A-2)X+(B+1)X^2} \qquad 0 < \varepsilon_c < \varepsilon_{co} \tag{7.11}$$

where,

$$X = \frac{\varepsilon}{\varepsilon_{c0}} \tag{7.12}$$

$$A = \frac{E_c \varepsilon_{c0}}{f_c'} \tag{7.13}$$

$$B = \frac{(A-1)^2}{0.55} - 1 \tag{7.14}$$

The strain at peak stress under uniaxial compression $\varepsilon_{c0}$ has been calculated by using the equation proposed by Nicolo et al. (1994) in Eq. (7.15), and corresponds to the strain at Point A in Figure 7.12.

$$\varepsilon_{c0} = 0.00076 + \sqrt{(0.626\, f_c' - 4.33) \times 10^{-7}} \tag{7.15}$$

The $\varepsilon_{cc}$ at point B, end of plateau AB, has been calculated based on the equation proposed by Samani and Attard (2012), as shown in Eq. (7.16) and Eq. (7.17).

$$\frac{\varepsilon_{cc}}{\varepsilon_{c0}} = e^{k} \tag{7.16}$$

$$k = (2.9224 - 0.00367\, f_c')\left(\frac{f_B}{f_c'}\right)^{0.3124+0.002 f_c'} \tag{7.17}$$

Confining stress $f_B$ for circular CFST is given in Eq. (7.18).

$$f_B = \frac{(1+0.027 f_y)\cdot e^{-0.02\frac{D}{t}}}{1+1.6e^{-1}\cdot (f_c')^{4.8}} \tag{7.18}$$

After the AB plateau, the softening branch BC was described in Eq. (7.19).

$$\sigma = f_r + (f_c' - f_r) exp\left[-\left(\frac{\varepsilon-\varepsilon_{cc}}{\alpha}\right)^{\beta}\right] \qquad \varepsilon \geq \varepsilon_{cc} \tag{7.19}$$

where,

$$\alpha = 0.04 - \frac{0.036}{1+e^{6.08\xi_c - 3.49}} \tag{7.20}$$

$\beta = 1$ for circular CFST (7.21)

The residual stress ($f_r$) of confined concrete was calculated by Eq. (7.22) for circular CFST.

$$f_r = 0.7\left(1 - e^{-1.38\xi_c}\right) f_c' \leq 0.25 f_c' \tag{7.22}$$

The steel model of CFST columns was proposed by Tao et al. (2012) for steel with a yield stress of 200 MPa to 800 MPa. The stress-strain curve of steel can be plotted in Figure 7.13. The steel was modelled by the following equations:

$$\sigma = \begin{cases} E_s \varepsilon & 0 \leq \varepsilon < \varepsilon_y \\ f_y & \varepsilon_y \leq \varepsilon < \varepsilon_p \\ f_u - (f_u - f_y)\cdot\left(\frac{\varepsilon_u - \varepsilon}{\varepsilon_u - \varepsilon_p}\right)^{p} & \varepsilon_p \leq \varepsilon < \varepsilon_u \\ f_u & \varepsilon \geq \varepsilon_u \end{cases} \tag{7.23}$$

in which,

$f_u$ = ultimate strength (MPa), as illustrated in Eq. (7.24)

$\varepsilon_y$ = yield strain

$\varepsilon_p$ = strain at the onset of stain hardening, illustrated by Eq. (7.25)

$p$ = strain hardening exponent given by Eq. (7.26)

$$f_u = \begin{cases} \left[1.6 - 2 \times 10^{-3}\left(f_y - 200\right)\right] f_y & 200 < f_y \leq 400 \text{ MPa} \\ \left[1.2 - 3.75 \times 10^{-4}\left(f_y - 400\right)\right] f_y & 400 < f_y \leq 800 \text{ MPa} \end{cases}$$

(7.24)

$$\varepsilon_p = \begin{cases} 15\varepsilon_y & f_y \leq 300 \text{ MPa} \\ \left[15 - 0.018\left(f_y - 300\right)\right]\varepsilon_y & 300 < f_y \leq 800 \text{ MPa} \end{cases} \quad (7.25)$$

$$p = E_p\left(\frac{\varepsilon_u - \varepsilon_p}{f_u - f_y}\right) \quad (7.26)$$

$$E_p = 0.02E_s \quad (7.27)$$

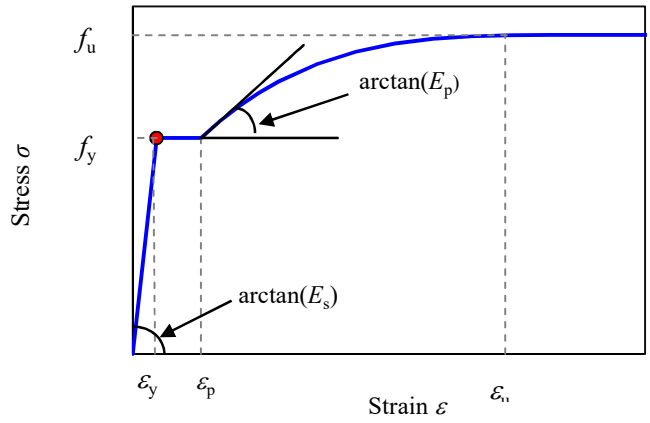


Figure 7.13. Model of steel in CFST column

*7.3.2.2 Verification of FE model*

For conventional CFST columns, considerable efforts have been made in the past to improve the accuracy of using FE models to predict the mechanical performance. Tao et al. (2013) collected a wide range of data to develop a refined FE model for CFST columns under axial compression. The concrete damaged plasticity material model was implemented to develop a three-stage strain hardening/softening

function for concrete with confinement by steel tube. The actual measured Young's modulus of concrete—as proved in Chapter 5 to be close to the ACI 318-14 (2015) prediction—was used in concrete.

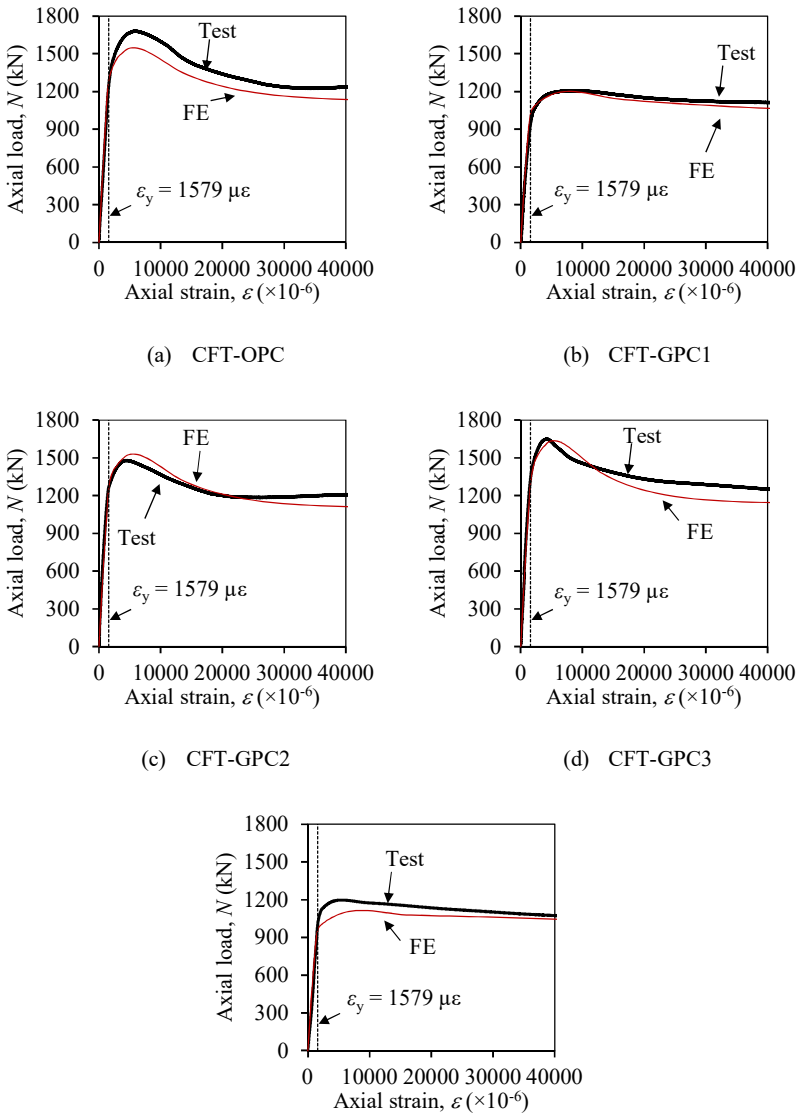


(a) CFT-OPC (b) CFT-GPC1

(c) CFT-GPC2 (d) CFT-GPC3

(e) CFT-GPC4

Figure 7.14. Comparison of *N*-*ε* curves for GCFST columns with FE model

The FE model has been proved to have high accuracy when modelling conventional CFST columns (Yu et al., 2016); this is further confirmed by the comparison between predicted and measured $N$–$\varepsilon$ curves for CFT-OPC, as shown in Figure 7.14 (e). The feasibility of using this model to predict the performance of GCFST columns at an ambient temperature is conducted in this part. As shown in Figure 7.14, the FE model also accurately predicts the axial load versus axial strain relationship of GCFST columns under compression. Both ascending and descending branches of load-strain curve are close to FE prediction. Using the model proposed by Tao et al. (2013) is able to get an accurate result before peak strength and conservative prediction after peak strength.

*7.3.2.3 Comparison with compressive stiffness*

The experiment test result and FE modelling result compressive stiffness are shown in Table 7.4. The FE result of each specimen has also been plotted in Figure 7.15 for comparison with test results. As can be seen, the FE model makes an accurate prediction for CFT-OPC. In general, the FE model gives a prediction close to test results on the compressive stiffness.

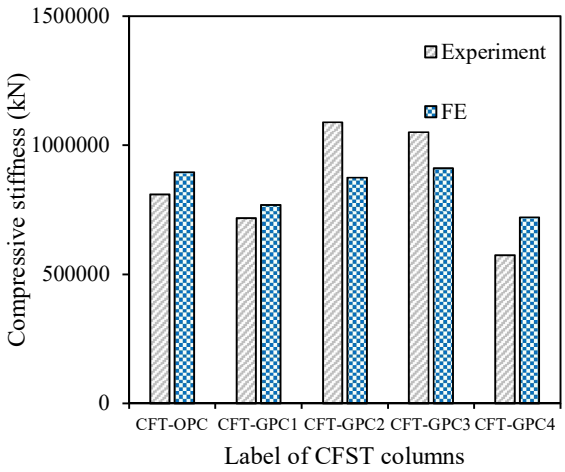

Figure 7.15. Comparison of compressive stiffness for GCFST columns with FE model

Table 7.4. Compressive stiffness (kN)

| Label | Experiment | FE model | |
|---|---|---|---|
| CFT-OPC | 809258 | 894959 | -10.6% |
| CFT-GPC1 | 717908 | 768630 | +7.1% |
| CFT-GPC2 | 1089054 | 874458 | -19.7% |
| CFT-GPC3 | 1050119 | 911167 | -13.2% |
| CFT-GPC4 | 574550 | 721093 | +25.5% |

### 7.3.3 Performance of CFST columns after elevated temperature exposure

*7.3.3.1 Axial load versus axial strain curves*

The failure mode of specimens after elevated temperature exposure is similar to that of specimens tested at an ambient temperature, as presented in Figure 7.16. The test results of CFST columns after exposure to elevated temperatures were reported in this part. Axial load ($N$) versus axial strain curves are shown in Figure 7.17. To get a more reasonable comparison, the results tested at ambient temperature are also plotted in each figure.


Figure 7.16. Tested specimens after exposure to elevated temperatures

After exposure to elevated temperatures, no post-peak descending phenomenon can be observed in GCFST columns cured at an ambient temperature. The post-peak branch

can be found in RES-GPC4 and RES-OPC specimens, and the descending branch of heat cured GCFST column is steeper than a conventional CFST column.

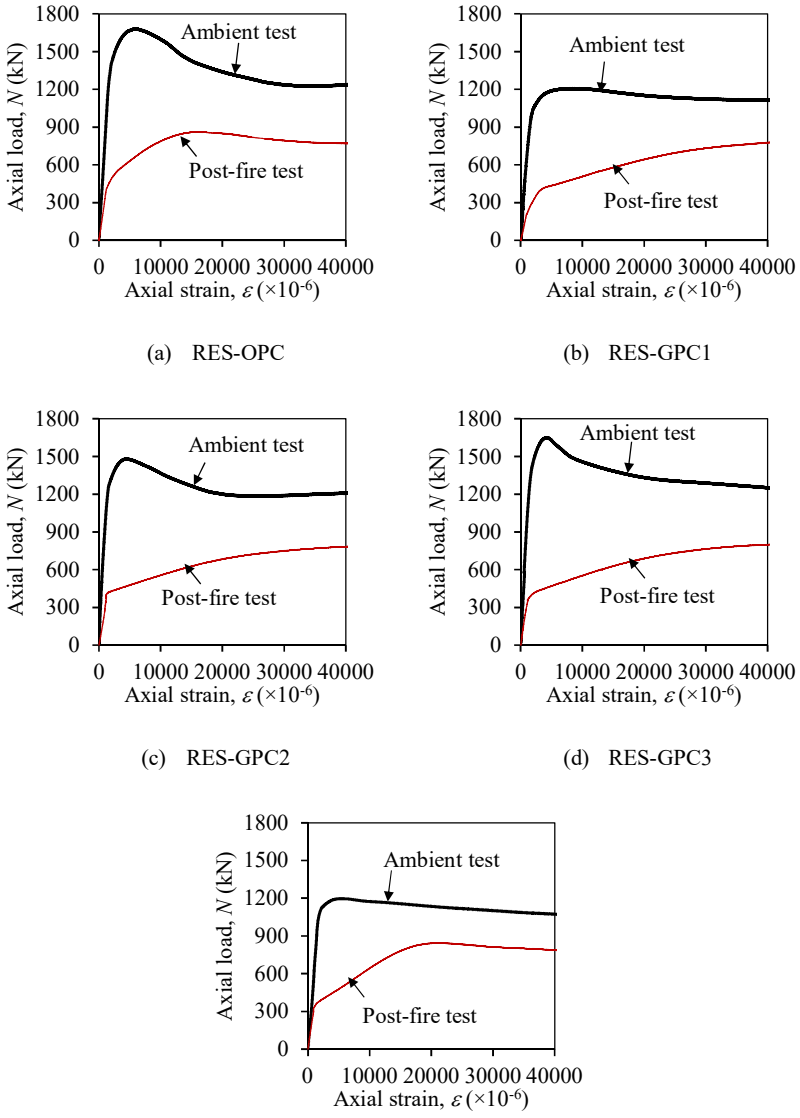


(a) RES-OPC (b) RES-GPC1

(c) RES-GPC2 (d) RES-GPC3

(e) RES-GPC4

Figure 7.17. Comparison of $N$-$\varepsilon$ curves for CFST with different concretes after exposure to elevated temperatures

It seems that the load-carrying capacities of GCFST columns (RES-GPC1, RES-GPC2 and RES-GPC3) after exposure to elevated temperatures have no relation with the

ambient test results. The first peak strengths for these three specimens are around 450 kN, and the curves are stable at around 800 kN. The heat cured GCFST (RES-GPC4) exhibited a totally different axial load to axial strain development curve compared to RES-GPC1, RES-GPC2 and RES-GPC3. No decreasing branch was observed on the curves of RES-GPC1, RES-GPC2 and RES-GPC3. By comparison, the load carrying capacity RES-GPC4 and RES-OPC decreased clearly after 15000-20000 με.

*7.3.3.2 Ultimate strength*

The residual ultimate strengths for conventional CFST and GCFST columns after fire exposure ($N_{u,r}$) are listed in Table 7.2. The definition of residual ultimate strength is similar to the definition of ultimate strength at room temperature. The $N_{u,r}$ is defined as the peak load corresponding to the axial strain of less than 0.01 if the load-strain curve has a descending branch. Otherwise, the residual ultimate strength is defined as the load at the strain of 0.01. A residual strength index (*RSI*) (Tao and Han, 2007) is defined to quantify the strength loss of CFST columns after fire exposure, as shown in Eq. (7.28).

$$RSI = \frac{N_{u,r}}{N_{ue}} \tag{7.28}$$

where $N_{u,r}$ is the residual ultimate strength of fire-exposed composite columns; $N_{ue}$ is the ultimate strength of columns tested at an ambient temperature.

A comparison between different CFST columns on the residual strength index is shown in Figure 7.18. The strength loss ratio (*RSI*) of CFST columns change along with different concrete core. Heat cured GCFST columns exhibit superior fire resistance which retain a 70.6% loading bearing capacity after fire exposure. The heat-cured GCFT has better post-fire performance than the ambient temperature cured

column. The *RSI* value decreases with the increase of the compressive strength of GPC, and the *RSI* value of RES-GPC3 is smaller than that of the conventional CFST column (RES-OPC). If post-fire performance of a structure is a concern, a heat cured GCFST column is recommended because of its high RSI value.

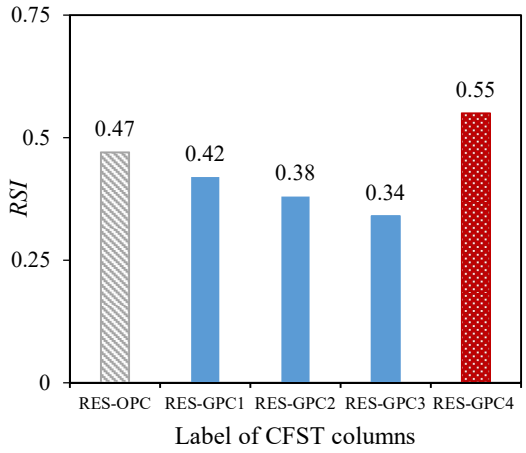


Figure 7.18. Comparison of different strength indexes

*7.3.3.3 Residual compressive stiffness*

The definition of residual compressive stiffness (*REA*) is the secant stiffness corresponding to the residual strength of $0.4N_{u,r}$, similar to the definition of compressive stiffness tested at an ambient temperature. The comparison results are shown in Figure 7.19 (a). By comparing different strength levels of GPCs, RES-GPC3 has higher *EA* than RES-GPC2. Considering RES-GPC1, RES-GPC2 and RES-GPC3 have similar residual compressive strengths, the difference of residual compressive stiffness of CFST columns is not contributed to concrete strength. After elevated temperature exposure, RES-GPC1 exhibits smaller *REA* results than RES-GPC2 and RES- GPC3. The liquid phase of GPC-1 evaporated at high temperature, and the shrinkage of GPC-1 might lead to a gap between the steel tube and concrete core of

RES-GPC1. The difference of the liquid content of GPC-1, GPC-2 and GPC-3 is accounted for by the difference of compressive stiffness of GCFST columns after elevated temperature exposure. The micro-crack development of the GPC-1 concrete core decreases the secant modulus. In the comparison of the influence between ambient cured GPC-2 and elevated cured GPC-4, RES-GPC4 has better behaviour than RES-GPC2 which complies to the test results in Figure 7.18.

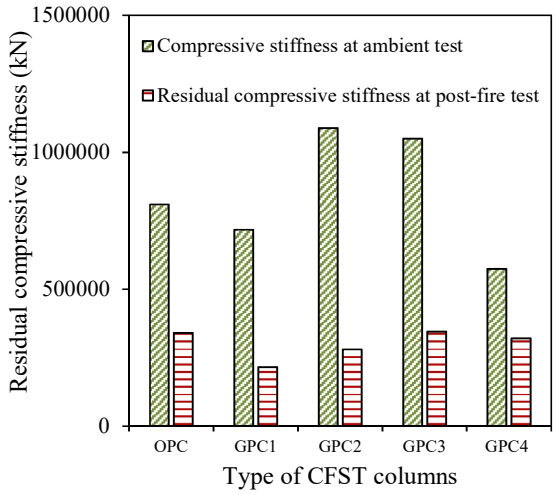


(a) Compressive stiffness

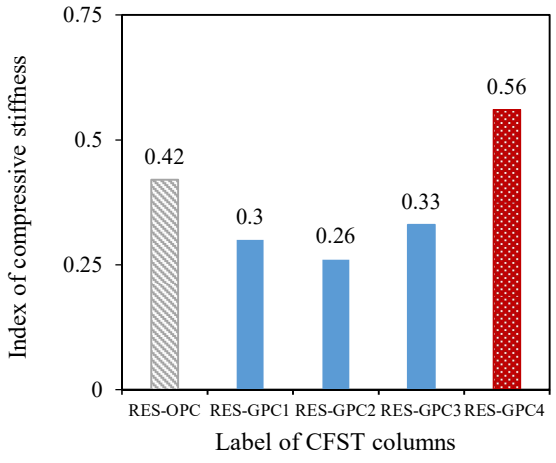


(b) Index of compressive stiffness

Figure 7.19. Comparison of compressive stiffness of CFST columns at ambient and post-fire test

### 7.3.4 Performance of CFST columns under combined temperature and loading

The tested specimens are presented in Figure 7.20. The control mode of the hydraulic machine was load control. With the increase of temperature, the load-carrying capacity decreased abruptly, and substantial deformation was observed on CFST columns, especially on HOT-OPC.

Figure 7.21 shows the comparison of axial deformation versus time ($\Delta$-$t$) relationships. Typically, a $\Delta$-$t$ curve has three stages (Tao et al., 2016), where in the initial stage the column starts to expand because of the thermal expansion. After the peak point is reached, the column starts to contract gradually due to strength loss at an elevated temperature. Finally, as the elevated temperature duration increases, the axial contraction deformation of the column increases sharply. The column fails when the load bearing capacity is no longer able to support the applied load.


Figure 7.20. Failed specimens under constant load and elevated temperature

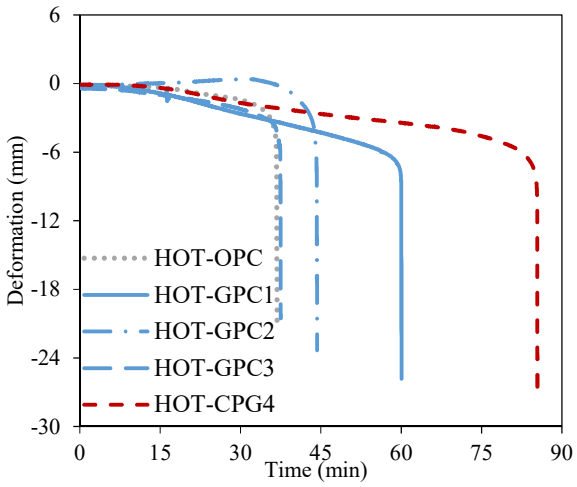


Figure 7.21. Axial deformation-time curves of CFST columns at heating stage

The test result of CFST columns under combined temperature and loading is different with the post-fire performance of CFST columns. Conventional CFST columns (HOT-OPC) exhibit the worst fire endurance, failing after 36 minutes of exposure. By comparison, heat cured GCFST columns have the best fire endurance, maintaining integrity under elevated temperatures for 85 minutes. Similar to residual strength tests on CFST, ambient temperature cured GCFST columns with low concrete strength level (HOT-GPC1) exhibit better fire endurance on fast heating regime. The fire endurance of HOT-GPC3, which has high strength GPC, is close to the performance of HOT-OPC. The initial thermal expansion of a HOT-GPC2 GCFST column is due to the temperature being more affected than other specimens; this could be due to the addition of extra water in the core GPC of a HOT-GPC2 GCFST column.

## 7.4 Summary

This chapter presents the experimental results and numerical modelling results of 15 CFST columns. The 15 experiments include 5 specimens tested at room temperature, 5 specimens tested at elevated temperatures and the remaining 5

specimens tested for residual strength after exposure to elevated temperatures. The following conclusions can be drawn within the scope of this study:

(1) The mechanical properties of GCFST columns, such as the axial load versus axial strain curve and the ultimate strength index and lateral to axial strain curve, are similar to those of conventional CFST columns. Two GCFST columns exhibit higher ductility than conventional CFST columns on average, while two GCFST columns have lower ductility than conventional CFST columns.

(2) The existing FE model proposed by Tao et al. (2013) can be used to accurately predict the load–deformation curves of GCFST columns at ambient temperature.

(3) GCFST columns exhibit better performance than the conventional CFST columns under elevated temperatures. The residual strength of GCFST columns were found slightly better than conventional CFST column. The fire endurance of CFST columns under combined loading and elevated temperature can be extensively improved by using GPC (especially heat cured GPC) as core concrete.

# Chapter 8 Conclusions and future research needs

## 8.1 Conclusions

This thesis has presented an in-depth study on the performance of GPC and the behaviour of CFST columns with GPC at both ambient and elevated temperatures. In relation to the objectives of this research, the major findings are summarised as follows:

(1) The addition of CAC in GPC can accelerate the geopolymerisation reaction at an ambient temperature. With the addition of CAC, the heat-curing regime was eliminated. The mechanical properties of the alkali-activated fly ash, blended with CAC, are improved significantly.

(2) The optimal geopolymer mixture design can be achieved using the Taguchi method. Alkali solution concentration plays a complex role; increasing the concentration will improve compressive strength while it will decrease workability. CAC replacement ratio is the most important factor for the mechanical properties. The optimal addition amount of CAC is 10% by mass of fly ash. Activator to binder ratio is crucial for workability; however, too much activator will diminish the compressive strength. Considering both compressive strength and workability, the optimal design is 10M alkali solution concentration, 10% CAC replacement and 45% activator to binder ratio.

(3) The conversion test was conducted on GPM cylinders and GPP samples. When undergoing a conversion test on a GPM specimen, there was no strength loss after the specimen cured at an elevated temperature. The TGA test was conducted on GPP samples, and no significant $C_3AH_6$ signal appeared on three GPP samples. The

strength test and material microstructure characterisations illustrate no severe risk of conversion existing in GPC.

(4) Both test results on workability and density of GPC presented in this thesis are comparable to those of conventional OPC. By varying the mixing designs of GPC, the slump results of fresh GPCs can be improved from 55 mm to 210 mm. The averaged density of hardened GPC is 2367.9 kg / $m^3$.

(5) This thesis confirmed the Young's modulus of GPC, tested by previous researchers, is lower than that of OPC. With the addition of CAC, the Young's modulus tested in this thesis was higher than that of conventional GPC reported by previous literature.

(6) The failure mode of GPM under elevated temperature was compared with typical fracture patterns defined in ASTM C39. The fracture patterns of GPM tended to form cones or diagonal fractures. Vertical cracks were less commonly observed than shear failure cracks.

(7) A parameter analysis was conducted on the hot strength of GPM. The results showed that activator concentration had little influence on the hot strength of GPM. By raising the amount of CAC from 5% to 20%, the strength increased at 600 °C, but a decrease in strength was observed at 800 °C; similar observations were made in regard to activator concentration: activator to binder ratio has little influence on the hot strength.

(8) GPC exhibited much better hot strength performance than reference OPC specimens. The residual strength of GPC was tested after exposure to elevated temperatures, and GPC exhibited a similar performance to OPC. Further, the

deformation of GPC at high temperatures under a constant load was examined. OPC failed earlier than geopolymer at 10 minutes in a brittle failure mode. The failure mode of GPC is much more ductile than that of OPC, although a significant improvement was not recorded on the duration time. The improved ductility makes the GPC safer than OPC in the application building during fire condition. The stress-strain curves of GPC and OPC were tested, and found to be similar, by the samples being exposed to elevated temperatures and cooled for seven days.

(9) The mechanical properties of GCFST columns—including axial load versus axial strain curve, ultimate strength index and lateral to axial strain curve—are similar to those of the conventional CFST columns. Two GCFST columns exhibited higher ductility than conventional CFST columns, while two GCFST columns exhibited lower ductility.

(10) The existing FE model proposed by previous researchers can be used to accurately predict the load-deformation curves of GCFST columns at an ambient temperature.

(11) GCFST columns were found to exhibit better fire resistance than the conventional CFST columns, whereas the residual strength of GCFST columns after exposure to elevated temperatures was also slightly improved. The fire endurance of CFST columns under combined loading and elevated temperature can be substantially improved by using GPC (especially heat cured GPC) as core concrete.

## 8.2 Recommendations for future research

This thesis examined fire-resistant GPC and its application in CFST columns. Although the objectives of this MPhil project have been successfully accomplished, a

number of issues could not be addressed due to equipment and time constraint. The following recommendations are suggested for future research:

(1) Study of shrinkage, creep and durability of GPC, along with the correlation between mechanical properties and durability of GPC.

(2) Study of the mechanical behaviour of GPC for a wider range of loading and temperature regimes. In order to further understand the fire resistance of GPC, tests need to be carried out on the thermal conductivity, capacity, diffusivity and coefficient of thermal expansion of GPC. In addition, the visualisation of heat transfer by using a thermal camera during the test can be investigated.

(3) The stress-strain curves of GPC under high temperatures should be investigated. Further requiring consideration are the effects of various parameters such as the aggregate type and size on the stress-strain curves of GPC. Studies of the performance of GPC under bi-axial and tri-axial loading are also required to understand the behaviour of this concrete under different loading conditions.

(4) Liquid alkali activated fly ash based GPC impedes the onsite application of GPC. Future research should consider the powder alkali activated GPC for on-site application.

(5) Further research is required to investigate the microscopic change of GPC under elevated temperatures and after elevated temperature exposure. Such knowledge is essential to providing a foundation for the future effort in improving the elevated temperature performance of GPC.

(6) GCFST slender columns should be investigated in future work, as well as the performance of such columns under eccentric loading.

# References

2015. Standard Specification for Coal Fly Ash and Raw or Calcined Natural Pozzolan for Use in Concrete. ASTM International.

318, A. C. Building Code Requirements for Structural Concrete (ACI 318-14): An ACI Standard: Commentary on Building Code Requirements for Structural Concrete (ACI 318R-14), an ACI Report. 2015. American Concrete Institute.

AIRPORT, B. 1996. Brisbane International Terminal.

ARIOZ, O. 2007. Effects of elevated temperatures on properties of concrete. *Fire safety journal,* 42**,** 516-522.

ASTM, C. 1996. 39, Standard test method for compressive strength of cylindrical concrete specimens. *Annual book of ASTM standards,* 4.

ATTARD, M. & SETUNGE, S. 1996. Stress-strain relationship of confined and unconfined concrete. *Materials Journal,* 93**,** 432-442.

AUSTRALIA, S. 2009. Concrete Structures (AS 3600-2009).

BAKHAREV, T. 2005. Geopolymeric materials prepared using Class F fly ash and elevated temperature curing. *Cement and Concrete Research,* 35**,** 1224-1232.

BOONSERM, K., SATA, V., PIMRAKSA, K. & CHINDAPRASIRT, P. 2012. Improved geopolymerization of bottom ash by incorporating fly ash and using waste gypsum as additive. *Cement and Concrete Composites,* 34**,** 819-824.

CAO, Y., TAO, Z., PAN, Z., MURPHY, T. & WUHRER, R. 2016a. Effect of calcium aluminate cement on workability and compressive strength of fly ash geopolymer mortar cured at ambient temperature. *Mechanics of Structures and Materials: Advancements and Challenges.* CRC Press.

CAO, Y., TAO, Z., PAN, Z., MURPHY, T. D. & WUHRER, R. Effect of calcium aluminate cement on workability and compressive strength of fly ash geopolymer mortar cured at ambient temperature. Mechanics of Structures and Materials: Advancements and Challenges: Proceedings of the 24th Australasian Conference on the Mechanics of Structures and Materials (ACMSM24), Perth, Australia, 6-9 December 2016, 2016b. 927-932.

CARREIRA, D. J. & CHU, K.-H. Stress-strain relationship for plain concrete in compression. Journal Proceedings, 1985. 797-804.

CHANG, Y.-F., CHEN, Y.-H., SHEU, M.-S. & YAO, G. C. 2006. Residual stress–strain relationship for concrete after exposure to high temperatures. *Cement and Concrete Research,* 36**,** 1999-2005.

CHENG, F.-P., KODUR, V. & WANG, T.-C. 2004. Stress-strain curves for high strength concrete at elevated temperatures. *Journal of Materials in Civil Engineering,* 16**,** 84-90.

CHENG, T. & CHIU, J. 2003. Fire-resistant geopolymer produced by granulated blast furnace slag. *Minerals Engineering,* 16**,** 205-210.

CHINDAPRASIRT, P., RATTANASAK, U., VONGVORADIT, P. & JENJIRAPANYA, S. 2012. Thermal treatment and utilization of Al-rich waste in high calcium fly ash geopolymeric materials. *International Journal of Minerals, Metallurgy, and Materials,* 19**,** 872-878.

COLLINS, F. & SANJAYAN, J. 1999. Strength and shrinkage properties of alkali-activated slag concrete placed into a large column. *Cement and concrete research,* 29**,** 659-666.

COLLINS, M. P., MITCHELL, D. & MACGREGOR, J. G. 1993. Structural design considerations for high-strength concrete. *Concrete international,* 15**,** 27-34.

COMMITEE, A. 2003. C09. ASTM C33-03, Standard Spesification for Concrete Agregates. ASTM International.

CONNOLLY, R. J. 1995. *The spalling of concrete in fires.* Aston University.

CROZIER, D. & SANJAYAN, J. 1999. Chemical and physical degradation of concrete at elevated temperatures. *Concrete in Australia,* 25**,** 18-20.

DAVIDOVITS, J. 1991. Geopolymers: inorganic polymeric new materials. *Journal of Thermal Analysis and calorimetry,* 37**,** 1633-1656.

DAVIDOVITS, J. 1993. Geopolymer cements to minimise carbon-dioxide greenhouse-warming. *Ceram. Trans.,* 37**,** 165-182.

DEXIN, X. 2012. *Structural Behaviour of Concrete Filled Steel Tubes With High Strength Materials.*

DING, J., FU, Y. & BEAUDOIN, J. 1996a. Study of hydration mechanisms in the high alumina cement-sodium silicate system. *Cement and concrete research,* 26**,** 799-804.

DING, J., FU, Y. & BEAUDOINT, J. 1996b. Effect of different inorganic salts/alkali on conversion-prevention in high alumina cement products. *Advanced cement based materials,* 4**,** 43-47.

DUXSON, P., FERNÁNDEZ-JIMÉNEZ, A., PROVIS, J. L., LUKEY, G. C., PALOMO, A. & VAN DEVENTER, J. 2007. Geopolymer technology: the current state of the art. *Journal of Materials Science,* 42**,** 2917-2933.

EN, C. 2004. 1–1. Eurocode 4: design of composite steel and concrete structures—Part 1.1: General rules and rules for buildings. *Brussels: European Committee for Standardization*.

ESPINOS, A., ROMERO, M. L., HOSPITALER, A., PASCUAL, A. M. & ALBERO, V. Advanced materials for concrete-filled tubular columns and connections. Structures, 2015. Elsevier, 105-113.

EUROCODE, C. 2004. 8: Design of structures for earthquake resistance—Part 1: General rules, seismic actions and rules for buildings (EN 1998-1: 2004). *European Committee for Normalization, Brussels*.

FERNÁNDEZ-JIMÉNEZ, A. & PALOMO, A. 2005. Composition and microstructure of alkali activated fly ash binder: effect of the activator. *Cement and concrete research,* 35**,** 1984-1992.

FERNÁNDEZ-JIMÉNEZ, A. & PUERTAS, F. 1997. Alkali-activated slag cements: kinetic studies. *Cement and Concrete Research,* 27**,** 359-368.

FERNANDEZ-JIMENEZ, A. M., PALOMO, A. & LOPEZ-HOMBRADOS, C. 2006. Engineering properties of alkali-activated fly ash concrete. *ACI Materials Journal,* 103**,** 106.

FERNÁNDEZ ‐ JIMÉNEZ, A., PALOMO, A., PASTOR, J. Y. & MARTIN, A. 2008a. New Cementitious Materials Based on Alkali ‐ Activated Fly Ash: Performance at High Temperatures. *Journal of the American Ceramic Society,* 91**,** 3308-3314.

FERNÁNDEZ ‐ JIMÉNEZ, A., PALOMO, A., VAZQUEZ, T., VALLEPU, R., TERAI, T. & IKEDA, K. 2008b. Alkaline activation of blends of metakaolin

and calcium aluminate. *Journal of the American Ceramic Society,* 91**,** 1231-1236.

GÖRHAN, G. & KÜRKLÜ, G. 2014. The influence of the NaOH solution on the properties of the fly ash-based geopolymer mortar cured at different temperatures. *Composites part b: engineering,* 58**,** 371-377.

GUERRIERI, M. & SANJAYAN, J. G. 2010. Behavior of combined fly ash/slag‐based geopolymers when exposed to high temperatures. *Fire and materials,* 34**,** 163-175.

HAN, L.-H., LI, W. & BJORHOVDE, R. 2014. Developments and advanced applications of concrete-filled steel tubular (CFST) structures: Members. *Journal of Constructional Steel Research,* 100**,** 211-228.

HAN, L.-H., WANG, W.-H. & YU, H.-X. 2010. Experimental behaviour of reinforced concrete (RC) beam to concrete-filled steel tubular (CFST) column frames subjected to ISO-834 standard fire. *Engineering Structures,* 32**,** 3130-3144.

HANJITSUWAN, S., PHOO-NGERNKHAM, T. & DAMRONGWIRIYANUPAP, N. 2017. Comparative study using Portland cement and calcium carbide residue as a promoter in bottom ash geopolymer mortar. *Construction and Building Materials,* 133**,** 128-134.

HARDJITO, D. 2005. *Studies of fly ash-based geopolymer concrete.*

HARDJITO, D. & RANGAN, B. V. 2005. Development and properties of low-calcium fly ash-based geopolymer concrete.

HEAH, C., KAMARUDIN, H., AL BAKRI, A. M., BINHUSSAIN, M., LUQMAN, M., NIZAR, I. K., RUZAIDI, C. & LIEW, Y. 2011. Effect of curing profile on kaolin-based geopolymers. *Physics Procedia,* 22**,** 305-311.

HEWLETT, P. 2003. *Lea's chemistry of cement and concrete*, Butterworth-Heinemann.

HUO, J., ZHANG, J., WANG, Z. & XIAO, Y. 2013. Effects of sustained axial load and cooling phase on post-fire behaviour of reinforced concrete stub columns. *Fire Safety Journal,* 59**,** 76-87.

HUSSIN, M., BHUTTA, M., AZREEN, M., RAMADHANSYAH, P. & MIRZA, J. 2015. Performance of blended ash geopolymer concrete at elevated temperatures. *Materials and Structures,* 48**,** 709-720.

JAMBUNATHAN, N., SANJAYAN, J., PAN, Z., LI, G., LIU, Y., KORAYEM, A., DUAN, W. & COLLINS, F. 2013a. The role of alumina on performance of alkali-activated slag paste exposed to 50 C. *Cement and Concrete Research,* 54**,** 143-150.

JAMBUNATHAN, N., SANJAYAN, J. G., PAN, Z., LI, G., LIU, Y., KORAYEM, A. H., DUAN, W. & COLLINS, F. 2013b. The role of alumina on performance of alkali-activated slag paste exposed to 50° C. *Cement and Concrete Research,* 54**,** 143-150.

JARKAS, A. 2012. Influence of Buildability Factors on Rebar Installation Labor Productivity of Columns. *Journal of Construction Engineering and Management,* 138**,** 258-267.

JAVIDAN, F., HEIDARPOUR, A., ZHAO, X.-L., HUTCHINSON, C. R. & MINKKINEN, J. 2016. Effect of weld on the mechanical properties of high strength and ultra-high strength steel tubes in fabricated hybrid sections. *Engineering Structures,* 118**,** 16-27.

JUNAID, M. T., KAYALI, O. & KHENNANE, A. 2017. Response of alkali activated low calcium fly-ash based geopolymer concrete under compressive load at elevated temperatures. *Materials and Structures,* 50**,** 50.

JUNAID, M. T., KHENNANE, A. & KAYALI, O. 2015. Performance of fly ash based geopolymer concrete made using non-pelletized fly ash aggregates after exposure to high temperatures. *Materials and Structures,* 48**,** 3357-3365.

KHAN, M., CASTEL, A., AKBARNEZHAD, A., FOSTER, S. J. & SMITH, M. 2016a. Utilisation of steel furnace slag coarse aggregate in a low calcium fly ash geopolymer concrete. *Cement and Concrete Research,* 89**,** 220-229.

KHAN, M., SHAIKH, F., HAO, Y. & HAO, H. 2016b. Workability and compressive strength properties of high strength geopolymer mortars. *Mechanics of Structures and Materials: Advancements and Challenges.* CRC Press.

KHAN, M. Z. N., HAO, Y. & HAO, H. 2016c. Synthesis of high strength ambient cured geopolymer composite by using low calcium fly ash. *Construction and Building Materials,* 125**,** 809-820.

KıRCA, Ö., YAMAN, İ. Ö. & TOKYAY, M. 2013. Compressive strength development of calcium aluminate cement–GGBFS blends. *Cement and Concrete Composites,* 35**,** 163-170.

LEE, N. & LEE, H. 2013. Setting and mechanical properties of alkali-activated fly ash/slag concrete manufactured at room temperature. *Construction and Building Materials,* 47**,** 1201-1209.

LEE, W. & VAN DEVENTER, J. 2004. The interface between natural siliceous aggregates and geopolymers. *Cement and Concrete Research,* 34**,** 195-206.

LI, C., SUN, H. & LI, L. 2010. A review: The comparison between alkali-activated slag (Si+ Ca) and metakaolin (Si+ Al) cements. *Cement and Concrete Research,* 40**,** 1341-1349.

LI, Y., LIU, X., YUAN, J. & WU, M. 2015. Toughness improvement of epoxy resin mortar by incorporation of ground calcium carbonate. *Construction and Building Materials,* 100**,** 122-128.

LIM, J. C. & OZBAKKALOGLU, T. 2014. Stress–strain model for normal-and light-weight concretes under uniaxial and triaxial compression. *Construction and Building Materials,* 71**,** 492-509.

LU, H., ZHAO, X.-L. & HAN, L.-H. 2011. FE modelling and fire resistance design of concrete filled double skin tubular columns. *Journal of Constructional Steel Research,* 67**,** 1733-1748.

MIJARSH, M., JOHARI, M. M. & AHMAD, Z. 2014. Synthesis of geopolymer from large amounts of treated palm oil fuel ash: application of the Taguchi method in investigating the main parameters affecting compressive strength. *Construction and Building Materials,* 52**,** 473-481.

MULTIPLEX 2005. Latitude.

NATH, P. & SARKER, P. K. 2014. Effect of GGBFS on setting, workability and early strength properties of fly ash geopolymer concrete cured in ambient condition. *Construction and Building Materials,* 66**,** 163-171.

NATH, P. & SARKER, P. K. 2015. Use of OPC to improve setting and early strength properties of low calcium fly ash geopolymer concrete cured at room temperature. *Cement and Concrete Composites,* 55**,** 205-214.

NEMATOLLAHI, B. & SANJAYAN, J. 2014. Effect of different superplasticizers and activator combinations on workability and strength of fly ash based geopolymer. *Materials & Design,* 57**,** 667-672.

NEVILLE, A. M. 1995. *Properties of concrete*, Longman London.

NGUYEN, K. T., AHN, N., LE, T. A. & LEE, K. 2016. Theoretical and experimental study on mechanical properties and flexural strength of fly ash-geopolymer concrete. *Construction and Building Materials,* 106**,** 65-77.

NICOLO, B. D., PANI, L. & POZZO, E. 1994. Strain of concrete at peak compressive stress for a wide range of compressive strengths. *Materials and Structures,* 27**,** 2206-210.

NOUSHINI, A., ASLANI, F., CASTEL, A., GILBERT, R. I., UY, B. & FOSTER, S. 2016. Compressive stress-strain model for low-calcium fly ash-based geopolymer and heat-cured Portland cement concrete. *Cement and Concrete Composites,* 73**,** 136-146.

OLIVIA, M. 2011. *Durability related properties of low calcium fly ash based geopolymer concrete.* Curtin University.

PACEWSKA, B., NOWACKA, M., WILIŃSKA, I., KUBISSA, W. & ANTONOVICH, V. 2011. Studies on the influence of spent FCC catalyst on hydration of calcium aluminate cements at ambient temperature. *Journal of thermal analysis and calorimetry,* 105**,** 129-140.

PACHECO-TORGAL, F., CASTRO-GOMES, J. & JALALI, S. 2007. Investigations about the effect of aggregates on strength and microstructure of geopolymeric mine waste mud binders. *Cement and Concrete Research,* 37**,** 933-941.

PALOMO, A., GRUTZECK, M. & BLANCO, M. 1999. Alkali-activated fly ashes: a cement for the future. *Cement and concrete research,* 29**,** 1323-1329.

PAN, Z. & SANJAYAN, J. G. 2012. Factors influencing softening temperature and hot-strength of geopolymers. *Cement and Concrete Composites,* 34**,** 261-264.

PAN, Z., SANJAYAN, J. G. & RANGAN, B. V. 2009. An investigation of the mechanisms for strength gain or loss of geopolymer mortar after exposure to elevated temperature. *Journal of Materials Science,* 44**,** 1873-1880.

PAN, Z., SANJAYAN, J. G. & RANGAN, B. V. 2011. Fracture properties of geopolymer paste and concrete. *Magazine of concrete research,* 63**,** 763-771.

POPOVICS, S. 1973. A numerical approach to the complete stress-strain curve of concrete. *Cement and concrete research,* 3**,** 583-599.

PROVIS, J. L. & VAN DEVENTER, J. S. 2014. *Alkali activated materials*, Springer.

PUERTAS, F., MARTíNEZ-RAMíREZ, S., ALONSO, S. & VAZQUEZ, T. 2000. Alkali-activated fly ash/slag cements: strength behaviour and hydration products. *Cement and Concrete Research,* 30**,** 1625-1632.

PULIGILLA, S. & MONDAL, P. 2013. Role of slag in microstructural development and hardening of fly ash-slag geopolymer. *Cement and Concrete Research,* 43**,** 70-80.

REIG, L., SORIANO, L., BORRACHERO, M., MONZÓ, J. & PAYÁ, J. 2016. Influence of calcium aluminate cement (CAC) on alkaline activation of red clay brick waste (RCBW). *Cement and Concrete Composites,* 65**,** 177-185.

RICKARD, W. D., GLUTH, G. J. & PISTOL, K. 2016. In-situ thermo-mechanical testing of fly ash geopolymer concretes made with quartz and expanded clay aggregates. *Cement and Concrete Research,* 80**,** 33-43.

RICKARD, W. D. & VAN RIESSEN, A. 2014. Performance of solid and cellular structured fly ash geopolymers exposed to a simulated fire. *Cement and Concrete Composites,* 48**,** 75-82.

RIVERA, O., LONG, W., WEISS JR, C., MOSER, R., WILLIAMS, B., TORRES-CANCEL, K., GORE, E. & ALLISON, P. 2016. Effect of elevated temperature on alkali-activated geopolymeric binders compared to portland cement-based binders. *Cement and Concrete Research,* 90**,** 43-51.

ROSS, P. J. 1988. Taguchi methods for quality engineering. McGraw-Hill, New York.

ROVNANÍK, P. 2010. Effect of curing temperature on the development of hard structure of metakaolin-based geopolymer. *Construction and Building Materials,* 24**,** 1176-1183.

SAMANI, A. K. & ATTARD, M. M. 2012. A stress–strain model for uniaxial and confined concrete under compression. *Engineering Structures,* 41**,** 335-349.

SANJAYAN, G. & STOCKS, L. 1993. Spalling of high-strength silica fume concrete in fire. *Materials Journal,* 90**,** 170-173.

SARGIN, M., GHOSH, S. & HANDA, V. 1971. Effects of lateral reinforcement upon the strength and deformation properties of concrete. *Magazine of concrete research,* 23**,** 99-110.

SARKER, P. K. & MCBEATH, S. 2015. Fire endurance of steel reinforced fly ash geopolymer concrete elements. *Construction and Building Materials,* 90**,** 91-98.

SATHONSAOWAPHAK, A., CHINDAPRASIRT, P. & PIMRAKSA, K. 2009. Workability and strength of lignite bottom ash geopolymer mortar. *Journal of Hazardous Materials,* 168**,** 44-50.

SHAIKH, F. & VIMONSATIT, V. 2015. Compressive strength of fly‐ash‐based geopolymer concrete at elevated temperatures. *Fire and Materials,* 39**,** 174-188.

SHAIKH, F. U. A. & HOSAN, A. 2016. Mechanical properties of steel fibre reinforced geopolymer concretes at elevated temperatures. *Construction and Building Materials,* 114**,** 15-28.

SHEHAB, H. K., EISA, A. S. & WAHBA, A. M. 2016. Mechanical properties of fly ash based geopolymer concrete with full and partial cement replacement. *Construction and Building Materials,* 126**,** 560-565.

SHI, C., JIMÉNEZ, A. F. & PALOMO, A. 2011. New cements for the 21st century: the pursuit of an alternative to Portland cement. *Cement and concrete research,* 41**,** 750-763.

SHI, X.-S., WANG, Q.-Y., ZHAO, X.-L. & COLLINS, F. G. 2015. Structural behaviour of geopolymeric recycled concrete filled steel tubular columns under axial loading. *Construction and Building Materials,* 81**,** 187-197.

SHOAIB, M., AHMED, S. & BALAHA, M. 2001. Effect of fire and cooling mode on the properties of slag mortars. *Cement and Concrete Research,* 31**,** 1533-1538.

SOFI, M., VAN DEVENTER, J., MENDIS, P. & LUKEY, G. 2007. Engineering properties of inorganic polymer concretes (IPCs). *Cement and Concrete Research,* 37**,** 251-257.

SOMNA, K., JATURAPITAKKUL, C., KAJITVICHYANUKUL, P. & CHINDAPRASIRT, P. 2011. NaOH-activated ground fly ash geopolymer cured at ambient temperature. *Fuel,* 90**,** 2118-2124.

SONG, T.-Y., HAN, L.-H. & UY, B. 2010. Performance of CFST column to steel beam joints subjected to simulated fire including the cooling phase. *Journal of constructional steel research,* 66**,** 591-604.

STANDARD, A. C78, 2010,"Standard Test Method for Flexural Strength of Concrete (Using Simple Beam with Third-Point Loading)", ASTM International, West Conshohocken, PA, 2010, DOI: 10.1520/C0078_C0078M-10.

STANDARD, A. C496 (2003). Standard Test Method for Splitting Tensile Strength of Cylindrical Concrete Specimens. *Annual Book of ASTM Standards,* 4.

STANDARD, A. 1997. Methods for fire tests on building materials, componets and structures. Part 4: Fire-resistance test of elements of construction. *AS1530,* 4.

STANDARD, A. 2002. C469 (2002) Standard test method for static modulus of elasticity and Poisson's ratio of concrete in compression. *ASTM International, West Conshohocken, PA. doi,* 10**,** 1520.

TAKE, C. slump tests for every test cylinders in accordance with ANSI. *ASTM C143*.

TALABÉR, J. 1993. FACTORS ACCELERATING TRANSFORMATION OF HIGH ALUMINA CEMENTS. *Periodica Polytechnica. Civil Engineering,* 37**,** 345.

TAO, Z., GHANNAM, M., SONG, T.-Y. & HAN, L.-H. 2016. Experimental and numerical investigation of concrete-filled stainless steel columns exposed to fire. *Journal of Constructional Steel Research,* 118**,** 120-134.

TAO, Z. & HAN, L.-H. 2007. Behaviour of fire-exposed concrete-filled steel tubular beam columns repaired with CFRP wraps. *Thin-walled structures,* 45**,** 63-76.

TAO, Z., WANG, X.-Q. & UY, B. 2012. Stress-strain curves of structural and reinforcing steels after exposure to elevated temperatures. *Journal of Materials in Civil Engineering,* 25**,** 1306-1316.

TAO, Z., WANG, Z.-B. & YU, Q. 2013. Finite element modelling of concrete-filled steel stub columns under axial compression. *Journal of Constructional Steel Research,* 89**,** 121-131.

VARMA, A. H., RICLES, J. M., SAUSE, R. & LU, L.-W. 2002. Experimental behavior of high strength square concrete-filled steel tube beam-columns. *Journal of Structural Engineering,* 128**,** 309-318.

WANG, W.-H., HAN, L.-H., LI, W. & JIA, Y.-H. 2014. Behavior of concrete-filled steel tubular stub columns and beams using dune sand as part of fine aggregate. *Construction and Building Materials,* 51**,** 352-363.

WANG, Y. C. 2003. *Steel and composite structures: Behaviour and design for fire safety*, CRC Press.

WANG, Z.-B., TAO, Z., HAN, L.-H., UY, B., LAM, D. & KANG, W.-H. 2017. Strength, stiffness and ductility of concrete-filled steel columns under axial compression. *Engineering Structures,* 135**,** 209-221.

WEE, T., CHIN, M. & MANSUR, M. 1996. Stress-strain relationship of high-strength concrete in compression. *Journal of Materials in Civil Engineering,* 8**,** 70-76.

WU, Z. & NAIK, T. R. 2003. Chemically activated blended cements. *Materials Journal,* 100**,** 434-440.

XU, H. & VAN DEVENTER, J. 2000. The geopolymerisation of alumino-silicate minerals. *International Journal of Mineral Processing,* 59**,** 247-266.

YANG, K.-H., MUN, J.-H., CHO, M.-S. & KANG, T. H. 2014. Stress-strain model for various unconfined concretes in compression. *ACI Structural Journal,* 111**,** 819.

YANG, Y.-F., CAO, K. & WANG, T.-Z. 2013. Experimental behavior of CFST stub columns after being exposed to freezing and thawing. *Cold Regions Science and Technology,* 89**,** 7-21.

YIN, J., ZHA, X.-X. & LI, L.-Y. 2006. Fire resistance of axially loaded concrete filled steel tube columns. *Journal of Constructional Steel Research,* 62**,** 723-729.

YOUNG, B. & ELLOBODY, E. 2006. Experimental investigation of concrete-filled cold-formed high strength stainless steel tube columns. *Journal of Constructional Steel Research,* 62**,** 484-492.

YU, X., TAO, Z. & SONG, T.-Y. 2016. Effect of different types of aggregates on the performance of concrete-filled steel tubular stub columns. *Materials and Structures,* 49**,** 3591-3605.